ANALYSIS AND OPTIMISATION OF SOFT ELECTROACTIVE LAMINATED COMPOSITES

by

Kudzai C.K. Mutasa MEng

Supervisor: Prof. Massimiliano Gei

A thesis in
Applied and Computational Mechanics.

A thesis presented for the degree of
Master of Philosophy in Engineering at
Cardiff University, United Kingdom.
August 2017

Declaration

This work has not been submitted in substance for any other degree or award at this or any other university or place of learning, nor is being submitted concurrently in candidature for any degree or other award.

Sign: .....(candidate) Date: .....

STATEMENT 1

This thesis is being submitted in partial fulfillment of the requirements for the degree of MPhil Engineering.

Sign: .....(candidate) Date: .....

STATEMENT 2

This thesis is the result of my own independent work/investigation, except where otherwise stated, and the thesis has not been edited by a third party beyond what is permitted by Cardiff University's Policy on the Use of Third Party Editors by Research Degree Students. Other sources are acknowledged by explicit references. The views expressed are my own.

Sign: .....(candidate) Date: .....

STATEMENT 3

I hereby give consent for my thesis, if accepted, to be available online in the Universitys Open Access repository and for inter-library loan, and for the title and summary to be made available to outside organisations.

Sign: .....(candidate) Date: .....

Acknowledgements

It would not have been possible to write this dissertation over the past year without the help and support of important people around me, all of whom are worth mentioning.

This body of work would first and foremost have not been possible without my supervisor, Professor Massimiliano Gei, whose brainchild is the foundation upon which this work is based upon. I am grateful that he has enhanced my critical thinking and sparked an accelerated rate of learning in me, as well as provided me with advice and support on both an academic and a personal level.

I would also like to thank the academic and technical staff at Cardiff University school of engineering for facilitating a smooth progression of my research. Finally, I would like to thank my parents, brothers and sister for their undying belief in my ambitions and for financial and emotional support throughout the duration of my studies.

Abstract

The aim of this study was to improve the overall electromechanical response of dielectric composite actuators. The microstructures of rank-1 and rank-2 laminates, composed of two materials of varying dielectric and shear moduli, were optimised for four types of actuation due to an applied nominal electric field.

A homogenization theory, established in the literature in finite electroelasticity for rank-1 layered composites, was specialized to the actuation types to develop a closed-form solution. A similar lamination methodology was then derived for rank-2 laminates to obtain a numerical solution. Expressions for specific sequentially laminated microstructures of rank-1 and rank-2 type were obtained so as to determine optimum microstructural configurations for maximum longitudinal stretch. These results were obtained iteratively using the Newton-Raphson method for a set of simultaneous equations.

Results for rank-1 laminates obtained in finite strain were found to produce actuation strains higher than those obtained by previous authors in small strain. Rank-2 laminates then presented an improvement in actuation strain compared to those obtained in small strain by the same authors. Ratios of shear and dielectric moduli were varied to obtain different contrasts and four parameters were defined to contribute to rank-2 laminate performance, namely two lamination angles and two volume fractions.

For all actuation types, rank-2 longitudinal stretch presented strong improvement from rank-1 laminates. Electromechanical instability was observed in rank-2 laminates for two of the four actuation types and a trade-off requirement was demonstrated between applied nominal electric field, shear and laminate microstructure for optimum performance.

At least a tenfold enhancement of phase electric fields was obtained for rank-2 laminates and the current configuration of lamination angles highlighted differences to the reference configuration. The ratios of shear and dielectric moduli were lastly perturbed and further enhancement of maximum longitudinal stretch obtained as a foundation for future work.

Contents

List of Figures

List of Tables

Chapter 1

Introduction

For a very long time, engineers and scientists have vehemently pursued motion-generating devices capable of mimicking the musculature and kinematics of the human form. Electro-active Polymers (EAPs) have gradually become the greatest prospect of generating a solution to this conundrum of providing small, light and affordable actuation capable of electrochemo-mechanical programming and manipulation. Dielectric elastomer actuators (DEAs), in particular, offer very good electromechanical capabilities in terms of achievable stresses, strains, response speeds, lifetimes, reliability and efficiency. Several applications have already been employed including robot arms, loudspeakers and variable-texture systems as discussed by Carpi et al. (2008) and Brochu & Pei (2010). However, one setback these type of actuators seem to present is that they require high electric fields as much as 10-100 V/μm as driving actuation which may limit their particular application, particularly in biomedical fields.

Most DEAs take advantage of large-scale deformations in the plane of the film. When exposed to high electric fields, DEAs contract in the direction of the electric field lines perpendicular to them due to Maxwell stress. The new devices are essentially rubbery capacitors in the form of two charged parallel plates sandwiching a dielectric material. On application of power, charges accumulate on opposite electrodes, attracting each other and squeezing down the polymer

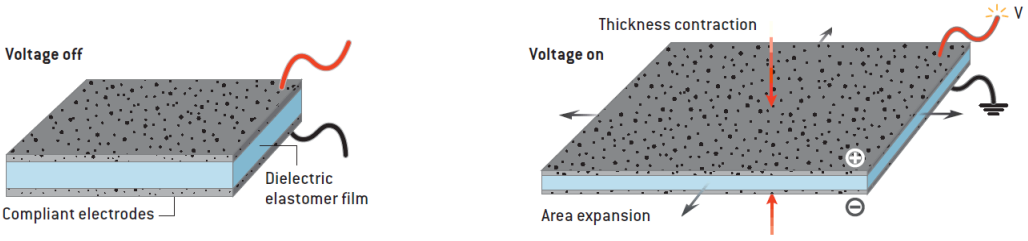

Figure 1.1: Basic mechanism of Dielectric Elastomer Actuators courtesy of Ashley (2003).

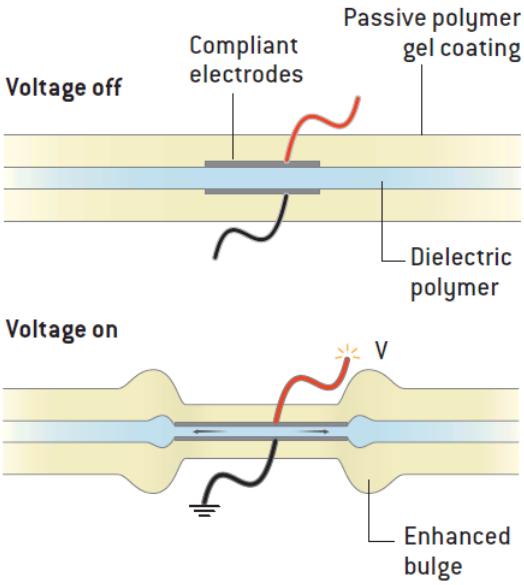

Figure 1.2: Mechanism of controllable surface textures using DEAs courtesy of Ashley (2003). As the film grows in the plane, the gel spreads out along with the expanding film and bunches up at the points at which the film compresses.

insulator, as presented in figure 1.1. One interesting application of DEAs is that presented by Ashley (2003) in figure 1.2 of changing the texture of a surface which can be desirable in areas such controlling air flow over surfaces of aircraft. The mechanism could be used for making "riblets" that improve the aerodynamic drag characteristics of aircraft wings, as investigated by Garcia-Mayoral & Jimenez (2011). Typical elastomers used as dielectrics in DEAs are silicone, acrylic or polyurethane while common compliant electrodes are usually based on carbon black or graphite powders.

The very nature of the electromechanical coupling mechanism has been an issue of numerous debates in the past: the aforementioned "Maxwell stress" has been attributed to account for the electromechanical response of these devices by Pelrine et al. (1998) whereas Dorfmann & Ogden (2005) and McMeeking & Landis (2005) proposed a different approach for electromechanical coupling based on the notion of total stress, where the coupling response is then included in the constitutive description, in agreement with the follow-up work by Suo et al. (2008). The general idea that can be extracted from either side of this debate is that the electromechanical behaviour is the result of the intrinsic electrical properties due to polarisation, as well as of the elastic mechanical ones.

In an effort to improve the overall electromechanical response of dielectric elastomers it is therefore crucial to focus intensely on properties that have a direct influence on achievable stresses and strains, such as the elastic or shear modulus and the dielectric constant. The scope of this work thus concerns dielectric elastomer composites, the particular classes of which are rank-1 and rank-2 laminates

composed of two materials of varying dielectric and shear moduli. Bertoldi & Gei (2011) mention that in order to design a new class of optimised devices based on dielectric composites, investigations are necessary focusing both on their failure under the applied loads and on the effect inclusions such as volume fraction, geometry and material properties have on their performance. This optimisation was also mentioned to be challenging due to the multiple failure modes that these materials possess, such that anyone undertaking such an optimisation should be on alert as to the possibility of instabilities presenting themselves at increased electrical excitation.

Thus the motivation of this study is threefold. My initial goal is to derive an explicit expression, from continuum mechanics fundamentals, for the effective energy-density function of the composites and to choose an appropriate lamination sequence such that the overall behaviour of the composite is transversely isotropic. The second goal shall then be to apply this theory by producing exact results for specific sequentially laminated microstructures of rank-1 and rank-2 type and determine optimum microstructural configurations for maximum longitudinal strain. Finally, these results shall be applied to various boundary-value problems, with key features of the overall laminate optimisation procedure for rank-1 and rank-2 laminates highlighted in an effort to provide an exhaustive and objective analysis of this process. What this study ultimately represents is a rigorous scientific optimisation methodology for rank-1 and rank-2 laminates of controlled electromechanical applied nominal electric fields for targeted maximum longitudinal stretch.

Chapter 2 embarks us on this study by introducing a continuum mechanics treatment for large strain finite elasticity, characterized by a typical non-linear stress-stretch relationship over large strain ranges. As the current configuration is distinct from the reference configuration, the electric balance equations will then be introduced so as to immediately plunge into the realm of electroelasticity with consistent stress tensors and equilibrium equations provided. I shall then prescribe the hyper-electroelastic, Neo-Hookean form of energy to this study and its response described by the strain energy function W, i.e. the stored energy per unit undeformed volume, which depends on the current state of deformation and electrical excitation.

Chapter 3 corresponds to a homogenization theory at finite strain for rank-1 layered composites introduced by Gei et al. (2013), recalled and specialized to be applied to four types of actuation. A similar lamination methodology will then be presented for rank-2 composites so as to obtain a numerical solution, while a closed-form solution would have been established for rank-1 laminates. An alternative energy formulation executed by Spinelli & Lopez-Pamies (2015) will be

presented in the context of this study with its interchangeable suitability to this study being highlighted.

In chapter 4, I will begin to distinguish the first two boundary-value problems in order to assess the behaviour of the heterogeneous devices described, with relevant results of the analysis illustrated. This chapter focuses solely on boundary-value problems in plane strain, beginning with an initial optimisation for each rank laminate in order to provide foundation for work in later sections. The initial results will be compared to those obtained by Tian et al. (2012) in an effort to provide initial validation. The study will then follow, in part, the sequence executed by the same aforementioned authors. An effort shall also be made to compare results of the two forms of plane strain problems. This chapter shall close with the exposition of the current electric field and configuration of rank-2 laminates.

Chapter 5 follows the structure of the previous chapter, except now for boundary-value problems in a three-dimensional environment. This three-dimensional representation aims to bring about a comparison with the plane-strain boundary-value problems, as well as discovery of any additional microstructural uniqueness occurring in rank-1 and rank-2 laminates. This then will enable a comparison of electromechanical instability occurrence in plane strain and three-dimensional environments. An attempt to reduce this instability, initially presented in the previous chapter, will be executed in its thoroughness for rank-2 laminates as well. Characterising these electromechanical instabilities however, is beyond the scope of this work and no general instability problems will be presented.

By the time I present chapter 6, I will be in a position to re-define the parameters that lead to microstructure optimisation, which are in the form of shear and dielectric moduli, and perturb these with guidance from information obtained in chapters 4 and 5 in order to introduce newly-configured rank-1 and rank-2 laminates. The current electric field will then be determined in a manner analogous to chapter 4 and comparison to these previous results also presented. These new laminates will also be investigated for the four boundary-value problems previously introduced. What this will then enable me to do is put forth a recommendation for strategies to employ in rank-1 and rank-2 sequentially-laminated composite design by enlisting all the observations presented throughout the text. This chapter in general is involved in providing a designer's perspective towards achieving the overall goal of this study, conducting an exhaustive approach of microstructure optimisation for rank-1 and rank-2 laminates as well as factors contributing to it.

In chapter 7, I discuss future work as well as summarise key points emphasised

throughout the text.

Chapter 2

General theoretical background on electroelasticity

2.1 Introduction

We shall begin by introducing continuum mechanics kinematics, mechanical balance laws and electric field equations relating to large strain hyper-electroelasticity. These will be defined in Lagrangian quantities in the reference configuration, with some forms of Eulerian quantities in the current configuration also presented. A description of kinematics of these two configurations will be presented in order to provide mechanical equilibrium equations and boundary conditions as well the neo-Hookean form of energy. This will be followed by electromechanical expressions as well as boundary conditions in terms of the aforementioned neo-Hookean energy. The now-called hyper-electroelasticity will also be presented in the form of an example boundary-value problem. In this text I will use Latin letters and Greek letters for *scalars*, bold-face Latin letters for *vectors*, bold-face Latin italicized letters for *second-order tensors* and bold-face calligraphic letters for *third order tensors*.

2.2 Analysis of deformation

Consider an electroelastic solid continuum occupying $\mathcal{B}^0 \subset \mathbb{R}^3$ in the undeformed stress-free configuration (in the absence of any electric field or mechanical load). Let the region, in three-dimensional euclidean space, occupied by the body in this configuration be denoted by $\mathcal{B}^0$, with boundary $\partial\mathcal{B}^0$ as shown by figure 2.1. Let $\mathbf{X}$ denote the position vector of a material point within the body in this configuration. Let us suppose the material is now deformed from the configuration $\mathcal{B}^0$ so that the point $\mathbf{X}$ occupies the position $\mathbf{x} = \mathcal{X}(\mathbf{X})$ in the deformed configuration, denoted by $\mathcal{B}$ which has boundary $\partial\mathcal{B}$. It should be noted that

time dependence is not considered in this study. The vector field $\mathcal{X}$, which is a one-to-one, orientation-preserving mapping with suitable regularity properties, describes the deformation of the body and is defined for $\mathbf{X} \in \mathcal{B}^0 \cup \partial\mathcal{B}^0$.

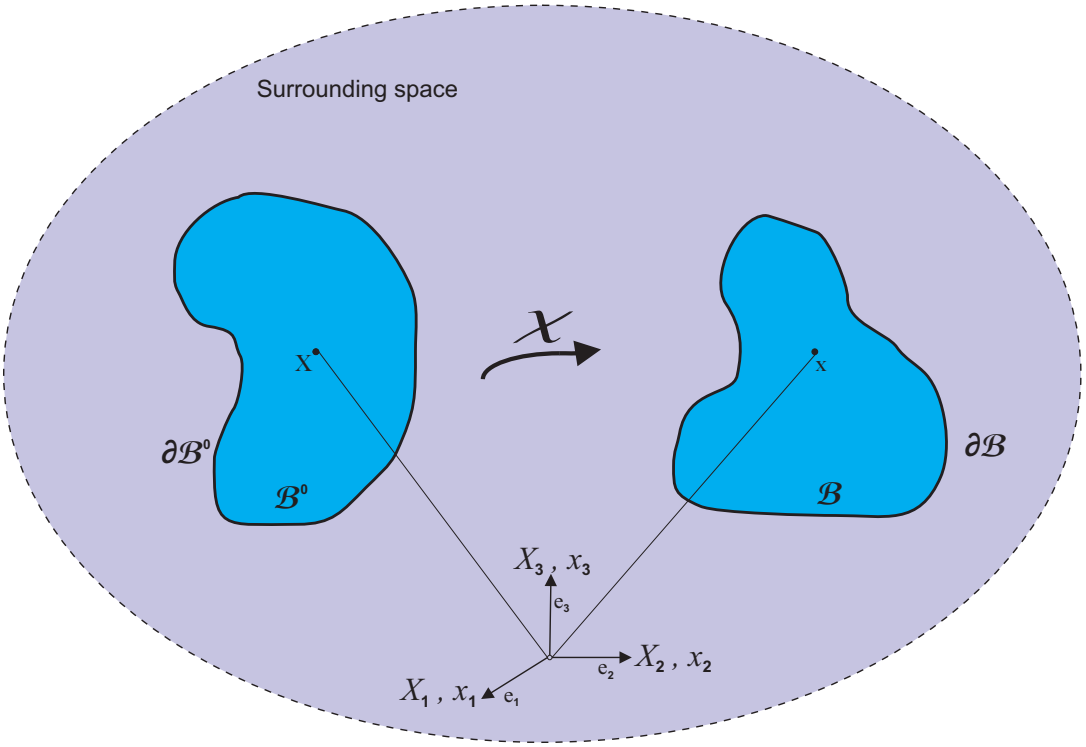

Figure 2.1: Configuration and deformation of a continuum body showing the reference and current configuration in three-dimensional euclidean space.

The deformation gradient tensor $\boldsymbol{F}$ relative to $\mathcal{B}^0$ is defined by

$$\boldsymbol{F} = \mathrm{Grad}\,\mathcal{X}, \qquad \mathbf{X} \in \mathcal{B}^0, \tag{2.1}$$

where Grad denotes the gradient operator with respect to $\mathbf{X}$. In Cartesian components, $F_{ij} = \{\mathrm{Grad}\,\mathcal{X}\}_{ij} = \partial x_i/\partial X_j$, where X_i and $x_i, i = 1, 2, 3$, are the components of $\mathbf{X}$ and $\mathbf{x}$, respectively. We also adopt the notation

$$J = \det \boldsymbol{F}, \tag{2.2}$$

with the standard convention $J > 0$. Associated with $\boldsymbol{F}$ are the (symmetric) right and left Cauchy-Green deformation tensors, here denoted $\boldsymbol{C}$ and $\boldsymbol{B}$, respectively, and defined by

$$\boldsymbol{C} = \boldsymbol{F}^{\mathrm{T}}\boldsymbol{F} = \boldsymbol{U}^2, \qquad \boldsymbol{B} = \boldsymbol{F}\boldsymbol{F}^{\mathrm{T}} = \boldsymbol{V}^2, \tag{2.3}$$

where $\boldsymbol{U}$, $\boldsymbol{V}$ are positive definite and symmetric tensors. The equation

$$\mathrm{d}\mathbf{x} = \boldsymbol{F}\mathrm{d}\mathbf{X}, \tag{2.4}$$

(in components, $\mathrm{d}x_i = F_{ij}\mathrm{d}X_j$) describes how an infinitesimal *line element* $\mathrm{d}\mathbf{X}$ of material at the point $\mathbf{X}$ transforms *linearly* under the deformation into the line element $\mathrm{d}\mathbf{x}$ at $\mathbf{x}$. Now let $\mathbf{dA}^0 \equiv \mathbf{n}^0\mathrm{d}A^0$ denote a vector surface area element on $\partial\mathcal{B}^0$, where $\mathbf{n}^0$ is the unit outward normal to the surface, and $\mathbf{dA} \equiv \mathbf{n}\,\mathrm{d}A$ the corresponding area element on $\partial\mathcal{B}$. The area elements are thus connected according to *Nanson's formula*, as follows:

$$\mathbf{n}\,\mathrm{d}A = J\boldsymbol{F}^{-\mathrm{T}}\mathbf{n}^0\mathrm{d}A^0, \tag{2.5}$$

where $\boldsymbol{F}^{-\mathrm{T}} = (\boldsymbol{F}^{-1})^{\mathrm{T}}$ and $^{\mathrm{T}}$ denotes the transpose. It should also be noted as mentioned by Fu & Ogden (2001) that, unlike a line element, the normal vector is not embedded in the material, i.e. $\mathbf{n}$ is not in general aligned with the same line element of material as $\mathbf{n}^0$.

The corresponding volumes $\mathrm{d}V^0$ in $\mathcal{B}^0$ and $\mathrm{d}V$ in $\mathcal{B}$ are related by the following:

$$\mathrm{d}V = J\mathrm{d}V^0. \tag{2.6}$$

In this case, $J = 1$ such that the volume in $\mathcal{B}^0$ is unchanged during deformation, which means that the deformation is *isochoric*. A material for which equation [2.2] is constrained to be satisfied for all deformation gradients $\boldsymbol{F}$ is said to be *incompressible*. From equation [2.4] the following expression is obtained

$$|\mathrm{d}\mathbf{x}|^2 = (\boldsymbol{F}\mathbf{m}^0)\cdot(\boldsymbol{F}\mathbf{m}^0)|\mathrm{d}\mathbf{X}|^2 = (\boldsymbol{F}^{\mathrm{T}}\boldsymbol{F}\mathbf{m}^0)\cdot\mathbf{m}^0|d\mathbf{X}|^2, \tag{2.7}$$

where the unit vector $\mathbf{m}^0$ has been introduced and is in the direction of $\mathrm{d}\mathbf{X}$ while $\cdot$ signifies the scalar product of two vectors. This means that the ratio $|\mathrm{d}\mathbf{x}|/|\mathrm{d}\mathbf{X}|$ of the lengths of a line element in the deformed and reference configurations is given by the following

$$\frac{|\mathrm{d}\mathbf{x}|}{|\mathrm{d}\mathbf{X}|} = |\boldsymbol{F}\mathbf{m}^0| = [\mathbf{m}^0\cdot(\boldsymbol{F}^{\mathrm{T}}\boldsymbol{F}\mathbf{m}^0)]^{1/2} \equiv \lambda(\mathbf{m}^0). \tag{2.8}$$

This equation defines the stretch $\lambda(\mathbf{m}^0)$ in the direction $\mathbf{m}^0$ at $\mathbf{x}$, and we note this restriction is according to the inequalities

$$0 < \lambda(\mathbf{m}^0) < \infty. \tag{2.9}$$

If there is no stretch in the direction $\mathbf{m}^0$, then $\lambda(\mathbf{m}^0) = 1$, and hence

$$(\boldsymbol{F}^{\mathrm{T}}\boldsymbol{F}\mathbf{m}^0)\cdot\mathbf{m}^0 = 1. \tag{2.10}$$

If there is no stretch in any direction, i.e. equation [2.10] holds for all $\mathbf{m}^0$, then it follows that $\boldsymbol{F}^{\mathrm{T}}\boldsymbol{F} = \boldsymbol{I}$, where $\boldsymbol{I}$ is the identity tensor. A suitable tensor measure

of strain is therefore $\boldsymbol{F}^{\mathrm{T}}\boldsymbol{F} - \boldsymbol{I}$ since this tensor vanishes when the material is unstrained. This leads to the definition of the Green strain tensor

$$\mathbf{G} = \frac{1}{2}(\boldsymbol{F}^{\mathrm{T}}\boldsymbol{F} - \boldsymbol{I}), \tag{2.11}$$

where $1/2$ is a normalization factor.

The deformation gradient can be decomposed according to the *polar decompositions*

$$\boldsymbol{F} = \boldsymbol{R}\boldsymbol{U} = \boldsymbol{V}\boldsymbol{R}, \tag{2.12}$$

where $\boldsymbol{R}$ is a proper orthogonal tensor and $\boldsymbol{U}, \boldsymbol{V}$ are positive definite and symmetric tensors. Each of the decompositions in [2.12] is unique and $\boldsymbol{U}$ and $\boldsymbol{V}$ are called the *right and left stretch tensors*, respectively. These stretch tensors can also be put in spectral form, and for $\boldsymbol{U}$ we have the *spectral decomposition*

$$\boldsymbol{U} = \sum_{i=1}^{3} \lambda_i \mathbf{u}^{(i)} \otimes \mathbf{u}^{(i)}, \tag{2.13}$$

where $\lambda_i > 0, i \in \{1, 2, 3\}$, are the principal stretches and $\mathbf{u}^{(i)}$, the unit eigenvectors of $\boldsymbol{U}$, are the Lagrangian principal axes, and $\otimes$ denotes the tensor product. Similarly, $\boldsymbol{V}$ has the spectral decomposition

$$\boldsymbol{V} = \sum_{i=1}^{3} \lambda_i \mathbf{v}^{(i)} \otimes \mathbf{v}^{(i)}, \tag{2.14}$$

where

$$\mathbf{v}^{(i)} = \boldsymbol{R}\mathbf{u}^{(i)}, \quad i \in \{1, 2, 3\}. \tag{2.15}$$

Let ρ and ρ_0 be the mass densities in $\mathcal{B}$ and $\mathcal{B}^0$, respectively. Then, since the material in the volume element $\mathrm{d}V$ is the same as that in $\mathrm{d}V^0$ the mass is conserved, i.e. $\rho \mathrm{d}V = \rho_0 \mathrm{d}V^0$, and hence, from [2.6] the mass conservation equation may be expressed in the form

$$\rho_0 = \rho J. \tag{2.16}$$

2.3 Stress tensors and equilibrium equations

The stress vector on the vector element area $\mathbf{dA}$, denoted by $\mathbf{t}$, depends on $\mathbf{n}$ according to the formula

$$\mathbf{t} = \boldsymbol{\sigma}\,\mathbf{n}, \tag{2.17}$$

where $\boldsymbol{\sigma}$ is a symmetric, second order tensor independent of $\mathbf{n}$ denoted the *Cauchy stress tensor*. Using equation [2.5] the force on $\mathbf{dA}$ may be written as follows:

$$\mathbf{t}\,\mathbf{dA} = \boldsymbol{S}\,\mathbf{n}^0 \mathbf{dA}^0, \tag{2.18}$$

where the Piola-Kirchoff stress tensor $\boldsymbol{S}$ is related to $\boldsymbol{\sigma}$ by

$$\boldsymbol{S} = J\boldsymbol{\sigma}\boldsymbol{F}^{-\mathrm{T}}. \tag{2.19}$$

If $\mathbf{b}$ denotes the body force per unit mass, then in integral form, the equilibrium equation for the body may be written with reference to either $\mathcal{B}^0$ or $\mathcal{B}$ below

$$\int_{\mathcal{B}} \rho \mathbf{b} \mathrm{d}V + \int_{\partial\mathcal{B}} \boldsymbol{\sigma}\,\mathbf{n}\,\mathrm{d}\mathbf{A} = \int_{\mathcal{B}^0} \rho_0 \mathbf{b} \mathrm{d}V^0 + \int_{\partial\mathcal{B}^0} \boldsymbol{S}\,\mathbf{n}^0\,\mathrm{d}\mathbf{A}^0 = \mathbf{0}, \tag{2.20}$$

and the resultant moment of the applied forces about a point $\mathbf{x}$ is

$$\int_{\mathcal{B}^0} \rho_0(\mathbf{x}-\mathbf{X}) \times \mathbf{b} \mathrm{d}V^0 + \int_{\partial\mathcal{B}^0} (\mathbf{x}-\mathbf{X}) \times \boldsymbol{S}\,\mathbf{n}^0 \mathrm{d}\mathbf{A}^0 = 0. \tag{2.21}$$

On use of the divergence theorem, equations [2.20] yield the equivalent equilibrium equations

$$\mathrm{div}\,\boldsymbol{\sigma} + \rho\mathbf{b} = \mathbf{0}, \tag{2.22}$$

$$\mathrm{Div}\,\boldsymbol{S} + \rho_0\mathbf{b} = \mathbf{0}, \tag{2.23}$$

where, in components, $\{\mathrm{Div}\,\boldsymbol{S}\}_i = S_{ij,j}$. Again Div and div represent the divergence operators in $\mathcal{B}^0$ and $\mathcal{B}$, respectively.

Considering the nonlinear theory of elasticity, electromechanical equilibrium along the deformation history, requires that

$$\mathrm{Div}\,\boldsymbol{S} = \mathbf{0}, \qquad \boldsymbol{S}\boldsymbol{F}^{\mathrm{T}} = (\boldsymbol{S}\boldsymbol{F}^{\mathrm{T}})^{\mathrm{T}}, \tag{2.24}$$

where $[2.24_1]$ is obtained from [2.20] while $[2.24_2]$ is obtained from [2.21]. The continuity of tractions can be imposed at the interface between two materials following on from equation [2.24] such that

$$[\![\boldsymbol{S}]\!]\mathbf{n}^0 = \boldsymbol{0}, \tag{2.25}$$

where the double square brackets denote the jump across a given interface i.e. $[\![f]\!] = f^A - f^B$ between two given materials A and B. We now consider the work done by the surface and body forces in a virtual displacement $\delta\mathbf{x}$ from the current configuration $\mathcal{B}$. By using the divergence theorem and equation [2.23], the resultant applied force on the body in $\mathcal{B}^0$, can be obtained by

$$\int_{\mathcal{B}^0} \rho_0 \mathbf{b} \cdot \delta\mathbf{x} \mathrm{d}V^0 + \int_{\partial\mathcal{B}^0} (\boldsymbol{S}\,\mathbf{n}^0) \cdot \delta\mathbf{x} \mathrm{d}\mathbf{A}^0 = \int_{\mathcal{B}^0} \mathrm{tr}(\boldsymbol{S}\delta\boldsymbol{F}^{\mathrm{T}}) \mathrm{d}V^0, \tag{2.26}$$

where the left-hand side of [2.26] represents the virtual work of the body and surface forces and in the integrand on the right-hand side tr denotes the trace of a second-order tensor, and $\delta\boldsymbol{F} = \mathrm{Grad}\delta\mathbf{x}$. The term on the right-hand side is the virtual work of the stresses in the bulk of the material. For a conservative system this latter work is recoverable and is stored as elastic strain energy W which has been well defined and explored by Ogden (1997).

2.4 Constitutive assumptions and energy formulations

2.4.1 Hyperelastic materials: strain energy functions

For conservative materials the mechanical response is described by a strain energy function W which reveals the stored energy per unit undeformed volume, depending on the current state of deformation. Analytical considerations provide that the function W of a hyperelastic material is a scalar-valued tensor function depending exclusively on the deformation gradient $\boldsymbol{F}$. For an incompressible hyperelastic solid, the stress-deformation relations introduced by Ogden (1997) can be represented as

$$\boldsymbol{S} = \frac{\partial W}{\partial \boldsymbol{F}} - p\boldsymbol{F}^{-\mathrm{T}}, \quad \boldsymbol{\sigma} = \boldsymbol{F}\frac{\partial W}{\partial \boldsymbol{F}} - p\boldsymbol{I}, \quad \det\boldsymbol{F} = 1, \tag{2.27}$$

where p is an arbitrary hydrostatic pressure, to be determined by boundary conditions. It should be noted that p has no effect on the deformation of an incompressible solid. For an isotropic hyperelastic material, W is a function of the following strain invariants $I_i\,(i = 1, 2, 3)$ defined as follows

$$I_1 = \mathrm{tr}\,\boldsymbol{C}, \quad I_2 = \frac{1}{2}((\mathrm{tr}\,\boldsymbol{C})^2 - \mathrm{tr}\,\boldsymbol{C}^2), \quad I_3 = \det\boldsymbol{C} = J^2. \tag{2.28}$$

The invariants of the right Cauchy-Green deformation tensor $\boldsymbol{C}$ can be defined in terms of the principal stretches as follows

$$\begin{aligned} I_1 &= \lambda_1^2 + \lambda_2^2 + \lambda_3^2, \\ I_2 &= \lambda_1^2\lambda_2^2 + \lambda_2^2\lambda_3^2 + \lambda_1^2\lambda_3^2, \\ I_3 &= \lambda_1^2\lambda_2^2\lambda_3^2, \end{aligned} \tag{2.29}$$

in the form $W = W(I_1, I_2, I_3)$. The first invariant, I_1, is found by Boyce & Arruda (2000) to correlate with the average polymer chain with regards to the macromolecular network structure of elastomeric materials. For convenience it is usual to require that the strain-energy function W should vanish in the reference configuration where $\boldsymbol{F} = \boldsymbol{I}$ so that $I_1 = I_2 = 3$ and $I_3 = 1$. The neo-Hookean strain energy model of hyper-elasticity used in this study is presented as follows:

$$W = \frac{\mu}{2}(\lambda_1^2 + \lambda_2^2 + \lambda_3^2 - 3) = \frac{\mu}{2}(I_1 - 3), \tag{2.30}$$

where μ is the initial shear modulus and J_m is a constant governing the maximum stretchability of the material, not to be confused with J.

2.5 Electric balance equations

It is considered now that the deformed configuration $\mathcal{B}$ arises from the combined application of mechanical loads and an electric field. The induced electric field $\mathbf{E}$ on the body satisfies the governing equation

$$\operatorname{curl} \mathbf{E} = \boldsymbol{0}, \tag{2.31}$$

in the entire space, with respect to the current coordinate system. Consequently, we define a scalar field, the electric potential ϕ, such that $\mathbf{E} = -\nabla_{\mathbf{x}}\phi$ where $\nabla_{\mathbf{x}}$ denotes the gradient with respect to the current coordinate system. The electric displacement field is

$$\mathbf{D} = \epsilon_0 \mathbf{E} + \mathbf{P}, \tag{2.32}$$

where ϵ_0 is the permittivity of the vacuum and $\mathbf{P}$ is the polarization, or the electric dipole-density. In the absence of free charges the electric displacement field is governed by the local equation

$$\operatorname{div} \mathbf{D} = 0. \tag{2.33}$$

It has previously been determined, and subsequently highlighted by Dorfmann & Ogden (2005), that the referential counterparts $\mathbf{E}^0$ and $\mathbf{D}^0$ of the electric field and the electric displacement are

$$\mathbf{E}^0 = \boldsymbol{F}^{\mathrm{T}}\mathbf{E}, \tag{2.34}$$

$$\mathbf{D}^0 = J\boldsymbol{F}^{-1}\mathbf{D}. \tag{2.35}$$

The corresponding electric field and electric displacement are governed by the equations

$$\operatorname{Div} \mathbf{D}^0 = 0, \quad \operatorname{Curl} \mathbf{E}^0 = \boldsymbol{0}. \tag{2.36}$$

Let us also assume the body $\mathcal{B}^0$ to be completely surrounded by an infinite free (vacuum) space such that $\mathbf{P} = \boldsymbol{0}$. In an electro-elastic problem, this means equations [2.31] and [2.33] must be satisfied in the surrounding space as well, such that equation [2.32] becomes

$$\mathbf{D} = \epsilon_0 \mathbf{E}. \tag{2.37}$$

In Lagrangian formulation, the standard continuity conditions for the electric displacement and the electric field through $\partial\mathcal{B}^0$ are

$$[\![\mathbf{D}^0]\!] \cdot \mathbf{n}^0 = -\omega^0, \quad \mathbf{n}^0 \times [\![\mathbf{E}^0]\!] = 0, \tag{2.38}$$

where ω is the surface charge distribution. Note that [2.25] and [2.38] are also valid across all interfaces between phases in a composite material.

2.6 Electro-elastic constitutive equations

The development of constitutive equations enables a clear determination of the relationship between the external electric input and the electromechanical response of the material in a composite. For each phase in the composite, it can be assumed to be hyperelastic and behaving as an ideal dielectric as already described i.e. $\mathbf{D} = \epsilon\mathbf{E}$, where the dielectric constant (or permittivity) ϵ is independent of the deformation. Considering thermodynamic arguments, $[2.27_1]$ can be recalled as introduced by Ogden (1997), while the constitutive law of electric displacement, can be expressed next to it as highlighted by Dorfmann & Ogden (2017) as follows

$$\boldsymbol{S} = \frac{\partial W}{\partial \boldsymbol{F}} - p\boldsymbol{F}^{-\mathrm{T}}, \quad \mathbf{D}^0 = -\frac{\partial W}{\partial \mathbf{E}^0}. \tag{2.39}$$

Assuming $\mathbf{E}^0$ as independent electric variable [i.e. $W = W(\boldsymbol{F}, \mathbf{E}^0)$], a form of energy with Neo-Hookean behaviour is given as:

$$W = \frac{\mu}{2}\left[\mathrm{tr}(\boldsymbol{F}^{\mathrm{T}}\boldsymbol{F}) - 3\right] - \frac{\epsilon}{2}(\boldsymbol{F}^{-\mathrm{T}}\mathbf{E}^0 \cdot \boldsymbol{F}^{-\mathrm{T}}\mathbf{E}^0). \tag{2.40}$$

According to the electroelastic theory of continua at finite strain highlighted by Dorfmann & Ogden (2005), direct equations can also be formulated in the current configuration $\mathcal{B}$. In reference to equations [2.24] and [2.36] where $\boldsymbol{\sigma}$ now refers to the total (true) stress, which replaces $\boldsymbol{S}$, analogous to [2.19], as follows:

$$\boldsymbol{\sigma} = \boldsymbol{S}\boldsymbol{F}^{\mathrm{T}}/J. \tag{2.41}$$

For the free energy [2.40], the explicit form of [2.39] can be obtained by substituting [2.34] and [2.35], leading to the following

$$\boldsymbol{S} + p\,\boldsymbol{F}^{-\mathrm{T}} - \mu\boldsymbol{F} = \frac{1}{\epsilon}\boldsymbol{F}\mathbf{D}^0 \otimes \mathbf{D}^0 = \epsilon\boldsymbol{F}^{-\mathrm{T}}\mathbf{E}^0 \otimes \boldsymbol{F}^{-1}\boldsymbol{F}^{-\mathrm{T}}\mathbf{E}^0, \tag{2.42}$$

which corresponds to the following

$$\boldsymbol{\sigma} + p\boldsymbol{I} - \mu\boldsymbol{F}\boldsymbol{F}^{\mathrm{T}} = \frac{1}{\epsilon}\mathbf{D} \otimes \mathbf{D} = \epsilon\mathbf{E} \otimes \mathbf{E}. \tag{2.43}$$

It should be noted that $[2.39]_2$ is included in equation [2.42].

2.6.1 Example boundary-value problem

An attempt shall now be made to solve a simple electromechanical problem of bi-axial strain so as to provide a framework for the interpretation and solution of boundary-value problems to be presented in the next chapter. To this end, we now consider an ideal dielectric membrane which is homogeneous, isotropic,

hyper-electro-elastic and incompressible. The body is subjected only to an electric field generated by a voltage difference between the stretchable electrodes coating the two extended surfaces, which are opposite to one another. Neglecting fringe effects, the perceived deformation is homogeneous, with the electric field vanishing outside the device, and inside it, uniformly aligned along direction x_2 given in figure 2.2.

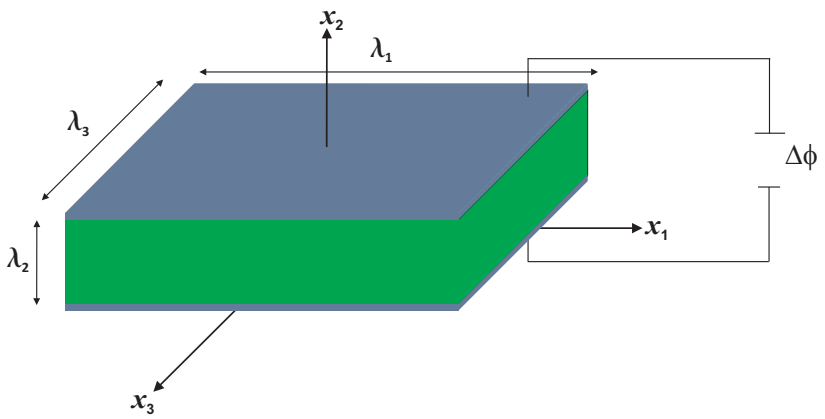

Figure 2.2: Current configuration of a planar soft dielectric actuator subjected to a voltage difference $\Delta\phi$.

The total change of energy stored, by performing a summation of all the contributions, is determined using equation [2.40]. The mechanical part of the energy function is found to depend only on the principal stretches. In this boundary-value problem, appropriate boundary conditions also need to be applied. These have been established in equations [2.25] and [2.38]. The deformation is defined by λ_1, λ_2 and λ_3 and the components of the deformation gradient $\boldsymbol{F}$ are given by the following

$$\boldsymbol{F} = \begin{bmatrix} \lambda_1 & 0 & 0 \\ 0 & \lambda_2 & 0 \\ 0 & 0 & \lambda_3 \end{bmatrix}. \qquad [2.44]$$

In the planar actuator presented in figure 2.2, any mechanical external force is applied to the elastomer and the electric field outside the body is assumed negligible, such that the total true and nominal stresses vanish identically throughout the actuator as implied by equation [2.25].

Substitution of equation [2.44] into [2.42] leads to the following

$$S_{11} = \lambda_1\mu - \frac{p}{\lambda_1}, \quad S_{22} = \epsilon\frac{E^0 \cdot E^0}{\lambda_2^2} - \frac{p}{\lambda_2} + \lambda_2\mu, \quad S_{33} = \frac{\mu}{\lambda_1\lambda_2} - p\lambda_1\lambda_2, \quad [2.45]$$

where $\mathbf{E}^0 = \Delta\phi/H^0$ along x_2 is the only non-vanishing component of the electric field and H^0 is the distance between electrodes. The associated stress state is such that the total Cauchy stress components $\sigma_{13} = \sigma_{23} = \sigma_{33} = 0$. Alternatively, imposing $S_{11} = S_{22} = S_{33} = 0$, incompressibility can also be used from $\lambda_1\lambda_2\lambda_3 = 1$ with $\lambda_1 = \lambda_3$ to determine that $\lambda_2 = 1/\lambda_1^2$. Thus it is possible to determine the 3 remaining unknowns λ_1, λ_2 and p in the form

$$\lambda_1 = \frac{\sqrt{(E^0)^2\epsilon + \lambda_2^4\mu}}{\lambda_2\sqrt{\mu}}, \quad \lambda_2 = \frac{\sqrt{\lambda_1^2 - \frac{\sqrt{\mu(-4(E^0)^2\epsilon + \lambda_1^4\mu)}}{\mu}}}{\sqrt{2}}, \quad p = \frac{(E^0)^2\epsilon}{\lambda_2^2} + \lambda_2^2\mu. \tag{2.46}$$

2.7 Conclusions

In this chapter I have introduced the theory of large strain finite elasticity based on the Neo-hookean model of elasticity. In the next chapter I will introduce a continuum mechanics treatment within the theory of deformable dielectrics for a rank-1 sequentially laminated composite. This treatment will then be applied to a rank-2 composite, of which a numerical solution shall be obtained.

Chapter 3

Sequentially laminated composites

3.1 Introduction

We will now expand a homogenization theory in finite strain for rank-1 layered composites, in a manner analogous to that introduced by Gei et al. (2013), and then extend this to rank-2 composites. Using interface-continuity conditions and constitutive laws, two constants that define the problem will be derived, α and $\tilde{\beta}$, and hence the phase-difference in hydrostatic pressure for each rank laminate. An alternative energy formulation executed by Lopez-Pamies (2014) shall then be highlighted and compared to the formulation already presented.

3.2 A description of the lamination procedure

In respect of the reference configuration, $\mathcal{B}^0$, consider a laminated composite presented in figure 3.1, composed of two distinct phases; one phase, "A" comprises of a stiff, high dielectric material while another phase, "B" composes entirely of a soft, low dielectric material with an arbitrary lamination angle θ. This is a rank-1 laminate. For purposes of this investigation we will assume the characteristic size of the heterogeneity is much smaller than the size of the actuator and the morphology of the actuator is such that the heterogeneous dielectric is macroscopically homogeneous. We consider the deformation of the actuator due to electromechanical coupling but with no external loads, thus the traction is zero. Geometrically, the layers are characterized by their thickness H^A and H^B and volume fractions given by $C^A_{R1} = H^A/(H^A + H^B)$ and $C^B_{R1} = 1 - C^A_{R1}$. Upon application of external electromechanical loading, the body reaches a current configuration $\mathcal{B}$.

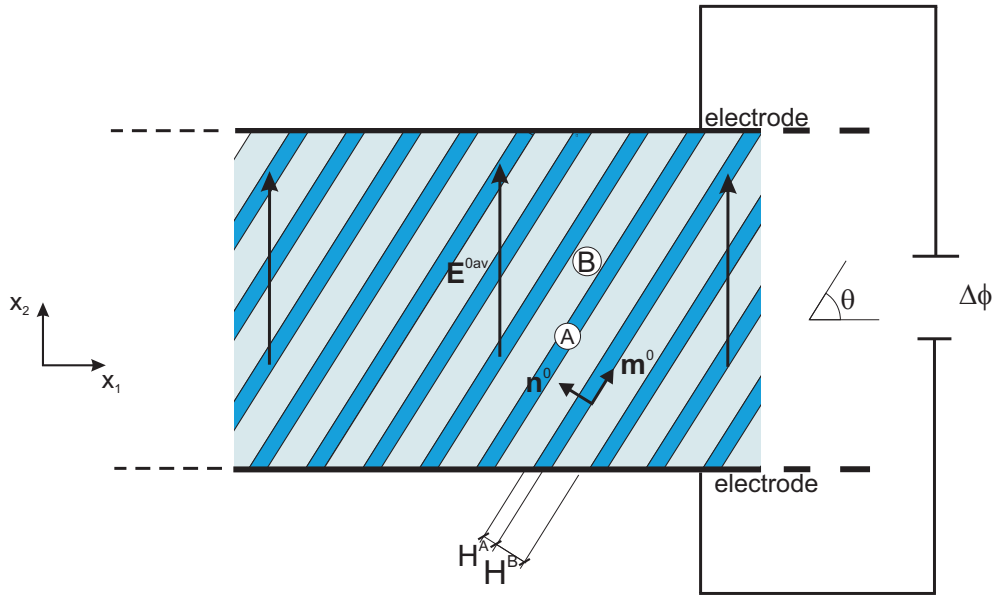

Figure 3.1: Geometry of the reference configuration of a two-phase layered dielectric actuator subjected to a electric field difference $\Delta\phi$ applied between electrodes.

Using these assumptions, the effective macroscopic behaviour of the system can be determined from homogenization theory previously executed in variation by Ogden (1974), DeBotton (2005), Gei et al. (2013) and Lopez-Pamies (2014). As electric field actuation is the area of interest in this body of work, the microscopic free energy in each phase, is introduced. Assuming $\mathbf{E}^0$ as independent electric variable (i.e. $W = W(\boldsymbol{F}, \mathbf{E}^0)$), the required expressions in reference to equation [2.40] are given below:

$$W^{\mathrm{A}} = \frac{\mu^A}{2}\left[\mathrm{tr}(\boldsymbol{F}^{\mathrm{T}}\boldsymbol{F}) - 3\right] - \frac{\epsilon^A}{2}(\boldsymbol{F}^{(-T)}\mathbf{E}^0 \cdot \boldsymbol{F}^{(-T)}\mathbf{E}^0), \qquad [3.1]$$

$$W^{\mathrm{B}} = \frac{\mu^B}{2}\left[\mathrm{tr}(\boldsymbol{F}^{\mathrm{T}}\boldsymbol{F}) - 3\right] - \frac{\epsilon^B}{2}(\boldsymbol{F}^{(-T)}\mathbf{E}^0 \cdot \boldsymbol{F}^{(-T)}\mathbf{E}^0), \qquad [3.2]$$

where μ^A and μ^B are the shear moduli in each phase while ϵ^A and ϵ^B are the dielectric moduli in each phase. The representation of [3.1] and [3.2], despite being identical, have expressions whose difference will be distinctive later when discussing rank-2 laminates. Continuity at all the internal interfaces between phases "A" and "B" is enforced imposing equations already described as equations [2.25] and [2.38]. The normal $\mathbf{n}^0$ is pointing toward "B" and can be easily related to angle θ. Following the approach of Gei et al. (2013), the heterogeneous actuator will be presented on similar bases of macroscopic average quantities $\boldsymbol{S}^{\mathrm{av}}$, $\boldsymbol{F}^{\mathrm{av}}$,

$\mathbf{D}^{0\mathrm{av}}$ and $\mathbf{E}^{0\mathrm{av}}$. These quantities sufficiently prescribe all conditions in which the validity of governing equations [2.25], [2.36] and [2.38] remains fulfilled in all points in the body. The macroscopic total stress and electric field can be obtained from the macroscopic average total energy W^{av} via constitutive relations presented in [2.39] now displayed as follows:

$$\boldsymbol{S}^{\mathrm{av}} = \frac{\partial W^{\mathrm{av}}}{\partial \boldsymbol{F}^{\mathrm{av}}} - p^{\mathrm{av}}(\boldsymbol{F}^{\mathrm{av}})^{-\mathrm{T}}, \qquad \mathbf{D}^{0\mathrm{av}} = -\frac{\partial W^{\mathrm{av}}}{\partial \mathbf{E}^{0\mathrm{av}}}, \tag{3.3}$$

where quantities with label 'av' prescribe the average over a representative volume of the composite. In the entirety of this homogenization theory, some of the assumptions made by Tevet-Deree (2008), as well as others already mentioned, will be applied and are summarised here, namely:

- Any difference between the macroscopic strain responses of the composites and those that would develop in the phases are solely due to the heterogeneity and the spatial arrangement of the phases. This arrangement of the phases in terms of lamination angle θ will be noted.

- As typical actuators mainly consist in very thin specimens, in all of them we disregard edge effects concentrated along the boundary of the electrodes or related to a lack of heterogeneity of the surface charge distribution. This implies the electric field outside the boundary vanishes identically and the Lagrangian electric field $\mathbf{E}^{0\mathrm{av}}$ is directed along x_2.

- We shall fix the rigid-body of the finite deformation such that the two straight boundaries remain aligned with x_1 and the electric fields $\mathbf{E}^{0\mathrm{av}}$ and $\mathbf{E}^{\mathrm{av}} = (\boldsymbol{F}^{\mathrm{av}})^{-\mathrm{T}}\mathbf{E}^{0\mathrm{av}}$ act along the orthogonal direction, namely

  $$\mathbf{E}^{0\mathrm{av}} = E^{0\mathrm{av}}\boldsymbol{e}_2, \qquad \mathbf{E}^{\mathrm{av}} = E^{\mathrm{av}}\boldsymbol{e}_2, \tag{3.4}$$

  where $\boldsymbol{e}_2$ is the unit vector associated with x_2.

- The electrodes are flexible with a negligible elastic moduli and thus do not extract mechanical traction on the dielectric layer.

- We consider the deformation of the actuator due to electromechanical coupling but with no external loads. This is enforced already by the traction boundary condition [2.25].

- In view of the dielectric anisotropy, the electric displacements, $\mathbf{D}^{0\mathrm{av}}$ and $\mathbf{D}^{\mathrm{av}}$ are not in general aligned with $\boldsymbol{e}_2$ and for the type of actuation being investigated, $E^{0\mathrm{av}} = \Delta\phi/H^0$, where H^0 is the distance between electrodes.

- Equation [2.38_2] (continuity of the tangential component of the electric field) can be also written as

$$[\![\mathbf{E}^0]\!] \cdot \mathbf{m}^0 = \mathbf{0}, \tag{3.5}$$

  where $\mathbf{m}^0$ is aligned with the interface and such that $\mathbf{n}^0 \cdot \mathbf{m}^0 = 0$ according to figure 3.1.

- The continuity at the interface in relation to the deformation gradient shall be determined as follows:

$$[\![\boldsymbol{F}]\!]\mathbf{m}^0 = \boldsymbol{0}. \tag{3.6}$$

- In all illustrative drawings presented, the requirement that the size of the layers of the core phase will be much smaller than the size of the layers in the rank-1 and rank-2 laminates is not strictly satisfied i.e. drawings are not to scale.

- The figures presented throughout this text will reflect a laminate configuration such that all points on the corresponding electromechanical loading path lie within the range $0 \leq \Delta\phi/H^0 \leq 100$ MV/m.

3.3 Homogenised solution of rank-1 and rank-2 laminates

3.3.1 Rank-1 solution

Based on the homogenisation procedure given in this section, Gei et al. (2013) mention how the behaviour expected of the laminate is that of a macroscopic behaviour both mechanically and electrically. The latter is evident from the eulerian constitutive relationship $\mathbf{D}^{\text{av}} = \boldsymbol{\epsilon}^{\text{av}}\mathbf{E}^{\text{av}}$, where matrix $\boldsymbol{\epsilon}^{\text{av}}$ depends on the properties of both phases, irrespective of the driving actuation. The aim is to obtain results for rank-1 layered dielectrics, specialised to the extended Neo-Hookean free energy in equation [3.1] or [3.2].

Considering the rank-1 geometry in consideration, the electric field outside the actuator vanishes and, with consideration that $\tilde{\mathbf{n}}^0$ as the outward unit normal to the boundaries of the actuator, the boundary conditions [2.38] are of the form presented below:

$$\mathbf{D}^{0\text{av}} \cdot \tilde{\mathbf{n}}^0 = -\omega^0, \quad \tilde{\mathbf{n}}^0 \times [\![\mathbf{E}^{0\text{av}}]\!] = \boldsymbol{0}, \tag{3.7}$$

the former implying equation [3.4]. Equations [$3.7_{1,2}$] state that the electric displacement is continuous across the interface and the electric field is continuous

along the interface, respectively. The jump in the electric displacement between the two phases can then be represented as follows:

$$[\![\mathbf{D}^0]\!] \cdot \mathbf{n}^0 = 0. \tag{3.8}$$

According to the theory of composite materials, the macroscopic deformation gradient $\boldsymbol{F}^{\text{av}}$, the macroscopic total first Piola-Kirchhoff stress $\boldsymbol{S}^{\text{av}}$ and the Lagrangian electric field $\mathbf{E}^{0\text{av}}$ are defined as

$$\boldsymbol{F}^{\text{av}} = C^A \boldsymbol{F}^A + C^B \boldsymbol{F}^B, \qquad \boldsymbol{S}^{\text{av}} = C^A \boldsymbol{S}^A + C^B \boldsymbol{S}^B, \qquad \mathbf{E}^{0\text{av}} = C^A \mathbf{E}^{0A} + C^B \mathbf{E}^{0B}. \tag{3.9}$$

Interface compatibility [3.6], together with eq. $[3.9]_1$ provide the relations:

$$\boldsymbol{F}^A = \boldsymbol{F}^{\text{av}} \left(\boldsymbol{I} + \alpha\, C^B \mathbf{m}^0 \otimes \mathbf{n}^0 \right), \quad \boldsymbol{F}^B = \boldsymbol{F}^{\text{av}} \left(\boldsymbol{I} - \alpha\, C^A \mathbf{m}^0 \otimes \mathbf{n}^0 \right), \tag{3.10}$$

where α is a real parameter. Considering $[2.38]_2$, it requires that the jump in $\mathbf{E}^0$ be along the direction normal to the layers, namely

$$\mathbf{E}^{0A} - \mathbf{E}^{0B} = \tilde{\beta} \mathbf{n}^0, \tag{3.11}$$

where $\tilde{\beta}$ is another real parameter. It follows from $[3.9]_2$ and [3.11] that

$$\mathbf{E}^{0A} = \mathbf{E}^{0\text{av}} + C^B \tilde{\beta} \mathbf{n}^0, \quad \mathbf{E}^{0B} = \mathbf{E}^{0\text{av}} - C^A \tilde{\beta} \mathbf{n}^0. \tag{3.12}$$

The scalar parameters α and $\tilde{\beta}$ are obtained by imposing the continuity of tractions from equation [2.25] and tangential components of the electric field $[2.38]_2$ at the interface after the substitution of the constitutive laws $[3.3]_{1,2}$. With both parameters being described by the free energy [3.1] and [3.2], their expressions were presented by Gei et al. (2013) as:

$$\alpha = \frac{\mu^B - \mu^A}{C^A \mu^B + C^B \mu^A} \frac{\boldsymbol{F}^{\text{av}} \mathbf{n}^0 \cdot \boldsymbol{F}^{\text{av}} \mathbf{m}^0}{\boldsymbol{F}^{\text{av}} \mathbf{m}^0 \cdot \boldsymbol{F}^{\text{av}} \mathbf{m}^0}, \tag{3.13}$$

$$\tilde{\beta} = \frac{\epsilon^B - \epsilon^A}{C^B \epsilon^A + C^A \epsilon^B} \frac{(\boldsymbol{F}^{\text{av}})^{-\text{T}} \mathbf{E}^{0\text{av}} \cdot (\boldsymbol{F}^{\text{av}})^{-\text{T}} \mathbf{n}^0}{(\boldsymbol{F}^{\text{av}})^{-\text{T}} \mathbf{n}^0 \cdot (\boldsymbol{F}^{\text{av}})^{-\text{T}} \mathbf{n}^0} + \alpha \mathbf{E}^{0\text{av}} \cdot \mathbf{m}^0. \tag{3.14}$$

Once α and $\tilde{\beta}$ have been determined, the macroscopic total stress and electric field can be determined through equations $[3.9]_{2,3}$. The jump in hydrostatic phase pressures p^A and p^B across each interface is obtained by multiplying the traction continuity condition [2.25] with the vector $(\boldsymbol{F}^{\text{av}})^{-\text{T}} \mathbf{n}^0$, yielding

$$\begin{aligned} p^B - p^A = \Bigg\{ & \left[(\boldsymbol{F}^{\text{av}})^{-\text{T}}\, \mathbf{E}^{0\text{av}} \cdot\, (\boldsymbol{F}^{\text{av}})^{-\text{T}}\, \mathbf{n}^0 \right]^2 \frac{\epsilon^A \epsilon^B (\epsilon^A - \epsilon^B)}{(C^B \epsilon^A + C^A \epsilon^B)^2} \\ & + \mu^B - \mu^A \Bigg\} \frac{1}{(\boldsymbol{F}^{\text{av}})^{-\text{T}}\, \mathbf{n}^0 \cdot\, (\boldsymbol{F}^{\text{av}})^{-\text{T}}\, \mathbf{n}^0}. \end{aligned} \tag{3.15}$$

Spinelli & Lopez-Pamies (2015) recorded simple explicit expressions for the macroscopic electroelastic response and stability of layered composites with any number of ideal dielectric elastic phases under general electromechanical loading conditions. The following set of invariants was expressed:

$$\begin{gathered} I_1 = \boldsymbol{F}^{\mathrm{av}} \cdot \boldsymbol{F}^{\mathrm{av}}, \quad I_2 = (\boldsymbol{F}^{\mathrm{av}})^{-\mathrm{T}} \cdot (\boldsymbol{F}^{\mathrm{av}})^{-\mathrm{T}}, \quad I_4 = \boldsymbol{F}^{\mathrm{av}}\mathbf{n}^0 \cdot \boldsymbol{F}^{\mathrm{av}}\mathbf{n}^0, \\ I_5 = (\boldsymbol{F}^{\mathrm{av}})^{\mathrm{T}}\boldsymbol{F}^{\mathrm{av}}\mathbf{n}^0 \cdot (\boldsymbol{F}^{\mathrm{av}})^{\mathrm{T}}\boldsymbol{F}^{\mathrm{av}}\mathbf{n}^0, \quad J_6 = \mathbf{E}^{0\mathrm{av}} \cdot \mathbf{E}^{\mathrm{av}}, \\ J_7 = (\boldsymbol{F}^{\mathrm{av}})^{-\mathrm{T}}\mathbf{E}^{0\mathrm{av}} \cdot (\boldsymbol{F}^{\mathrm{av}})^{-\mathrm{T}}\mathbf{E}^{0\mathrm{av}}, \\ J_8 = (\boldsymbol{F}^{\mathrm{av}})^{-1}(\boldsymbol{F}^{\mathrm{av}})^{-\mathrm{T}}\mathbf{E}^{0\mathrm{av}} \cdot (\boldsymbol{F}^{\mathrm{av}})^{-1}(\boldsymbol{F}^{\mathrm{av}})^{-\mathrm{T}}\mathbf{E}^{0\mathrm{av}}, \\ J_9 = \mathbf{E}^{0\mathrm{av}} \cdot \mathbf{n}^0, \quad J_{10} = (\boldsymbol{F}^{\mathrm{av}})^{-\mathrm{T}}\mathbf{E}^{0\mathrm{av}} \cdot (\boldsymbol{F}^{\mathrm{av}})^{-\mathrm{T}}\mathbf{n}^0. \end{gathered} \tag{3.16}$$

The effective free energy function is then represented as

$$\begin{aligned} W^{\mathrm{av}}(\boldsymbol{F}^{\mathrm{av}}, \mathbf{E}^{0\mathrm{av}}) = \frac{\mu^{\mathrm{av}}}{2}[I_1 - 3] - \frac{\mu^{\mathrm{av}} - \mu^{\mathrm{Hav}}}{2}\Big[I_4 - \frac{1}{I_2 - I_1 I_4 + I_5}\Big] \\ -\frac{\epsilon^{\mathrm{av}}}{2}J_7 + \frac{(\epsilon^{\mathrm{av}} - \epsilon^{\mathrm{Hav}})J_{10}^2}{2[I_2 - I_1 I_4 + I_5]}, \end{aligned} \tag{3.17}$$

where

$$\mu^{\mathrm{av}} = C_{R1}^A \mu^A + C_{R1}^B \mu^B, \qquad \mu^{\mathrm{Hav}} = \left(\frac{C_{R1}^A}{\mu^A} + \frac{C_{R1}^B}{\mu^B}\right)^{-1}, \tag{3.18}$$

$$\epsilon^{\mathrm{av}} = C_{R1}^A \epsilon^A + C_{R1}^B \epsilon^B, \qquad \epsilon^{\mathrm{Hav}} = \left(\frac{C_{R1}^A}{\epsilon^A} + \frac{C_{R1}^B}{\epsilon^B}\right)^{-1}. \tag{3.19}$$

What equation [3.17] emphasises is that the resulting free energy for rank-1 laminated composites is not of the separable form. In the next section, this theory shall be adapted to a rank-2 composite in order to fully optimize the geometry of rank-2 composites in a manner analogous to rank-1 composites. This will all be carried out for various boundary conditions.

3.3.2 Rank-2 solution

A rank-2 laminate can be created by layering a rank-1 laminate with either a third phase whose material parameters differ from the two materials used to construct the rank-1 laminate, or by using one of the constituent phases already present in the laminate. The latter construction process will be adopted in this study. We shall now laminate a rank-1 laminate with the compliant phase of low dielectric constant, denoted already as material "B" in order to obtain a particulate microstructure of the stiff and high dielectric inclusions surrounded by a compliant and low dielectric matrix as presented in figure 3.2.

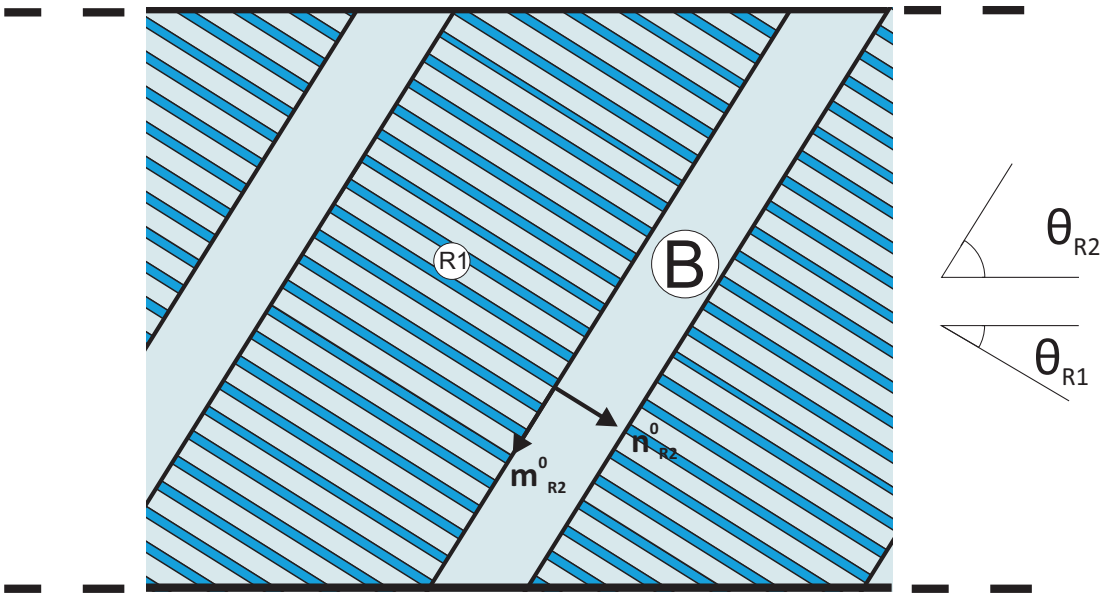

Figure 3.2: Geometry of the reference configuration of a two-phase rank-2 composite consisting of a rank-1 composite laminated with a soft homogeneous phase. θ_{R1} is negative in the figure.

As before, it is assumed that the characteristic size of the layers in the rank-1 laminate, denoted the core, is smaller in comparison with the corresponding size of the layers of the homogeneous soft phase, denoted the matrix. Following this construction process, it is implicitly assumed that the deformation in the rank-2 composite is piecewise constant with a different constant in each of the three different phases. It should be noted that this assumption violates the requirement that $\mathcal{X}(\mathbf{X})$ will be locally continuous at the interface between the inner rank-1 composite and the third phase. However, since we have already established that the characteristic size of the layers of the rank-1 composite is substantially smaller than the corresponding size of the layers of the rank-2 composite, the local fluctuations of the actual fields, whose wavelength is comparable with the thickness of the layers in the rank-1 laminate, will decay a few wavelengths from the interface. These fluctuations are mentioned by DeBotton (2005) to have only a negligible effect on the macroscopic response of the composite.

Following on from the rank-1 lamination process, optimum configurations for C^B_{R1} and θ_{R1}, will be determined through an iterative approach using the Newton-Raphson method, but now the volume fraction of the soft phase and lamination angle in the layered rank-1 laminate present the possibility of the configuration requiring re-optimisation. Figure 3.3 displays this configuration whereby holis-

tically, the configuration is exactly the same as that of the previously discussed rank-1 laminate with a new unit normal and tangent to the interface denoted $\mathbf{n}^0_{\mathrm{R}2}$ and $\mathbf{m}^0_{\mathrm{R}2}$ respectively, aligned with the interface as shown.

The process of determining the free energy of the rank-2 composite is essentially the same process executed for the rank-1 composite, with the inner rank one material treated as a homogenized material, whose subscript shall be denoted "R1". The subsequent free energy will now be prescribed to be "$W^{\mathrm{av}}_{\mathrm{R}2}$ " and arbitrary lamination direction "$\mathbf{n}^0_{\mathrm{R}2}$". According to this schematic, there are two independent microstructural parameters for each composite and thus four independent parameters for the rank-2 composite. Namely, these are the volume fraction of the soft phase in the core (C^B_{R1}), the volume fraction of the core in the composite (C^{R1}) and the lamination angles of the two laminates (θ_{R1}, θ_{R2}).

Specifically, at each stage the core of a rank-1 composite is laminated with an identical homogeneous constituent, the matrix phase. By following this lamination procedure the end result is a particulate composite consisting of an inclusion phase which is embedded in a matrix phase. In terms of the macroscopic energy of the composite, the expression for the energy of a rank-2 composite becomes the following.

$$W^{\mathrm{av}}_{\mathrm{R}2} = W^{\mathrm{R}1} C^{R1} + W^{\mathrm{B}}_{\mathrm{R}2} C^B_{R2}, \qquad [3.20]$$

where, as W^{av} represents the total macroscopic energy of the rank-1 laminate, $W^{\mathrm{av}}_{\mathrm{R}2}$ represents the total macroscopic energy of the rank-2 laminate. The energy of the soft phase is that presented in equation [3.2] while that of phase "R1" is the same as that in equation [3.17]. It is now apparent that the energy of phase "R1" is exactly the same as the total energy of the rank-1 laminate W^{av}. In section 3.3, we have obtained explicit expressions for the nominal macroscopic total stress in terms of the overall deformation gradient $\boldsymbol{F}^{\mathrm{av}}$ and the applied nominal electric field $\mathbf{E}^{0\mathrm{av}}$. For a rank-2 laminate, corresponding Euler-Lagrange equations cannot be solved analytically and thus numerical solutions need to be determined. Here we have introduced new subscripts which should not be muddled with those corresponding to the rank-1 solution. The subscript *always* corresponds to the rank of the laminate being considered.

Due to the electric field, there are mechanically induced stresses corresponding to phases "$\mathrm{A}_{\mathrm{R}1}$" and "$\mathrm{B}_{\mathrm{R}1}$" microscopically which contribute to the overall macroscopic actuation strain on the rank-1 composite. Thus when considering the rank-2 laminate, these microscopic contributions of mechanically induced stress are "R1" and "$\mathrm{B}_{\mathrm{R}2}$"[1] where "$\mathrm{B}_{\mathrm{R}2}$" represents the soft homogeneous phase

[1]Phases $\mathrm{B}_{\mathrm{R}2}$ and $\mathrm{B}_{\mathrm{R}1}$ are of the same material, however for purposes of this section it is useful to distinguish them. For the rest of this study, the soft phase will be specified for the laminate being discussed.

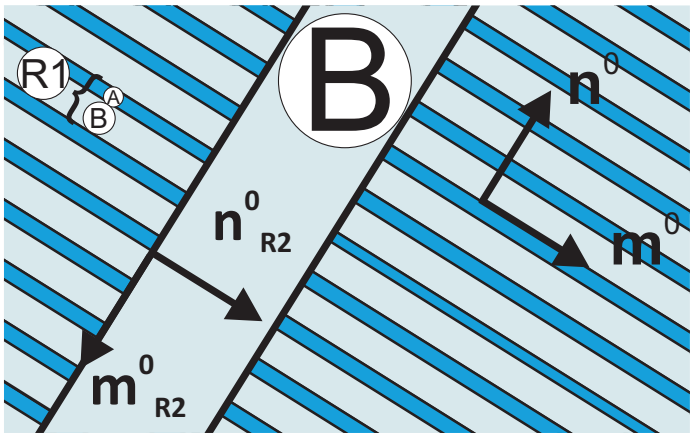

Figure 3.3: Geometry of a rank-2 laminate zoomed in to display unit normals and tangents and volume fractions present at each layer.

layered with the anisotropic rank-1 laminate. This implies that for all intents and purposes and in agreement with the lamination process already established, only phases "A_{R1}", "B_{R1}" and "B_{R2}" exist in the rank-2 composite as displayed in figure 3.3. This maintains the earlier declaration that a rank-1 composite is being laminated with a homogeneous matrix phase. Thus the rank-1 relations to the rank-2 laminate can now be expressed as follows:

$$C^{R1} = C^{A}_{R1} + C^{B}_{R1}, \qquad \boldsymbol{S}^{\mathrm{av}}_{R2} = \boldsymbol{S}^{\mathrm{R1}} C^{R1} + \boldsymbol{S}^{B} C^{B}_{R2}. \tag{3.21}$$

The macroscopic deformation gradient and average electric field in relation to the rank-2 laminate can also be expressed as follows.

$$\boldsymbol{F}^{\mathrm{av}}_{R2} = C^{R1}\boldsymbol{F}^{R1} + C^{B}_{R2}\boldsymbol{F}^{B}, \qquad \mathbf{E}^{0\mathrm{av}}_{R2} = C^{R1}\mathbf{E}^{0R1} + C^{B}_{R2}\mathbf{E}^{0B}. \tag{3.22}$$

with $\boldsymbol{F}^{R1} = C^{A}_{R1}\boldsymbol{F}^{A} + C^{B}_{R1}\boldsymbol{F}^{B}$. From a computational point of view, it should be noted that equation $[3.21_2]$ is significantly simpler than the rank-2 equivalent of equation $[3.3_1]$ since $[3.21_2]$ includes the already defined total first Piola-Kirchhoff stress which need not be computed again. Whereas $[3.3_1]$ depends not only on rank-2 equivalents of $\boldsymbol{F}^{\mathrm{av}}$ and its partial derivative, but also on the phase pressures in all three phases. It should be noted that, despite the clear interface between phases "B" and "R1" in figure 3.2, only two materials compose the rank-2 laminate such that in reality there is no actual interface between B_{R1} and B_{R2}. The remaining rectangular orientation of the stiff phase may also imply infinite stresses at the "corners" of the interfaces therefore these corners can be smoothed as presented by Rudykh et al. (2011).

Determination of the numerical solution for a rank-2 laminate is now possible and was executed using equation [2.25] which defines the traction continuity and

[3.8] for the electric displacement and thus the jump between phases "R1" and "$\mathrm{B_{R2}}$." These jump conditions are combined with the imposition of respective boundary conditions for the specific boundary-value problem e.g. $S_{11} = S_{22} = S_{33} = 0$ as presented in the example in section 2.6.1. These sets of equations can then be solved simultaneously for determination of rank-2 laminate parameters α_{R2}, $\tilde{\beta}_{R2}$, λ and one of the phase pressures, in this case p^{R1}. The corresponding parameters for rank-1 laminates were also solved in a likewise manner in section 3.3.1. The sets of simultaneous equations were solved by iteration using a Newton-Raphson method in MATHEMATICA® commercial software.

3.4 An alternative energy formulation

Lopez-Pamies (2014) also developed an analytical, nonlinear homogenisation framework for determining the overall response of elastomeric composites subject to finite deformations. The strategy executed involved an iterated homogenization procedure that provides an exact solution for energy W^{av} in terms of an auxiliary dilute problem. The second step, similar to that carried out by DeBotton (2005), consisted of the construction of suitable classes of sequential laminates. The alternative definition of the effective free energy function was given by

$$W(\boldsymbol{F}^{\mathrm{av}}, \mathbf{E}^{0\mathrm{av}}) = \min_{\boldsymbol{F}^{\mathrm{av}} \in \mathcal{K}} \max_{\mathbf{E}^{0\mathrm{av}} \in \mathcal{E}} \int_{\partial \mathcal{B}^0} W(\mathbf{X}, \boldsymbol{F}, \mathbf{E}^0) d\mathbf{X}. \qquad [3.23]$$

Where $\mathcal{K}$ and $\mathcal{E}$ denote sufficiently large sets of admissible deformation gradients and electric fields. The problem of computation of Euler-Lagrange solutions was executed by adopting a semi-inverse approach in which the sets $\mathcal{K}$ and $\mathcal{E}$ of admissible deformation gradients and electric fields were restricted to include only certain classes of sub-fields. The maximization and minimization operations in equation [3.23] are over suitably restricted sets $\mathcal{K}$ and $\mathcal{E}$ of deformation gradient tensors $\boldsymbol{F}^{\mathrm{av}}$ and electric fields $\mathbf{E}^{0\mathrm{av}}$, whose precision however shall not be specified in this text.

Lopez-Pamies (2014) applied the same lamination procedure already presented for rank-1 laminates in section 3.2, followed by determination of expressions analogous to equations [3.10] and [3.12]. Considering solely piecewise constant deformation gradients and electric fields, the effective stored-energy function of the rank-1 laminate was expressed in a similar form to that by DeBotton (2005) as

$$W^{\mathrm{av}}(\boldsymbol{F}^{\mathrm{av}}, \mathbf{E}^{\mathrm{av}}) = \min_{\alpha} \max_{\tilde{\beta}} \{C^{\mathrm{A}} W^{\mathrm{A}}(\boldsymbol{F}^{\mathrm{A}}, \mathbf{E}^{0\mathrm{A}}) + C^{\mathrm{B}} W^{\mathrm{B}}(\boldsymbol{F}^{\mathrm{B}}, \mathbf{E}^{0\mathrm{B}})\}. \qquad [3.24]$$

The minimisation condition with respect to α implies mechanical equilibrium (equation [2.25]) whereas the maximisation with respect to $\tilde{\beta}$ implies Gauss' law

(equation [2.36]) across material interfaces. Following the formulation presented, the jump conditions implied are similar to those already presented in equations [2.25], $[2.38]_2$ and [3.6].

The rank-2 formulation follows that already presented, with the same piecewise constant deformation gradients and electric fields. The effective free energy function of the corresponding rank-2 laminate is given by an expression analogous to [3.24], presented as follows:

$$\begin{aligned} W^{\mathrm{av}}_{\mathrm{R2}}(\boldsymbol{F}^{\mathrm{av}},\mathbf{E}^{0\mathrm{av}}) =& \min_{\alpha_{R2}} \max_{\tilde{\beta}_{R2}} \big\{ C^{\mathrm{B}}_{\mathrm{R2}} W^{\mathrm{R1}}(\boldsymbol{F}^{\mathrm{R1}} + C^{\mathrm{R1}} \alpha_{R2} \mathbf{m}^0_{\mathrm{R2}} \otimes \mathbf{n}^0_{\mathrm{R2}}, \mathbf{E}^{0\mathrm{R1}} + C^{\mathrm{R1}} \beta_{R2} \mathbf{n}^0_{\mathrm{R2}}) \\ & + C^{\mathrm{R1}} W^{\mathrm{av}}_{\mathrm{R1}}(\boldsymbol{F}^{\mathrm{R1}} - C^{\mathrm{B}}_{\mathrm{R2}} \alpha_{R2} \mathbf{m}^0_{\mathrm{R2}} \otimes \mathbf{n}^0_{\mathrm{R2}}, \mathbf{E}^{0\mathrm{R1}} - C^{\mathrm{B}}_{\mathrm{R2}} \beta_{R2} \mathbf{n}^0_{\mathrm{R2}}) \big\}. \end{aligned} \tag{3.25}$$

In comparison to the previously formulated rank-2 energy in equation [3.20], equation [3.25] has been restricted to per-layer fields to correspond to the unique exact effective stored-energy function. Thus, when performing computations, equation [3.25] is more convenient as equation [3.20] requires first establishing the rank-1 solution, then supplementing of this solution into the rank-2 problem which then leads to the rank-2 solution. However, both equations [3.20] and [3.25] produce the exact same closed-form solution when applied to rank-1 laminates, and subsequent rank-2 solution. Thus in the microstructure optimisation process, both forms of the energy can be utilised interchangeably. Although, it is emphasised that the theory of [3.25] is entrenched in a derivation whose procedure is mathematically-intensive. Thus it is not the prime driver of the optimisation process used in this study. Checks were also successfully completed to ensure that [3.25] will satisfy all conditions in this study.

3.5 Conclusions

Chapter 4

Boundary value problems in plane strain

4.1 Introduction

This chapter focuses solely on boundary-value problems in a plane strain environment of two types. The first boundary-value problem will refer to plane strain with shear strains considered while the second will relate to plane strain with no shear strains considered. We shall begin with an initial optimisation for each rank laminate to provide a basic framework of the optimisation process. The initial results in finite strain will be compared to those obtained by Tian et al. (2012), which were reported for small strain. An effort shall also be made to compare results of the different plane-strain boundary-value problems, in an attempt to observe the effect of shear strains on rank-1 and rank-2 laminates of this type. This chapter shall round off with exposing the current state of lamination angles and phase electric fields in rank-2 laminates.

In the previous work accomplished by Tian et al. (2012), it was investigated that the electromechanical coupling, rather the macroscopic strain, induced in the composite through the application of a unit electric field, can be amplified by many orders of magnitude by a combination of constituent materials with high contrast and a highly complex and poly-disperse micro-structure. For varying contrasts, whose shear and dielectric moduli were equal, results were obtained for optimum configurations. Beginning from these micro-structure arrangements, the formulations in section 3.2 will be used to optimise the micro-structure of rank-1 and rank-2 laminates in order to determine the maximum achievable longitudinal stretch. The lamination process has already been described in section 3.2, relating to a stiff phase "A" with a high dielectric constant and a compliant phase "B" with a low dielectric constant. These two phases will have material parameters of $\epsilon^A = 100\,\epsilon_0$, $\epsilon^B = 10\,\epsilon_0$, $\mu^A = 100$ MPa and $\mu^B = 10$ MPa such that the

contrast between materials will be given by $\mu^A/\mu^B = \epsilon^A/\epsilon^B = 10$. This contrast will be increased in steps of $\{10^x,\, x = 1, 2..., 4\}$ and results for each contrast presented. Initially, the contrast of 100 and corresponding configuration obtained by Tian et al. (2012) was selected as the template contrast so as to compare results obtained by the same author in small strain with results obtained in this study in finite strain. For any initial optimisation in this study for all boundary-value problems, the contrast of 100 will be the reference for any initial optimisation and then the contrast will be varied to produce the results in the order of contrasts already described.

4.2 Plane strain with in-plane vanishing tractions

4.2.1 Initial optimisation: rank-1 laminates

Consider now a boundary-value problem where the device will deform macroscopically at vanishing tractions, specifically, for the conditions

$$S_{11}^{\text{av}} = 0, \qquad S_{12}^{\text{av}} = 0, \qquad S_{22}^{\text{av}} = 0, \tag{4.1}$$

along the electric activation. Due to the intrinsic macroscopic mechanical anisotropy, the deformation gradient is imposed to be as follows

$$\boldsymbol{F}^{\text{av}} = \begin{bmatrix} \lambda & \xi/\lambda & 0 \\ 0 & 1/\lambda & 0 \\ 0 & 0 & 1 \end{bmatrix}, \tag{4.2}$$

where ξ is the amount of shear related to the shear angle γ in the current configuration i.e. $\tan\gamma = \xi$, λ is the longitudinal stretch and λ_{max} is the maximum longitudinal stretch along an electromechanical equilibrium path. For plane strain, it should be noted that $S_{33}^{\text{av}} \neq 0$ as it is associated with the out of plane stretch constrained due to there being no strain along direction x_3. It was determined, by DeBotton (2005) and Tian et al. (2012), that for rank-1 laminates the actuation strain δl[1] mainly depends on the relative angle between the direction of the applied nominal electric field and the interface i.e. θ_{R1}, but only a little on the volume fraction of the phases (C_{R1}^A, C_{R1}^B). Due to the combination of the two phases, the rank-1 laminate is highly anisotropic such that the actuation strain in some directions is larger than when compared to the homogeneous strain. Thus this optimisation process will also aim to confirm these observations.

[1] where $\delta l = \lambda - 1$ e.g. when $\lambda = 1.03$ then $\delta l = 3\%$.

The results for rank-1 laminates at a contrast of 100 and applied nominal electric field of 100 MV/m are presented on table 4.1 and figure 4.1. The interpretation of these configurations is as follows: HS_mS refers to the stretch due to a homogeneous material in small strain obtained by Tian et al. (2012) while HL_gS refers to the stretch due to a homogeneous soft material obtained in this study in large strain. The curve TS_mS in figure 4.1 refers to the result obtained by Tian et al. (2012) for a rank-1 laminate while TL_gS refers to the performance of the geometry found by Tian et al. (2012), this time taking into account non-linear effects in large strain. Finally, $R1L_gS$ corresponds to the optimised configuration for λ_{max} for a rank-1 laminate obtained in this study. It is evident that there is an improvement in λ_{max} for a rank-1 laminate from the soft material such that the actuation is homogeneous, similar to the improvement obtained by Tian et al. (2012). Specifically, the longitudinal stretch[2] has improved by 12% from homogeneous, similar to the improvement obtained by Tian et al. (2012). As presented on table 4.1, a homogeneous strain ($\lambda_{max} - 1$) of 2.21% was obtained by Tian et al. (2012) in small strain in response to a nominal electric field of 100 MV/m whereas in finite strain a homogeneous strain of 2.34% was obtained presenting an improvement of 6%. The two sets of results for a soft material such that the actuation is homogeneous provide the foundation of significant enhancement of longitudinal strain to be obtained once the new optimal θ_{R1} and C^B_{R1} configurations have been obtained.

Case	λ_{max}	ξ	C^B_{R1}	$\theta_{R1}[^\circ]$
HS_mS	1.022100		1	
HL_gS	1.023440		1	
TS_mS	1.024800	not known	0.5	61.2
TL_gS	1.026213	-0.00926	0.5	61.2
$R1L_gS$	1.026214	-0.00949	0.5	60.9

Table 4.1: Rank-1 laminate longitudinal stretch, amount of shear and microstructure configurations. HS_mS and HL_gS refer to the stretches due to homogeneous materials in small strain obtained by Tian et al. (2012) and in finite strain obtained in this study, respectively. Curve TS_mS refers to the result obtained by Tian et al. (2012) while TL_gS refers to the performance of the geometry of TS_mS, this time taking account non-linear effects. $R1L_gS$ is the rank-1 optimum configuration in finite strain.

[2]The difference between λ and λ_{max} is recalled here. λ refers to any point along the curves for a corresponding applied nominal electric field, whereas λ_{max} refers to the maximum longitudinal stretch obtained when the laminate is optimised at a *specific* target electric field. The same differentiation will be applied to the amount of shear ξ and ξ_{max}.

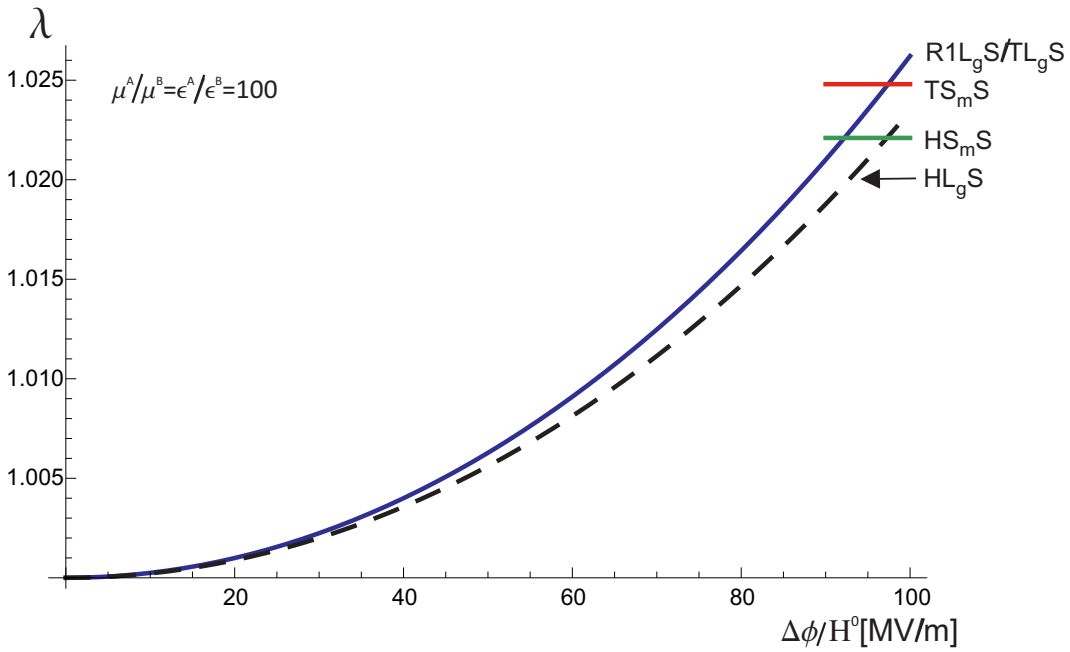

Figure 4.1: Longitudinal stretch obtained due increasing applied nominal electric field for rank-1 laminates and a soft material such that the actuation is homogeneous relating to table 4.1. Curves for $R1L_gS$ and TL_gS are found to be near identical and thus are superimposed and homogeneous curve for large strain is black dotted/HL_gS. Straight lines refer to small strain results obtained by Tian et al. (2012) for a soft material such that the actuation is homogeneous (Green line/HS_mS) and Rank-1 laminate (Red line/TS_mS). Configurations are presented on table 4.1.

4.2.2 Influence of increasing contrast on rank-1 laminates

The optimum configurations at increasing contrast and corresponding λ_{max} for rank-1 laminates are presented on table 4.2. When these configurations at different contrasts are compared, the values of θ_{R1} and C^B_{R1} corresponding to λ_{max} are exactly the same. This is also confirmed by investigating optimum laminate configurations at increasing contrasts and this is reflected in figure 4.2(b) showing the influence of varying θ_{R1} at a constant applied nominal electric field of 100 MV/m. The effect of increasing contrasts is minimum in this boundary-value problem as displayed in figure 4.2(a) which displays that as the applied nominal electric field is increased for a set configuration there is little difference in λ_{max} at increasing contrasts. This implies that for rank-1 laminates with shear strain considered there is no great benefit in varying the contrast when the ratios of shear to dielectric moduli are equal.

The absolute values of phase electric fields have also been presented on table 4.2 and it is noticeable that with increasing contrast the absolute value of electric field in phase "A" is almost constant and much lower in comparison to that for

Curve	$\mu^A/\mu^B = \epsilon^A/\epsilon^B$	λ_{max}	ξ	E^A_{R1} [MV/m]	E^B_{R1} [MV/m]	C^B_{R1}	$\theta_{R1}[^\circ]$
Yellow	10	1.025373	-0.00663	89.2	128.8	0.5	60.9
Red	100	1.026313	-0.00949	88.9	134.9	0.5	60.9
Green	1000	1.026316	-0.00984	88.9	135.6	0.5	60.9
Blue	10 000	1.026326	-0.00987	88.9	135.7	0.5	60.9

Table 4.2: (a) Rank-1 laminate microstructure configurations and corresponding longitudinal stretch and phase electric fields for contrasts of $\{10^x,\, x = 1, 2..., 4\}$ corresponding to figure 4.2(a) for a boundary-value problem of plane strain with in-plane vanishing tractions.

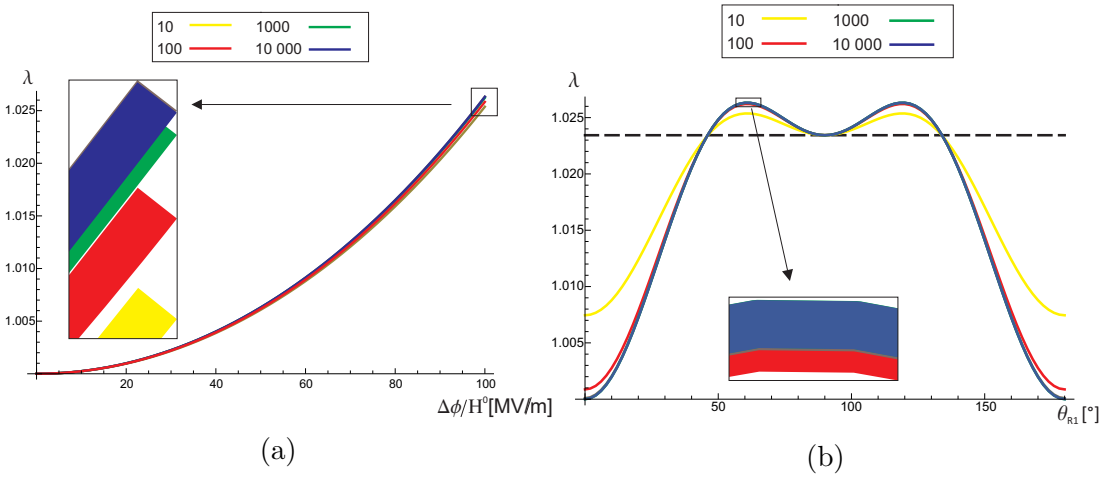

Figure 4.2: (a) Resulting longitudinal stretch when varying applied nominal electric field up to 100 MV/m at optimum configurations reflected on table 4.2 and (b) influence of varying lamination angle at increasing contrasts of $\{10^x,\, x = 1, 2..., 4\}$ for the range $0^\circ \leq \theta_{R1} \leq 180^\circ$ at an applied nominal electric field of 100 MV/m with maximum values of λ corresponding to those on table 4.2.

phase "B." What this implies is that the deformation experienced is greater in the soft phase and is a result of the greater ability of the soft phase to deform, while the stiffer phase does not contribute greatly to the overall laminate deformation. From a contrast of 10 to that of 100, the phase electric field of the soft phase has increased but does not increase greatly at higher contrasts after that. Thus at higher contrasts and in single phases the electric fields remain almost constant, which can be attributed to the similar amounts stiff and soft phase in each of the rank-1 laminates. These equal amounts of stiff to soft phase, along with the lack of change of optimum lamination angle with increasing contrast, also enforces the aforementioned fact that the soft phase is dominant in the deformation of rank-1 laminates as all other parameters are unchanging.

At a contrast of 100, the effect of the configuration on the amount of shear for a rank-1 laminate is presented in figures 4.3(a) and 4.3(b). With regards to volume fraction, it is interesting that the influence of volume fraction is less pronounced at $C^B_{R1} \geq 0.9$ and $C^A_{R1} \leq 0.1$ as compared to $C^B_{R1} = 0.7$ or $C^A_{R1} = 0.3$

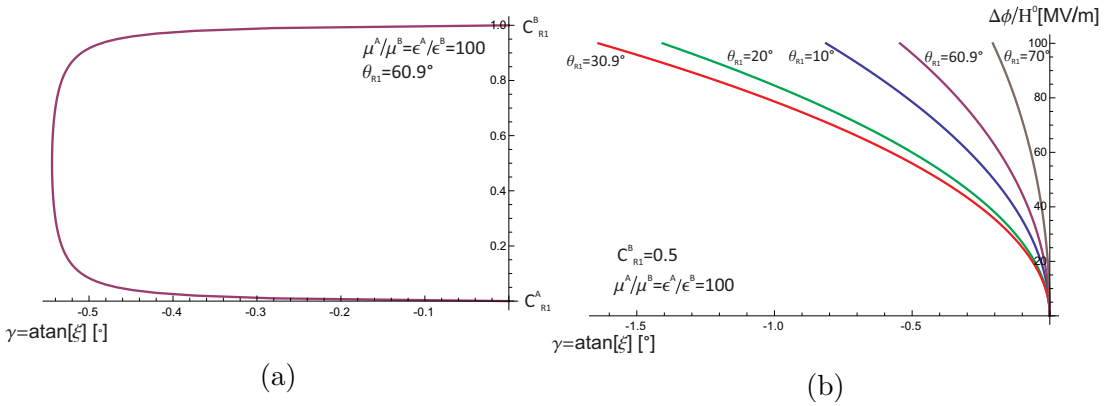

Figure 4.3: (a) Influence of increasing volume fraction on the shear angle of a rank-1 laminate at a contrast of 100 and lamination angle of 60.9° and (b) resulting shear angle and various values for θ_{R1} with increasing applied nominal electric field.

in figure 4.3(a). Compare this behaviour with statements made earlier relating to phase electric fields on table 4.2. This confirms that the phase electric fields reflected are due to the inherent nature of the phases i.e. stiff and more dielectric or soft and less dielectric as the effect of volume fraction is the same at either extreme of stiff or soft phase. If the lamination angle is unchanging, it is evident that both greater stretch and shear are experienced when the volume fraction is 0.5. At $C^B_{R1} = 0.5$, this configuration is one of the many presented in figure 4.3(b) and what is unique here is that the lamination angle corresponding with λ_{max} is not the same as the lamination angle corresponding to the greatest amount of shear (ξ_{max}) experienced at an applied nominal electric field of 100 MV/m. For example, the curve relating to $\theta_{R1} = 70°$ does not give a great amount of shear relative to $\theta_{R1} = 20°$, due to a stiffening effect that the material seems to undergo as it evolves through various lamination angles. This is revealed by comparing figures 4.2(b) and 4.3(b) where the gradient at $\theta_{R1} = 20°$ in figure 4.2(b) is greater than at $\theta_{R1} = 70°$. This implies θ_{R1} influences both λ and ξ concurrently. The non-linear nature of finite strain is observed through the fact that at $\theta_{R1} = 30.9°$ the maximum shear angle is experienced and then decreases after that at points such as $\theta_{R1} = 20°$. The value of applied nominal electric field should not be taken for granted here as Gei et al. (2013) presents similar results to figure 4.3(b) for much greater voltages. Therefore within the limit of applied nominal electric field presented of 100 MV/m, one can establish either a lamination angle corresponding to λ_{max}, which is not the same as θ_{R1} that provides maximum shear.

The results obtained now enable one to pose the following question: if optimisation for λ_{max} is possible, what of a configuration in which the laminate is optimised for shear? If the rank-1 laminates are optimised for maximum amount

of shear or ξ_{max}, new configurations now given by table 4.3 are established. Therefore for a boundary-value problem of plane strain with in-plane vanishing tractions, it is possible to optimise rank-1 laminates for either maximum γ[3], or λ_{max}. Most of the phenomena exactly experienced relating to volume fraction and lamination angle with increasing contrast are observed in these curves as well, with minimum improvement in amount of shear at higher order contrasts.

It should be noted that the amount of shear experienced as shown on table 4.3 is very small. However, even if the numerical value of amount of shear is small, this does not mean that the contributory effect of shear itself to the overall longitudinal stretch is also small. A new optimum lamination angle has been obtained when the laminates are optimised for configurations which provide the maximum amount of shear. The lamination angle θ_{R1} has changed significantly from 60.9° to 30.9° for most contrasts. Shear strains have therefore effectively driven this lamination angle evolution, despite their perceived low values. Figure 4.4(b) shows how shear angle changes with varying volume fraction and what is emphasised here is that C^B_{R1} represents a point of symmetry in which the exact same curves are obtained at the same values of C^A_{R1} similar to figure 4.3(a). There is a stiffening of the laminate which is more pronounced at specific volume fractions as the contrast increases, with the curve for a contrast of 10 000 showing near straight line behaviour at the maximum shear angle as the volume fraction of the soft phase approaches 1, implying a soft material such that the actuation is homogeneous. It should also be noted that the amounts of phase electric fields experienced for ξ_{max} optimisation on table 4.3 are similar to those presented on table 4.2.

Curve	μ^A/μ^B	ξ_{max}	λ	C^B_{R1}	$\theta_{R1}[^\circ]$
Yellow	10	-0.02013	1.01744	0.5	30.8
Red	100	-0.02861	1.01505	0.5	30.9
Green	1000	-0.02963	1.01477	0.5	30.9
Blue	10 000	-0.02973	1.01474	0.5	30.9

Table 4.3: Rank-1 laminate configurations and corresponding maximum amount of shear for contrasts of $\{10^x,\ x = 1, 2..., 4\}$ corresponding to figure 4.4 for a boundary-value problem of plane strain with vanishing tractions.

4.2.3 Initial optimisation: rank-2 laminates

It is useful to continue this optimisation process by first comparing figures 3.1 and 3.2. It has already been established that symmetrical behaviour of longitudi-

[3]where shear angle $\gamma = \text{atan}[\xi]$ as presented in figure 4.9(c)

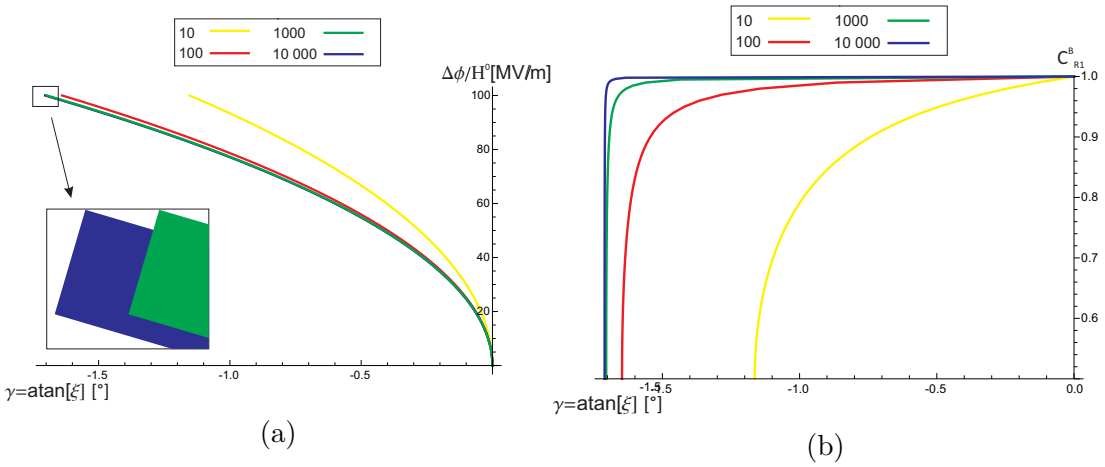

Figure 4.4: (a) Shear angle presented as a result of increasing applied nominal electric field for increasing contrasts presented on table 4.3 for rank-1 laminates (b) shear angle presented as a result of increasing volume fraction of the soft phase for increasing contrasts presented on table 4.3 for rank-1 laminates.

nal stretch is present at various lamination angles for a rank-1 laminate and thus for rank-2 laminates, one can deduce that the more complicated microstructure would create barriers to this symmetrical behaviour. Therefore for rank-2 laminates, the microstructure is now more complex and it should be expected that the various contrasts will present profound differences to each other.

Recalling the formulation for rank-2 laminates, when the specimen is subjected to plane-strain loading conditions, the out of plane stress component has to be taken into consideration. Each single phase is treated as an incompressible neo-Hookean dielectric material with energy as in equation [2.40] and [3.20]. As we have already established, an optimum configuration is expected for a set volume fraction and lamination angle. The method of solution of rank-2 laminates has already been presented in section 3.3.2.

Optimum configurations for rank-2 laminates are shown in figure 4.5. The interpretation of these curves is as follows: for the same contrast of 100, different optimum configurations were found to be present at different applied nominal electric fields, given in table 4.4. At an applied nominal electric field of 100 MV/m, the configuration for λ_{max} for a rank-2 laminate is the one presented with configuration on table 4.4 as $\mathrm{R2L_gS}$. The nominal electric field was then reduced to 50 MV/m and the corresponding configuration for λ_{max} determined, presented as $\mathrm{R2L_gS50}$. $\mathrm{R2TS_mS}$ is the configuration determined by Tian et al. (2012) in small strain while $\mathrm{R2TL_gS}$ is the same configuration in large strain. It is evident that at $\Delta\phi/H^0 = 50$ MV/m, the corresponding configuration for λ_{max} is different to the one when the configuration is determined at an applied

nominal electric field of 100 MV/m. At $\Delta\phi/H^0$ =50 MV/m in figure 4.5, the curve R2L$_g$S50 presents a value of λ_{max} greater than that of λ for R2L$_g$S at this point. The same phenomena would be obtained for configurations optimised for any other nominal electric fields up to 100 MV/m. This confirms the presence of an optimum configuration that provides λ_{max} at a set applied nominal electric field. The curve R2TL$_g$S presents an improved value for λ_{max} to R2TS$_m$S of 12% while R2L$_g$S presents an improvement of 5% from R2TL$_g$S. Using the new laminate configuration obtained (R2L$_g$S), an improvement in strain of 78% from R1L$_g$S was obtained, while R2L$_g$S presents a 20% improvement from R2TS$_m$S and confirming the approach of this study.

Case	λ	ξ	C^B_{R1}	$\theta_{R1}[^\circ]$	C^{R1}	$\theta_{R2}[^\circ]$
R2TS$_m$S	1.10299	not known	0.531	60.3	0.964	14.6
R2TL$_g$S	1.11795	0.07241	0.531	60.3	0.964	14.6
R2L$_g$S50	1.12033	0.08228	0.507	61.4	0.963	15.0
R2L$_g$S	1.12405	0.11811	0.508	65.1	0.963	12.3

Table 4.4: Rank-2 laminate configurations obtained for a contrast of 100 and applied nominal electric field of 100 MV/m and in small strain (R2TS$_m$S) by Tian et al. (2012), the same configuration in large strain (R2TL$_g$S), optimum configuration for λ in large strain at an applied nominal electric field of 50 MV/m (R2L$_g$S50) and optimum configuration for λ in large strain at a nominal electric field of 100 MV/m (R2L$_g$S). Corresponding curves are presented in figure 4.5.

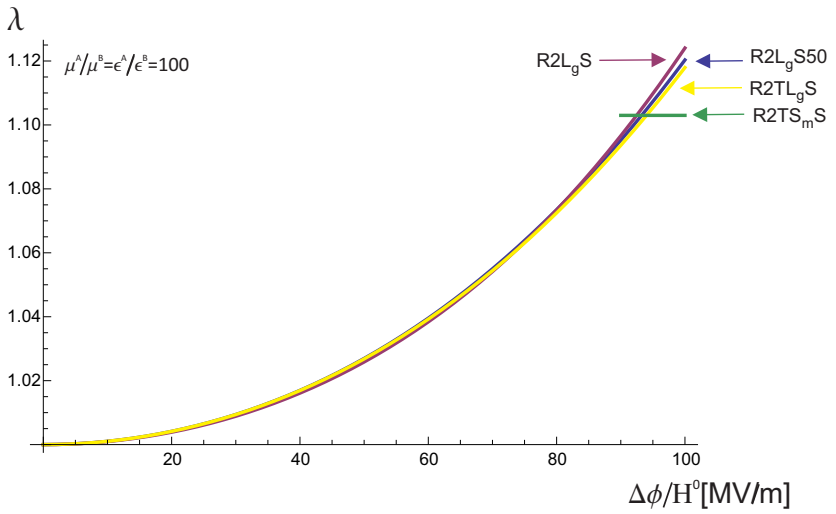

Figure 4.5: Rank-2 laminate influence of increasing applied nominal electric field on longitudinal stretch obtained for a contrast of 100 and applied nominal electric field of 100 MV/m in small strain ($R2TS_mS$) by Tian et al. (2012), the same configuration in large strain ($R2TL_gS$), optimum configuration in large strain at an applied nominal electric field of 50 MV/m ($R2L_gS50$) and optimum configuration in large strain at a nominal electric field of 100 MV/m ($R2L_gS$). Corresponding configurations are presented on table 4.4.

4.2.4 Influence of increasing contrast on rank-2 laminates

Table 4.5 presents results obtained by Tian et al. (2012) in small strain while table 4.6 shows the results obtained for contrasts up to 10 000 for λ_{max} and maximal strain δl. At the lowest contrast of 10, the effect of electric field was found to be less pronounced such that the improvement in the rank-2 laminate from the rank-1 is very small. This brings to suggestion the theory that for a material that is at very low contrasts at which the dielectric and shear moduli are equal, there is little benefit in using a rank-2 laminate as opposed to a rank-1 laminate for actuation purposes. A substantial increase in λ_{max} from the homogeneous value has been obtained at contrasts of 1000 and higher. It is evident that results obtained from contrasts of 100 upwards reflect a remarkable improvement in maximum longitudinal stretch attainable in large strain.

At the point of interest which is 100 MV/m, the statement that λ_{max} increases with increasing contrast for a rank-1 laminate also applies to rank-2 laminates, as well as applying in both small strain according to Tian et al. (2012), and large strain in this study. The amount of strain however is considerably high at a contrast of 10 000 which may imply a difficult configuration to configure, as we shall observe when the laminates are optimised for ξ_{max}. Table 4.6 shows that the amount of shear is increasing in magnitude with increasing contrast. Comparing tables 4.5 and 4.6, the configurations obtained in both studies for contrasts of

Line	$\mu^A/\mu^B = \epsilon^A/\epsilon^B$	λ_{max}	$\delta l/\delta l_{Hom}$	C^B_{R1}	$\theta_{R1}[^\circ]$	C^{R1}	$\theta_{R2}[^\circ]$
Black	10	1.02542	1.15	0.569	61.9	0.819	21.4
Red	100	1.10298	4.66	0.531	60.3	0.964	14.6
Green	1000	1.82720	37.43	0.584	63.1	0.992	27.5
Blue	10 000	5.98488	225.56	0.690	62.8	0.997	42.3

Table 4.5: Rank-2 laminate configurations at contrasts of $\{10^x,\ x = 1, 2..., 4\}$ at maximum longitudinal stretch and longitudinal strain obtained for a contrast of 100 and applied nominal electric field of 100 MV/m by Tian et al. (2012) i.e. R2TS$_m$S. Values were initially presented as maximal strain and have been converted in terms of stretch in this table. Points have also been represented as straight lines in figure 4.6.

Curve	$\mu^A/\mu^B = \epsilon^A/\epsilon^B$	λ_{max}	$\delta l/\delta l_{Hom}$	ξ	%gain	C^B_{R1}	$\theta_{R1}[^\circ]$	C^{R1}	$\theta_{R2}[^\circ]$
Yellow	10	1.02705	1.15	0.00134	6	0.563	62.1	0.831	20.1
Red	100	1.12405	5.29	0.11811	16	0.508	65.1	0.963	12.3
Green	1000	2.47891	63.10	0.24845	26	0.498	70	0.990	-20.0
Blue	10 000	7.22270	265.47	-7.91313	17	0.518	88.0	0.988	-51.0

Table 4.6: Rank-2 laminate configurations (R2L$_g$S) and amount of shear at contrasts of $\{10^x,\ x = 1, 2..., 4\}$ at maximum longitudinal stretch, Longitudinal strain and percentage gain in λ_{max} are presented in comparison to Tian et al. (2012) in small strain (R2TS$_m$S). Corresponding curves are presented in figure 4.6.

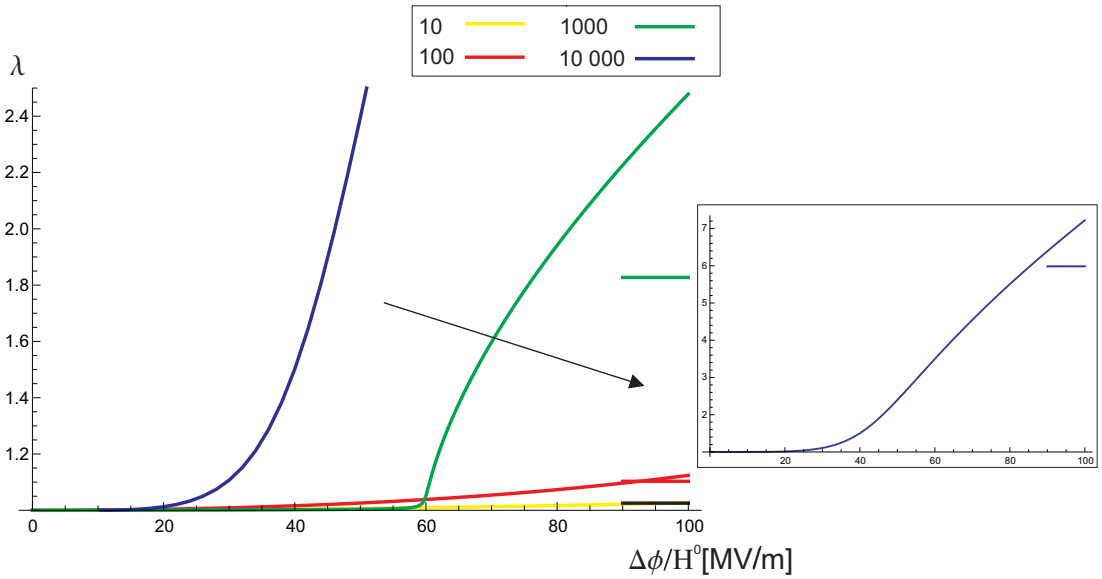

Figure 4.6: Influence of applied nominal electric field on longitudinal stretch for rank-2 laminates at contrasts of $\{10^x,\ x = 1, 2..., 4\}$ for the range $1 \leq \lambda \leq 2.5$ in large strain with horizontal lines representing values obtained by Tian et al. (2012) in small strain (R2TS$_m$S). Sub-image displays the full curve and corresponding line at a contrast of 10 000. Laminate configurations are presented on table 4.6.

10 and 100 show great similarity. However as the contrast is increased to 1000

and 10 000, the non-linear effects in this study present a greater effect on the optimum configuration.

As already established for rank-1 laminates, laminate optimisation in terms of ξ_{max} can also be performed for rank-2 laminates and this optimisation provides crucial insight into the effective influence of microstructural interactions of rank-2 laminates. Figure 4.7 displays the applied nominal electric field influence on shear angle and we observe that different configurations are obtained due to an optimisation for maximum shear angle. At contrasts of 10 and 100 we observe a positive overall maximum shear angle on table 4.7, implying the material is shearing in a counter-clockwise direction and then at all higher contrasts ξ_{max} is negative implying a clockwise shearing.

Curve	$\mu^A/\mu^B = \epsilon^A/\epsilon^B$	ξ_{max}	λ	$\delta l/\delta l_{Hom}$	C^B_{R1}	$\theta_{R1}[^\circ]$	C^{R1}	$\theta_{R2}[^\circ]$
Yellow	10	0.01176	1.02334	0.99	0.563	87.3	0.810	33.3
Red	100	0.26417	1.06172	2.63	0.505	90.0	0.967	31.1
Green	1000	-0.95326	1.92680	39.54	0.502	47.0	0.994	-44.0
Blue	10 000	-20.9042	7.01465	256.60	0.529	58.8	0.980	-90.0

Table 4.7: Rank-2 laminate configurations at contrasts of $\{10^x,\ x = 1, 2..., 4\}$ when laminates were optimized for maximum amount of shear. Corresponding curves within the range -40° $\leq \gamma \leq$ 20° are presented in figure 4.7.

Let us try and envision the interaction between shear angle and both lamination angles for a moment: If we consider contrasts of 10 and 100, there are positive shear angles at λ_{max} as well as positive inclinations of θ_{R1} and θ_{R2}. At a contrast of 1000, θ_{R1} is positive with θ_{R2} negative and the corresponding γ of approximately -44° as displayed in figure 4.7. An increase in contrast from 100 to 1000 has resulted in a change of shear inclination of the rank-2 laminate. At a contrast of 1000, the laminate starts with almost no shear i.e. shear values that are very small and negative, then as the amount of applied nominal electric field increases at $\Delta\phi/H^0$ =60MV/m, a distinctly negative inclination presents itself.

One important point to highlight is that that the optimisation process can present amounts of shear of either positive or negative value. Thus the definition of ξ_{max} in this study refers in actual fact to $|\xi_{max}|$ such that the largest amount of shear is the parameter in consideration. Figure 4.7 only displays the shear curves up to -40° in an effort to try and minimise the shear angles experienced. The reason for this being that shear angles that are too great imply relatively high shear forces at the interfaces between phases, in such a manner as to possibly trigger failure within the composite. In the context of material design, high shear forces would therefore be unfavourable. This was particularly experienced for the configuration that presents maximum shear at a contrast of 10 000. It can then

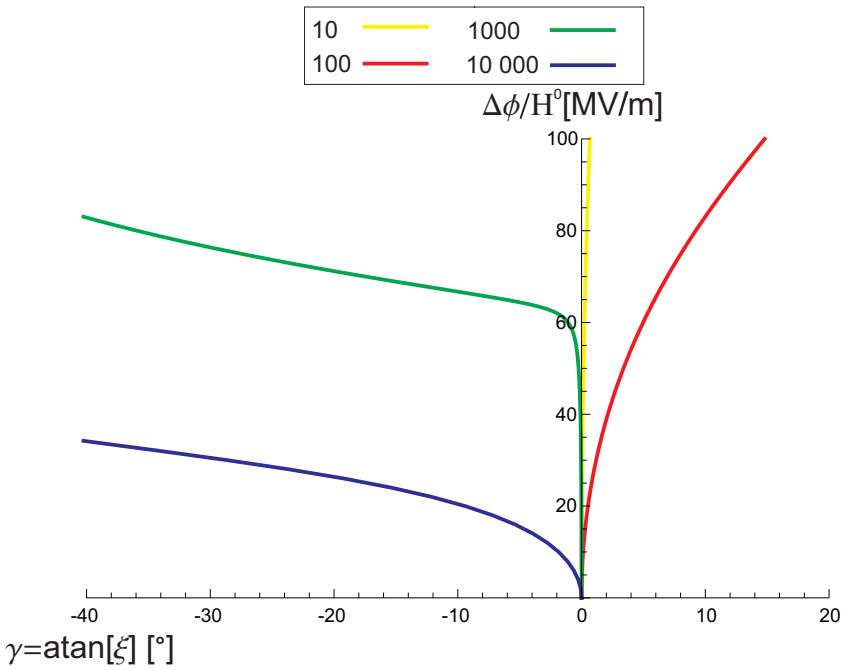

Figure 4.7: Influence of increasing applied nominal electric field on shear angle at contrasts of $\{10^x,\ x = 1, 2..., 4\}$ for rank-2 laminates limited to the range -40° $\leq \gamma \leq$ 20°. Corresponding configurations for optimisation for absolute ξ_{max} beyond this range are presented on table 4.7.

be argued that an optimum configuration for a low fixed shear angle can be determined to try and keep shear angles at a minimum. Also at a contrast of 10 000, it is evident that even at low applied nominal electric fields below 40 MV/m, the shear angle is already unsuitably high, implying that as contrast is increased, it is imperative to strive for lower shear angles for laminate programming purposes.

Figure 4.8 shows the influence of the two main volume fractions on the shear angle at a contrast of 100. What is emphasised here is that the volume fraction of the core in the laminate provides maximum shear effects at $0.9 \leq C^{R1} \leq 1$ while the volume fraction of the soft phase in the core maintains most effective behaviour for shear angle at $C^B_{R1} \approx 0.5$, similar to the rank-1 behaviour presented earlier in figure 4.4(b) and rank-2 behaviour on table 4.7. The stiff phase in the core is required to establish a contrast in the laminate for electromechanical behaviour. When considering the rank-1 anisotropic phase embedded in the rank-2 laminate, it should be acknowledged that the stiff phase makes up nearly half of this phase thus reinforcing the requirement that the stiff phase plays just as crucial a role in laminate performance as the soft phase.

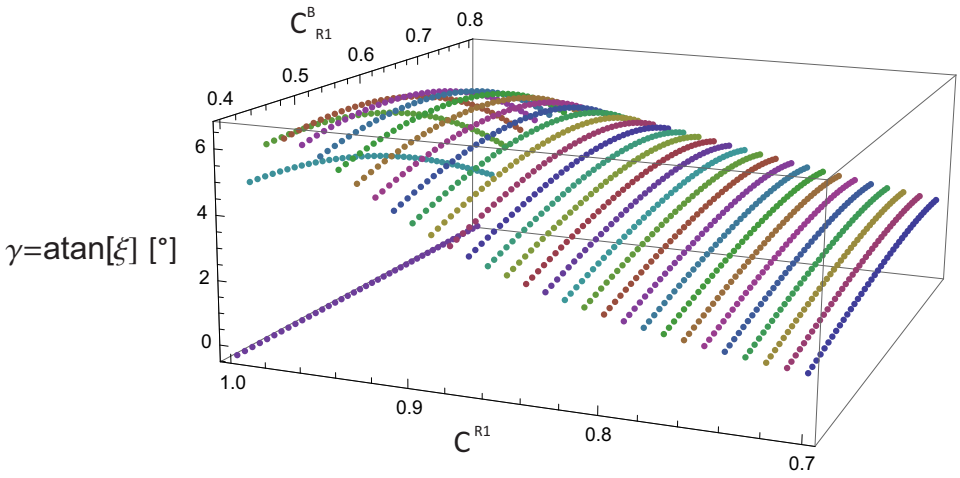

Figure 4.8: Microstructure interaction of C^{R1} and C^{B}_{R1} with shear angle. Each point corresponds to a unique value for shear angle. $\mu^A/\mu^B = \epsilon^A/\epsilon^B = 100$, $\theta_{R1} = 64.9°$, $\theta_{R2} = 11.2°$.

4.3 Plane strain without shear strain consideration

4.3.1 Influence of increasing contrast on rank-1 laminates

Let us maintain the Cartesian coordinate system already introduced and consider a deformation such that the actuation will deform the specimen macroscopically in such a manner as to obtain principal strain directions corresponding to x_1 and x_2 such that the admissible deformation gradient becomes the following

$$\boldsymbol{F}^{\text{av}} = \begin{bmatrix} \lambda & 0 & 0 \\ 0 & 1/\lambda & 0 \\ 0 & 0 & 1 \end{bmatrix}. \qquad [4.3]$$

For this boundary-value problem, the influence of increasing contrast on λ_{max} is more enhanced as presented on table 4.8 and figure 4.10(a). Comparing each of the curves presented in figure 4.10(a), it is evident that an increase in contrast leads to an amplification in the longitudinal stretch of rank-1 laminates greater than in figure 4.2(a). This is attributed to the increase in contrast providing a more enhanced electromechanical interaction within the material. It is evident on table 4.8 that lamination angle provides a profound influence on longitudinal stretch at all contrasts. An addition of stiff phase to the homogeneous material increases λ_{max}, and then at increasing contrasts, for equal amounts of the soft and stiff phases, the lamination angle changes only slightly but this slight change in θ_{R1} is evidently contributing to a profound increase in λ_{max}.

Having established that there is a strong influence of lamination angle on a rank-1 laminate, figure 4.10(b) displays the evolution of λ for $0 \leq \theta_{R1} \leq \pi$ for

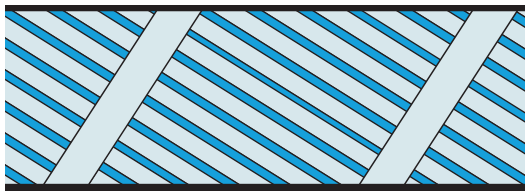

(a) Undeformed configuration

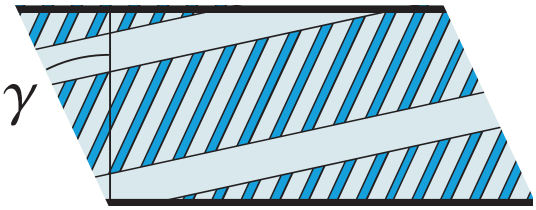

(b) $R2L_gS$ configuration

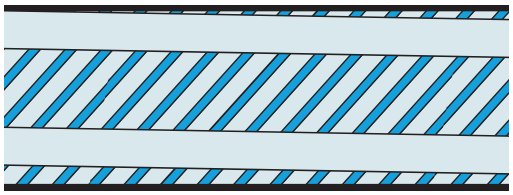

(c) C_2 configuration

Figure 4.9: Geometry of rank-2 laminates at various configurations at a contrast of 100: (a) Undeformed configuration, (b) Optimum configuration discussed in section 4.2.3 on table 4.4 and (c) Optimum configuration discussed in section 4.3.4 on table 4.13. Phases embedded in the laminates are not drawn to scale.

various contrasts. It is evident there is symmetry of the curves at all contrasts at $\pi/2$ as already presented for the previous boundary value problem in figure 4.2(b). This phenomenon can also be used to predict that a similar symmetry would be present at $\theta_{R1} = \pi$ as well as $\theta_{R1} = \frac{3}{4}\pi$. The symmetrical behaviour at opposing lamination angles reflects the fact that rank-1 laminates are piecewise constant. What is also of note is the fact that λ approaches values below 1 at certain angles in this particular boundary-value problem, implying a shrinking in the material at certain configurations. This behaviour may imply a tunable laminate however will not be explored in this study as the supreme focus is on optimisation for positive longitudinal stretch. Considering the volume fraction of all laminates in figure 4.10(a), the weighting of C^A_{R1} and C^B_{R1} in all laminates is equal, similar to tables 4.2 and 4.3.

Curve	$\mu^A/\mu^B = \epsilon^A/\epsilon^B$	λ_{max}	C^B_{R1}	$\theta_{R1}[^\circ]$
Yellow	10	1.02768	0.5	57.0
Red	100	1.04505	0.5	52.1
Green	1000	1.07906	0.5	51.0
Blue	10 000	1.10509	0.5	51.3

Table 4.8: Rank-1 laminate configurations and maximum longitudinal stretch at contrasts of $\{10^x,\, x = 1, 2..., 4\}$. Corresponding curves are presented in figures 4.10(a) and 4.10(b).

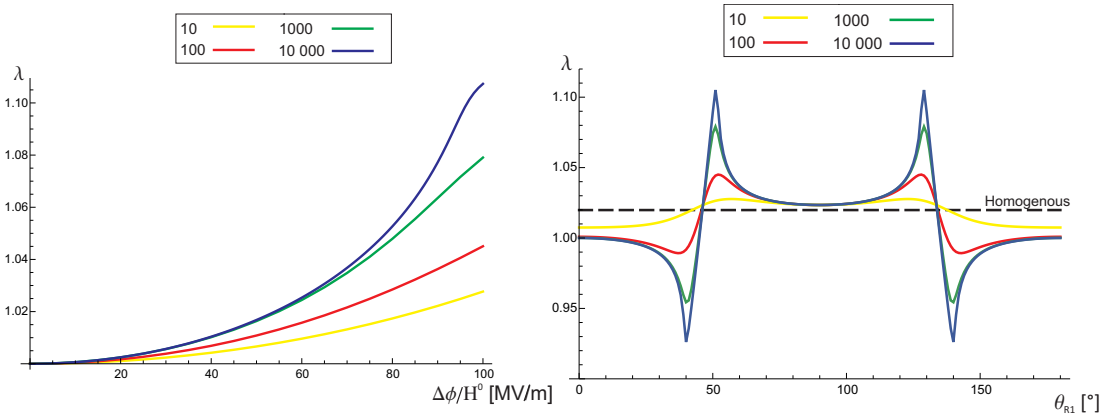

Figure 4.10: (a) Influence of applied nominal electric field on maximum longitudinal stretch at contrasts of $\{10^x,\, x = 1, 2..., 4\}$ presented on table 4.8 for rank-1 laminates and (b) lamination angle evolution for rank-1 laminates and corresponding longitudinal stretch at contrasts of $\{10^x,\, x = 1, 2..., 4\}$ and constant applied nominal electric field of 100 MV/m for $0^\circ \leq \theta_{R1} \leq 180^\circ$ presented on table 4.8.

A note on micro-structure sensitivity for rank-1 laminates

Let us consider the statement earlier introduced in section 4.2.1, that λ depends on the relative angle between the direction of the applied nominal electric field and θ_{R1} but only a little on the volume fraction of the phases when shear strains are considered. This statement shall now be confirmed for validity also when shear strains are not considered. Figure 4.11 displays numerous configurations obtained when volume fraction and lamination angle are simultaneously optimised within prescribed limits at a contrast of 100 at an applied nominal electric field of 100 MV/m. The optimum lamination angle for a rank-1 laminate at a contrast of 100 when shear strains are not considered has already been determined to be 52.1° on table 4.8 which also lies in figure 4.11. Let us for example, consider the point labelled 'v'. From this point, if the volume fraction of $C^B_{R1} = 0.6$ is maintained as constant and lamination angle increased, the corresponding curve of λ (blue dots) has a set of completely different values as compared to the curve starting at 'v' at constant $\theta_{R1} = 54°$ with decreasing volume fraction (top to bottom). If the change in lamination angle with changing volume fraction is observed as presented in figure 4.11 it is evident that for range of $0.4 \leq C^B_{R1} \leq 0.6$, which represents 20% of the possible range of volume fraction, there is only a change in λ of approximately 0.03. Whereas for the range $50° \leq \theta_{R1} \leq 54°$, which represents approximately 4% of the possible range of angles taking into account symmetry, there is a change of 0.09 which confirms the aforementioned prediction that θ_{R1} presents a greater influence on λ. Once again the non-linear phenomenon present at finite strain is evident from the numerous configurations possible.

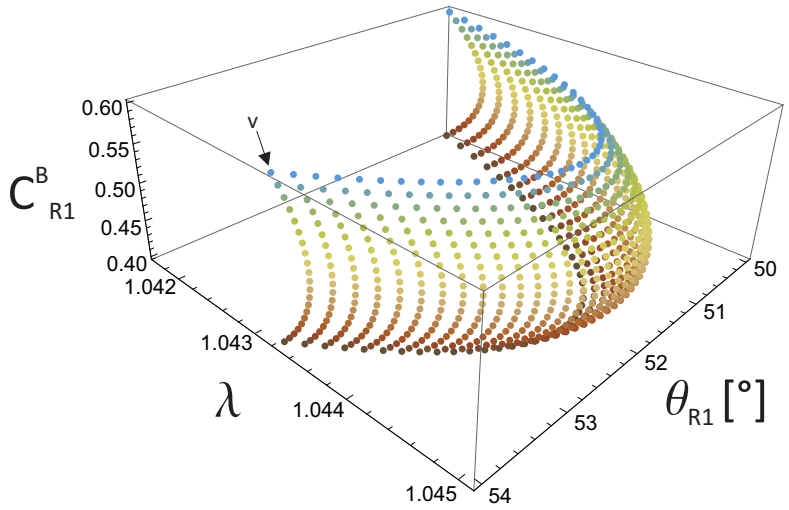

Figure 4.11: Microstructure perturbation of a rank-1 laminate presented showing longitudinal stretch when volume fraction of the soft phase and lamination angle are optimised simultaneously for the ranges $0.4 \leq C^B_{R1} \leq 0.6$ and $50° \leq \theta_{R1} \leq 54°$ at a contrast of 100 and applied nominal electric field of 100 MV/m.

4.3.2 Influence of increasing contrast on rank-2 laminates

Figure 4.12 displays the evolution of λ up to λ_{max} with increasing applied nominal electric field for different contrasts and the corresponding configurations are presented on table 4.9. Comparing this behaviour with that obtained for the rank-1 laminate in figure 4.10(a), it is evident that the rank-2 laminates provide a remarkable improvement in λ_{max} from rank-1 laminates, in agreement with the initial hypothesis of this study. Once again, each contrast appears to present a different microstructural arrangement from the next. Let us begin with analysing the microstructure evolution of the laminate corresponding with a contrast of 10. What is initially evident when comparing tables 4.8 and 4.9 is that there is once again no improvement in λ_{max} from rank-1 to rank-2 laminates. This can be inferred when realising that θ_{R1} has not changed and the matrix phase is parallel to the core in the rank-2 laminate. This means the rank-2 laminate configuration is essentially identical to the rank-1 configuration presented earlier on table 4.8 and the new homogeneous phase therefore provides no electromechanical influence on the rank-2 laminate.

Curve	$\mu^A/\mu^B = \epsilon^A/\epsilon^B$	λ_{max}	C^B_{R1}	$\theta_{R1}[^\circ]$	C^{R1}	$\theta_{R2}[^\circ]$
Yellow	10	1.02768	0.499	57.0	0.998	57.0
Red	100	1.10629	0.513	51.2	0.965	-1.0
Green	1000	1.85719	0.491	60.0	0.987	-9.0
Blue	10 000	2.19007	0.506	58.9	0.991	-13.0

Table 4.9: Rank-2 laminate configurations at contrasts of $\{10^x,\, x = 1, 2..., 4\}$ experiencing plane strain with no shear strains considered. Corresponding laminate configurations are presented in figure 4.12.

For a contrast of 100, with regards to volume fraction, the weighting of the matrix in the rank-2 composite, i.e. C^{R1}, has decreased significantly from the contrast of 10, possibly influenced by the new orientation of the matrix due to the drastic change in θ_{R2}. For a contrast of 1000, we observe non-monotonic behaviour for the first time in figure 4.12. An inflexion point is observed which drastically leads to a decrease in applied nominal electric field with increasing λ, and then an increase at a second inflexion point up to λ_{max}. This region in which the inflexion points occur can be attributed to the presence of electromechanical instability in the laminate due to the constraint $S^{\text{av}}_{12} \neq 0$. The fact that this electromechanical instability begins to be observed only at higher contrasts, which then leads to a further improvement in λ_{max}, implies an increase in response to applied nominal electric field with increasing contrast for a rank-2 laminate. This is confirmed when it is noticed that the presence of electromechanical instability becomes more enhanced at the higher contrast of 10 000. The range between inflexion points is much greater for a contrast of 10 000 implying an even more

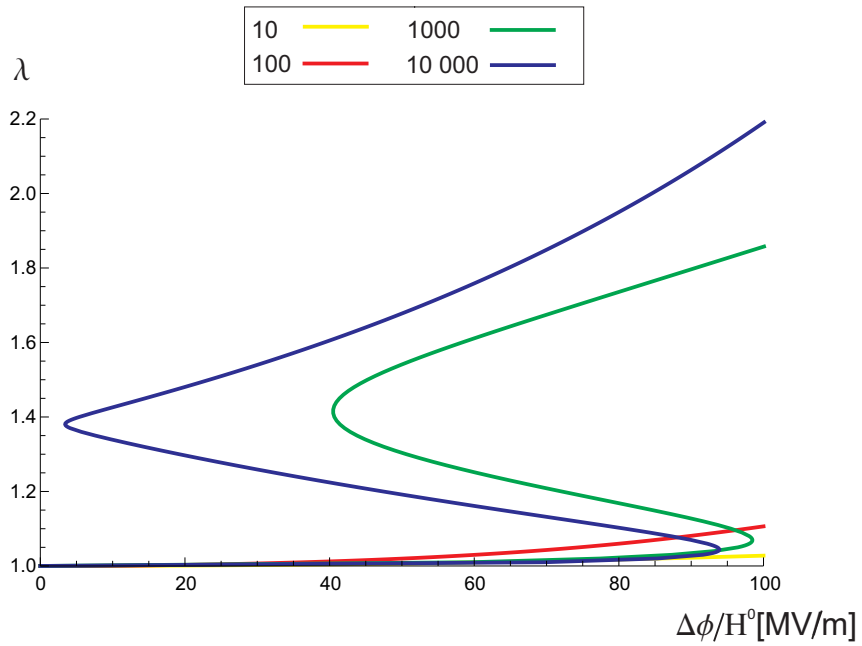

Figure 4.12: Influence of increasing applied nominal electric field on maximum longitudinal stretch at contrasts of $\{10^x, x = 1, 2..., 4\}$ for rank-2 laminates experiencing plane strain with no shear strain considered. Corresponding configurations are presented on table 4.9.

enhanced presence of instability. The fact this behaviour is due to electromechanical instability can also be established if some curves are analysed concurrently. For the range $0\,\text{MV/m} \leq \Delta\phi/H^0 \leq 88$ MV/m, the curves for contrasts of 10, 1000 and 10 000 present a similar evolution up until the point at which instability is experienced. The lower contrast curve of 10 can be utilised to serve as control curves for the higher contrast curves. It also appears that there may be a specific contrast at which instability in rank-2 laminates is triggered. Also, up to $\Delta\phi/H^0$ =88 MV/m, one may consider that it would be beneficial to limit the applied nominal electric field to this amount to limit electromechanical instability but the non-linearity presented in section 4.2.3 should be kept in mind. such that it is very possible that electromechanical instability exists at lower applied electric fields as well.

Also note how in the vicinity of $\lambda \approx 1.05$ and $\lambda \approx 1.4$ on the electromechanical loading paths of 1000 and 10 000, the curves are only just within the required limit of $0\,\text{MV/m} \leq \Delta\phi/H^0 \leq 100$ MV/m. Recall how in section 3.2 it was emphasised that all points for each laminate must lie within the range presented. This means that λ can in fact be increased when the rank-2 laminates are optimised at 100 MV/m however, points on the electromechanical loading path would then lie outside of this aforementioned range. Therefore in the context of this study, these configurations would not be ideal however it does emphasise the severe

effect of electromechanical instability as well as the non-linear effect as will be discussed in the section 4.3.3.

A note on microstructure sensitivity of Rank-2 laminates

Let us analyse the scenario relating to a contrast of 100 when shear strains are not considered more closely. Figure 4.13 displays the perturbation of the two lamination angles θ_{R1} and θ_{R2} for the optimum configuration when volume fraction is maintained as on table 4.9. What is emphasised here is as that one cannot simply maintain one lamination angle and perturb the other to attain λ_{max}. Both lamination angles are important, even though it is evident that the change in λ due to θ_{R1} is more rapid than due to θ_{R2} for ranges of the same magnitude. Despite the fact that some points share a similar λ, each individual point maintains its own α, $\tilde{\beta}$, α_{R2}, $\tilde{\beta}_{R2}$ and phase pressures therefore these points are neither equivalent nor reflections of each other along x_2 as was the case for rank-1 laminates. The same may be deduced when volume fractions are analysed in a similar manner, as displayed in figure 4.14. As we have already established, in reality C^{R1} also contains phase "B." Therefore this particular figure is representative of the interaction between the core and the matrix due to "B_{R1}" and "B_{R2}" already defined in the rank-2 solution in section 3.3.2.

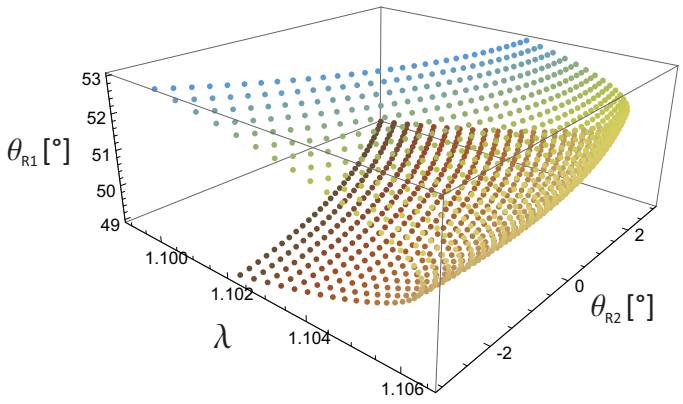

Figure 4.13: Lamination angle of the anisotropic phase in the rank-2 laminate for the range $49° \leq \theta_{R1} \leq 53°$ shown against the lamination angle of the rank-2 laminate for the range $-2° \leq \theta_{R1} \leq 2°$ and corresponding values of longitudinal stretch obtained at a contrast of 100. C^B_{R1} =0.513, C^{R1} =0.965.

What is evident for rank-1 laminates, and now also rank-2 laminates, is that the lamination angles reach a configuration upon which they cannot present a greater value for λ, thus dubbed λ_{max}. Despite the curves presented referring to a contrast of 100, this behaviour has been established thoroughly for rank-1 laminates in figure 4.10(b) and thus refers to all contrasts for rank-2 laminates.

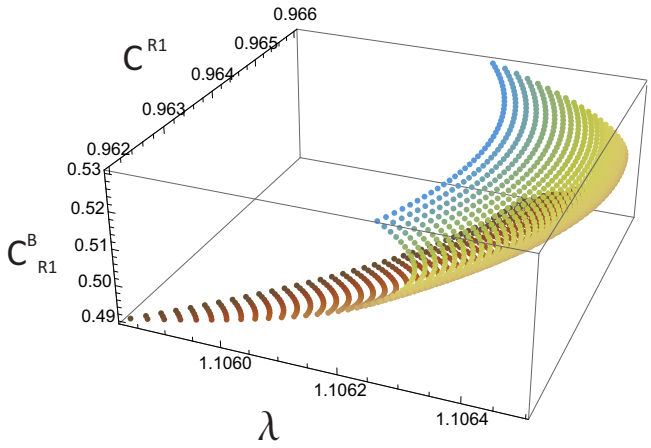

Figure 4.14: Volume fraction of the matrix in the rank-2 laminate for the range $0.49 \leq C^B_{R1} \leq 0.53$ shown against the volume fraction of the core in the rank-2 laminate for the range $0.961 \leq C^B_{R1} \leq 0.966$ and corresponding values of longitudinal stretch obtained at a contrast of 100. $\theta_{R1} = 51.2°$, $\theta_{R2} = -1°$.

Therefore this implies that for θ_{R1} and θ_{R2} there are "peaks" which in combination, in the form of figure 4.10(b), lead to a limit of maximum longitudinal stretch. At contrasts of 1000 and 10 000 however, applied nominal electric field leads to electromechanical interactions which, through electromechanical instability, enable an enhancement of longitudinal stretch to an absolute limit. This also means that the laminate configuration can possibly be modified to enable monotonic behaviour for these contrasts and this shall be investigated in the next section.

4.3.3 Non-monotonic behaviour of rank-2 laminates

In order to thoroughly analyse the influence of microstructure configuration on electromechanical instability, three curves are presented at a contrast of 1000 in figure 4.15. The first relates to optimisation relating to λ_{max} with observable electromechanical instability as on table 4.9, from here on titled N_1. The second relates to an example configuration that makes an attempt at reduction of this instability to present the limit of strict-monotonic behaviour titled N_2 and the third relates to an example configuration which provides a curve without any inflexion-related behaviour to serve as comparison of the aforementioned two curves and this is titled N_3. These configurations are presented on table 4.10.

For all curves, the main parameter found to contribute to reducing the electromechanical instability on table 4.10 was found to be θ_{R1} due to the fact it presented the greatest variation of longitudinal stretch in section 4.3.2. What is evident from these three curves is that in the process of laminate microstruc-

ture optimisation, electromechanical instabilities need to be taken into account such that a trade off between λ_{max} and electromechanical instability needs to be established. If one requires to use a configuration with no predictable instabilities at this contrast, it is advisable to utilise a type of configuration similar to that presented by N_3 as the configuration corresponding to N_2, despite presenting monotonic behaviour, is at the limit of electromechanical instability. One can therefore determine threshold[4] configurations for λ_{max} within the range $0\,\mathrm{MV/M} \leq \Delta\phi/H^0 \leq 100$ MV/m. However, it should be emphasised that curves N_2 and N_3 present example configurations possible to present this behaviour as in reality there are many different configurations that can be determined to present this type of behaviour.

Curve	λ_{max}	C^B_{R1}	$\theta_{R1}[^\circ]$	C^{R1}	$\theta_{R2}[^\circ]$
N_1	1.85719	0.491	60.0	0.987	-9.0
N_2	1.40554	0.490	50.5	0.987	-14.9
N_3	1.27908	0.489	47.0	0.987	-1.0

Table 4.10: Rank-2 laminate configurations determined for maximum longitudinal stretch at a maximum applied nominal electric field of 100 MV/m and contrast of 1000. N_1 - absolute λ_{max} with non-monotonic behaviour present for corresponding curve, N_2 - controlled optimum to to present the limit of monotonic behaviour and N_3 - comparison curve where no instabilities are observed. Corresponding curves are presented in figure 4.15.

For the same contrast of 1000, the applied nominal electric field at determination of λ_{max} has now also been varied, similar to section 4.2.3. Configurations corresponding to λ_{max} determined at various applied nominal electric fields of 20 MV/m (N_1L_g20), 50 MV/m (N_1L_g50) and N_1 at 100 MV/m are shown on table 4.11 and figure 4.16. At this contrast, we observe a modification in the concavity of the curves for different applied nominal electric fields. Beginning with the curve corresponding to N_1L_g20 in the manner described in section 4.2.3, there is monotonic behaviour. Monotonic behaviour is observed for the curves corresponding to configurations determined for N_1L_g50 and the already introduced N_1.

As shown by the table 4.11, the configurations are vastly different if C^B_{R1}, θ_{R1} and θ_{R2} specifically are analysed. There is a decrease in θ_{R1} with decreasing applied nominal electric field from the configuration for 50 MV/m to the one for 100 MV/m, possibly due to θ_{R2} increasing in a manner to become more horizontal. A more horizontal homogeneous phase possibly leads to the creation of more conductive pathways of the homogeneous phase of the rank-2 laminate. Comparing

[4]The threshold may be dependent on computational ability such that there is always the possibility that a numerical search misses the global optimum. However in this study effort has been made to establish these optimum configurations to the best of the author's ability.

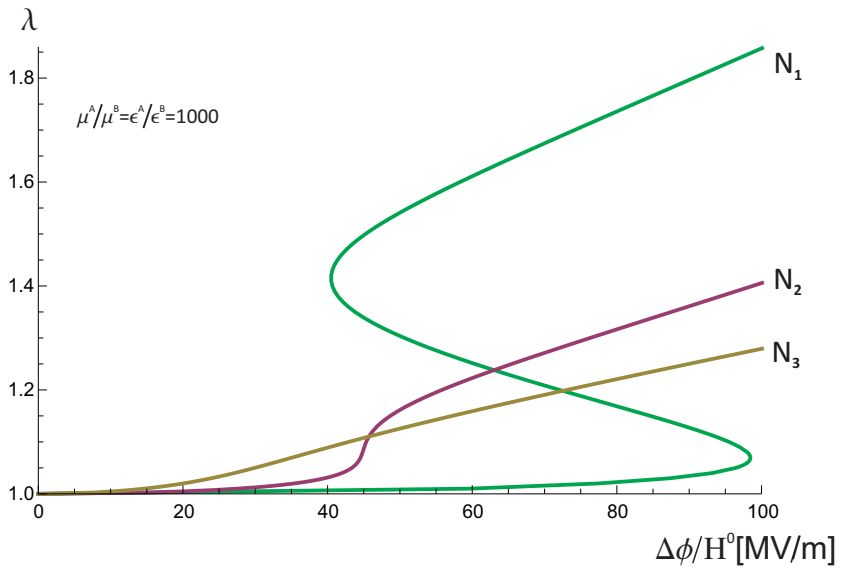

Figure 4.15: Influence of increasing applied nominal electric field on longitudinal stretch at a maximum applied nominal electric field of 100 MV/m and contrast of 1000 for rank-2 laminates. N_1 - absolute λ_{max} with non-monotonic behaviour present for corresponding curve, N_2 - controlled optimum to to present the limit of monotonic behaviour and N_3 - comparison curve where no instabilities are observed. Laminate configurations are presented on table 4.10.

figures 4.15 and 4.16, it is evident that observable electromechanical instabilities can be controlled through either reduction of θ_{R1} or reduction of applied nominal electric field when the microstructure is optimised.

	λ	C^B_{R1}	$\theta_{R1}[^\circ]$	C^{R1}	$\theta_{R2}[^\circ]$
N_1	1.85719	0.491	60.0	0.987	-9.0
N_1L_g50	1.32895	0.512	50.0	0.994	-1.0
N_1L_g20	1.19962	0.504	46.5	0.996	-0.4

Table 4.11: Rank-2 laminate configurations determined for maximum longitudinal stretch at maximum increasing applied nominal electric fields of 20 MV/m (N_1L_g20), 50 MV/m (N_1L_g50) and 100 MV/m (N_1). Curves are presented in figure 4.16.

Other forms of instabilities that may occur in electro-elastic laminates have been defined as macroscopic and microscopic instabilities as discussed by Lopez-Pamies (2006), Bertoldi & Gei (2011) and Rudykh (2012). An observation of these instabilities would bring to light some more interactions between the two constituent phases with relation to the construction and layout of the composite however, specific characterisation of these instabilities is beyond the scope of this work.

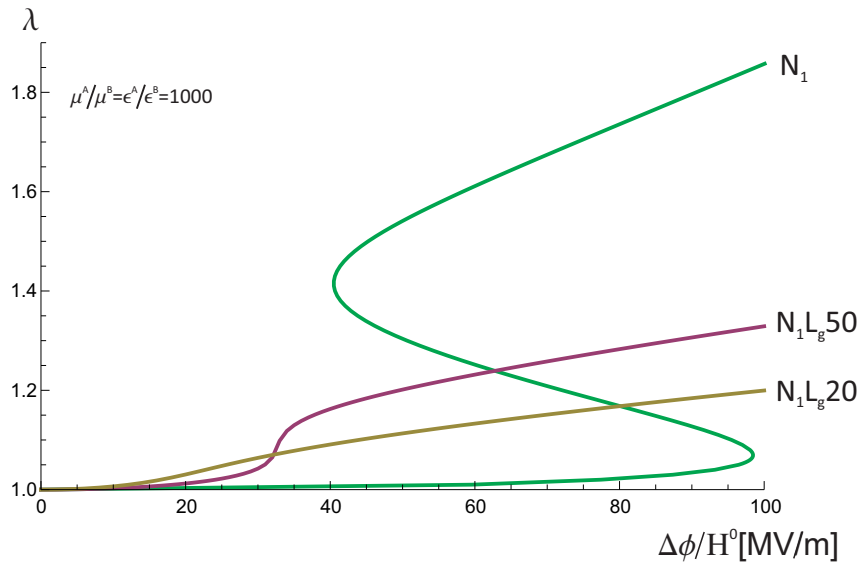

Figure 4.16: Influence of increasing applied nominal electric field on longitudinal stretch for configurations determined for various applied nominal electric fields of 20 MV/m (N_1L_g20), 50 MV/m (N_1L_g50) and 100 MV/m (N_1) at a contrast of 1000. Corresponding configurations are presented on table 4.11.

4.3.4 Comparison between plane strain boundary-value problems

Rank-1 laminates

This section shall be dedicated to comparing the two already presented boundary-value problems with the aim of possibly exposing the influence of shear strain on observable electromechanical instability. It is useful to begin first with rank-1 laminates briefly before proceeding to rank-2 laminates. Thus let us begin by revisiting figures 4.2(b) and 4.10(b) where the same phenomena with increasing lamination angle are observed in both boundary-value problems for $0 \leq \theta_{R1} \leq \pi$. The phenomenon apparent in this comparison is that a boundary-value problem in which shear strain is accounted for results in a dampening of the fluctuation of λ with varying θ_{R1}. This also means that when shear strains are not considered a higher value of λ_{max} is obtained than that previously observed if tables 4.2 and 4.8 are compared. Figure 4.17(b) displays the feature that when shear strains are considered for a rank-1 laminate ($R1L_gS$), the value for λ_{max} at optimum laminate configuration is lower than that experienced when shear strains are not considered (B_1). This is confirmed by curve B_2 which presents the same configuration as for $R1L_gS$ but with no shear strains considered. It should be mentioned that curve B_1 is identical to the red curve in figure 4.10(a) while $R1L_gS$ corresponds to the red curve in figure 4.2(a) and has also been defined earlier in section 4.2.1.

Curve	λ_{max}	ξ	C^B_{R1}	$\theta_{R1}[^\circ]$
B_1	1.04505		0.5	52.1
B_2	1.03369		0.5	60.9
$R1L_gS$	1.02632	-0.00949	0.5	60.9

Table 4.12: Rank-1 laminate configurations obtained at a contrast of 100 and electric field of 100 MV/m. B_1 relates to the optimum configuration when shear strains are not considered and B_2 relates to the performance at vanishing in-plane tractions, this time without considering shear stains. $R1L_gS$ has been defined earlier in section 4.2.1. Corresponding curves are presented in figure 4.17.

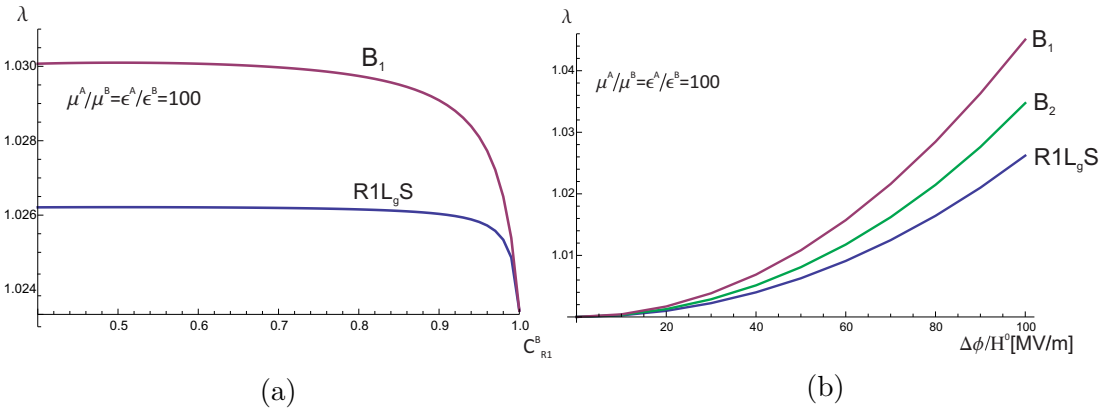

Figure 4.17: (a) Rank-1 laminate influence of increasing volume fraction on longitudinal stretch and (b) influence of increasing applied nominal electric field on maximum longitudinal stretch. Curve B_1 relates to the optimum configuration when shear strains are not considered, B_2 relates to the performance at vanishing in-plane tractions, this time without considering shear strains. $R1L_gS$ has been defined earlier in section 4.2.1. Corresponding configurations are presented on table 4.12.

What is demonstrated by figure 4.10(a) is that for a rank-1 laminate, there is a strong influence of lamination angle on the optimum laminate configuration as well as the fact that when shear strains are not considered, higher values for λ_{max} are obtained. Gei et al. (2013) showed that at low electric field/charge, λ will be very close to that computed in the plane strain boundary-value problem, while diverging at higher electrical excitations. This is confirmed in figure 4.17(b) where, at voltages less than 50 MV/m there is little difference in the curves corresponding to λ_{max} under different boundary conditions. Let us now investigate the influence of volume fraction on the same two boundary conditions. A comparison is presented in figure 4.17(a). It is useful to note that the influence of volume fraction on longitudinal stretch is very similar when shear strains are considered and when they are not, with the only difference being the magnitude of λ_{max}.

Rank-2 laminates

For rank-2 laminates, only specific contrasts shall be compared. The contrast of 100, despite not having presented any unique instability-related behaviour, will be mentioned so as to provide a comparison with the contrast of 1000 at which instability was observed, in a manner consistent with introducing N_3 in section 4.3.3. Beginning with table 4.13 and figure 4.18(a) for the already determined contrast of 100, the curves considered include that already obtained for plane strain with shear strain considered which is exactly the same as the red curve in figure 4.6 and R2L$_g$S. C_2 refers to a curve determined by immersing the laminate configuration that is optimum in a boundary-value problem of absent shear strain into an environment in which shear strains are considered. C_3 is identical to the red curve in figure 4.12, relating to a boundary-value problem of no shear strain considered while C_4 is identical to the red curve in figure 4.7 optimised for ξ_{max}.

Curve	Shear considered?	λ	ξ	C^B_{R1}	$\theta_{R1}[^\circ]$	C^{R1}	$\theta_{R2}[^\circ]$
R2L$_g$S	Yes	1.12405	0.11811	0.508	65.1	0.963	12.3
C_2	Yes	1.10683	0.01528	0.513	51.2	0.965	-1.0
C_3	No	1.10629		0.513	51.2	0.965	-1.0
C_4	Yes	1.06172	0.26417	0.505	90.0	0.967	31.1

Table 4.13: Various Rank-2 laminate configurations and corresponding longitudinal stretch and amount of shear at a contrast of 100 and applied nominal electric field of 100 MV/m. R2L$_g$S - optimum configuration when shear strains are considered, C_2 - optimum configuration when shear strains are not considered and resulting longitudinal stretch and amount of shear when computed in an environment taking into account shear strain, C_3 - optimum configuration when shear strains are not considered and C_4 - optimum configuration to obtain maximum amount of shear and corresponding longitudinal stretch. Corresponding curves presented in figure 4.18.

Of the curves presented, it is evident that the boundary-value problem with shear strain considered results in an increase in λ_{max} and the microstructure configurations related to R2L$_g$S, C_2 and C_4 are completely dissimilar except for the value of C^{R1} which have very small differences. This demonstrates some possible relation between C^{R1} and contrast as the laminates all share the same contrast. A larger value of λ in R2L$_g$S and C_2 is due to liberation of S^{av}_{12}. As slight enhancement of λ_{max} is experienced even for configuration C_2 from C_3 this confirms this injection of additional favourable conditions due to shear strain consideration. It is also of note that at θ_{R1} for C_4 is 90° which reflects some sort of direct influence of applied nominal electric field on deformation of the anisotropic phase. This is logical if one considers that the stiff phase is less contributory to the overall deformation of the laminate as discussed in section 4.2.2.

The rank-1 laminate behaviour presented in figure 4.3(b) can be compared to the rank-2 laminate behaviour in figure 4.18(b). What rank-2 laminates now

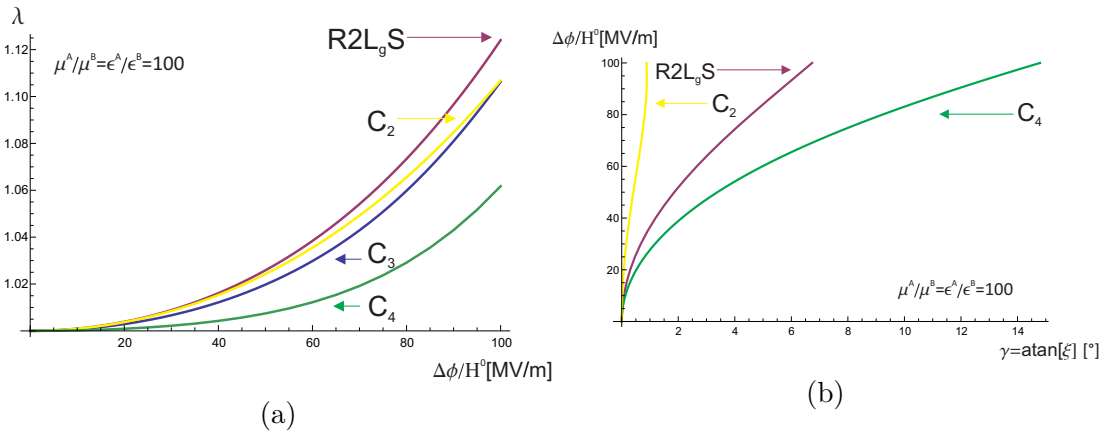

Figure 4.18: (a) Influence of increasing applied nominal electric field on longitudinal stretch on laminate configurations R2L$_g$S, C$_2$ and C$_3$ described on table 4.13. (b) Influence of applied nominal electric field on shear angle on laminate configurations R2L$_g$S and C$_4$ described on table 4.13.

provide is an increase in the soft, more compliant phase to maximise deformation when shear strains are considered. This has presented itself in the form of an improved value for corresponding λ_{max} for C$_2$ at the same configuration for C$_3$. It is noticeable that throughout a large range of applied nominal electric field the performance of C$_2$ is better than the performance of C$_3$ in figure 4.18(b), only showing minimal difference at $\Delta\phi/H^0$ =100 MV/m such that the amount of shear reflects an internal deformation which can only be observed through figure 4.18(b).

The phenomena described for a contrast of 100 is also experienced at a contrast of 1000 in figure 4.19, where consideration of shear effects leads to an increased value in λ of 16% in comparison to that previously experienced when shear is not considered. This again confirms the fact that increasing contrast leads to amplified effects in a rank-2 laminate as λ increases from figure 4.18(a) to 4.19(a). There are now interesting effects due to shear strain presented in figure 4.19(a) for applied nominal electric field and 4.19(b) for amount of shear. Curve C$_5$ relates to a configuration that presents λ_{max} at a contrast of 1000 when shear strains are considered, identical to the green curve in figure 4.6. C$_6$ is identical to the green curve in figure 4.7 relating to a configuration optimised for ξ_{max} at a contrast of 1000. Curves C$_7$ and N$_1$, in a manner analogous to that executed for a contrast of 100 for C$_3$ and C$_4$, represent corresponding longitudinal stretches for identical configurations when shear strains are considered, and when they are not considered, respectively.

What is now unique at this contrast is the phenomenon observed with regards to the inflexion point previously encountered for N$_1$. A boundary-value problem

Curve	Shear considered?	λ	ξ	C^B_{R1}	$\theta_{R1}[^\circ]$	C^{R1}	$\theta_{R2}[^\circ]$
C_5	Yes	2.47891	0.24845	0.498	70.0	0.990	-20.0
C_6	Yes	1.92680	-0.95326	0.502	47.0	0.994	-44.0
C_7	Yes	2.15951	-0.38556	0.491	60.0	0.987	-9.0
N_1	No	1.85719		0.491	60.0	0.987	-9.0

Table 4.14: Various Rank-2 laminate configurations and corresponding longitudinal stretch and amount of shear at a contrast of 1000 and applied nominal electric field of 100 MV/m. C_5 - optimum configuration for λ_{max} when shear strains are considered, C_6 - optimum configuration for ξ_{max} and corresponding longitudinal stretch, C_7 - optimum configuration when shear strains are not considered and resulting longitudinal stretch and amount of shear when computed in an environment taking into account shear strain and N_1 - optimum configuration for λ_{max} when shear strains are not considered. Corresponding curves presented in figure 4.19.

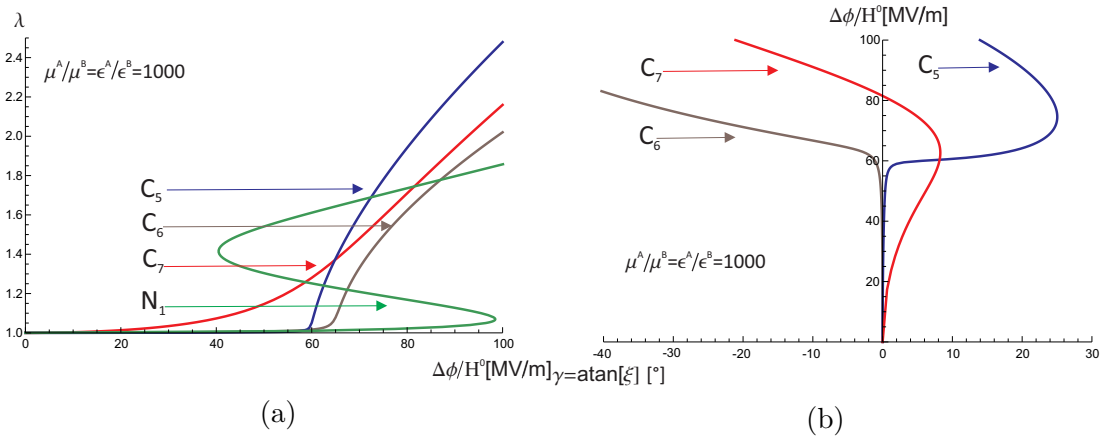

(a) (b)

Figure 4.19: (a) Influence of increasing applied nominal electric field on longitudinal stretch on laminate configurations C_5, C_6 and C_7, N_1 described on table 4.13. (b) Influence of applied nominal electric field on shear angle on laminate configurations C_5, C_6 and C_7 described on table 4.14.

taking into account shear strain not only provides an enhancement in λ_{max}, but also affects electromechanical stability of a rank-2 laminate as non-monotonic behaviour is not present on C_7 in figure 4.19(a) for the same configuration N_1. It seems when shear strains are not considered for a rank-2 laminate at a contrast of 1000 (N_1), a constrictive-type effect on λ is experienced in the laminate which results in non-monotonic behaviour. When shear strains are considered for the optimum configuration (C_5), the laminate stretches minimally up until severe enhancement of λ is first experienced. At this point of $\Delta\phi/H^0 \approx$65 MV/m, the deformation increases greatly up until λ_{max}.

Configurations C_5, C_6 and C_7 all begin with very small and positive shear angles at lower applied nominal electric fields and then as the applied nominal electric field is increased, C_6 and C_7 evolve towards the negative direction af-

ter $\Delta\phi/H^0 \approx$55 MV/m. With regards to C_5, the behaviour presented in figure 4.19(b) presents a new perspective of what is happening inside the rank-2 laminate in figure 4.19(a), thus ξ consideration can also be used as a tool to observe laminate evolutionary behaviour when the electromechanical loading path is analysed. At $\Delta\phi/H^0 \approx$55 MV/m for C_5, while λ is increasing somewhat steadily, the shear angle is increasing and then at $\Delta\phi/H^0 \approx$75 MV/m, it begins to decrease up until λ_{max}. It should be noted that electromechanical instabilities may be existent at lower applied nominal electric fields but in the figures presented, it is only *observable* electromechanical instabilities that are discussed.

4.3.5 Current configuration of lamination angles for rank-2 laminates

Rank-1 laminates at a contrast of 100

The lamination angles for rank-2 laminates have been shown to be unique to each type of boundary-value problems determined and now that the optimum configurations in the reference configurations have been determined, it would be beneficial to understand the microstructural step-change evolution that lamination angles undergo when the applied nominal electric field is increased within the material. Let us begin with our reference boundary-value problem, that of equal shear and dielectric moduli at a contrast of 100. The input configuration has already been presented in section 4.3.2 and the corresponding microstructural evolution is now presented in this section. These configurations are presented in figure 4.20 where the rank-2 laminate evolution begins at 0 MV/m with the reference configuration already presented on table 4.9. As the applied nominal electric field is increased, θ_{R1} begins to decrease while θ_{R2} increases. However, θ_{R1} decreases by a much larger value than the reflected increase of θ_{R2}. Reference back to figure 4.9 is advised if one desires to generate a mental model of the possible lamination angle evolution taking place at any coincident points of applied nominal electric field. What these evolutions reflect is the greater contribution θ_{R1} provides to the overall laminate deformation, as compared to θ_{R2}.

Rank-2 laminates at a contrast of 1000

Let us now consider the contrast of 1000 at which the unique behaviour and inflexion point were encountered. It is useful to recap the three curves earlier presented in section 4.3.3 such that we can complete the comparison that had commenced in the aforementioned section. The description of the three curves will be re-visited as follows. One, titled N_1, with the optimisation relating to λ_{max} with clear instability, the second (N_2) with an attempt at reduction of this instability to present the limit of monotonic behaviour and a presented lower

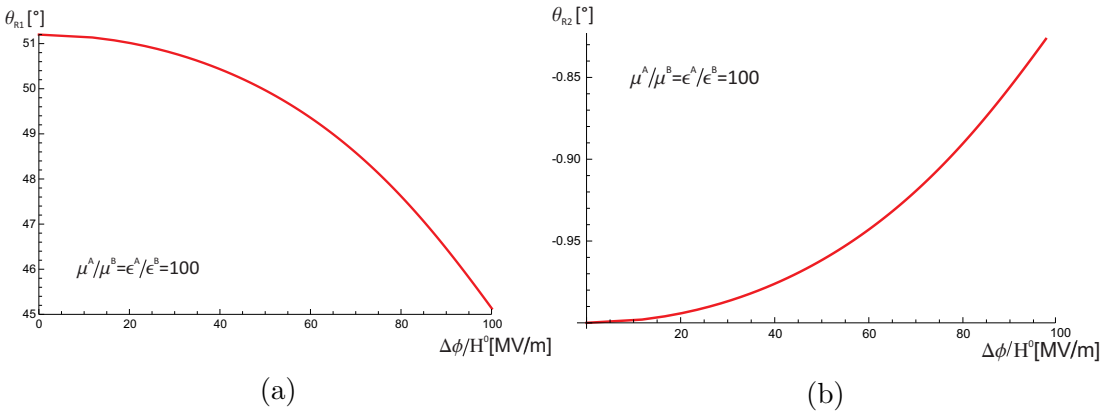

(a) (b)

Figure 4.20: Current configuration with increasing applied nominal electric field at a contrast of 100 of (a) anisotropic phase of and (b) homogeneous phase of a rank-2 laminate with no shear strain considered.

corresponding λ and the third (N_3), a curve presented at a configuration without any inflexion-related behaviour to serve as comparison for N_1 and N_2.

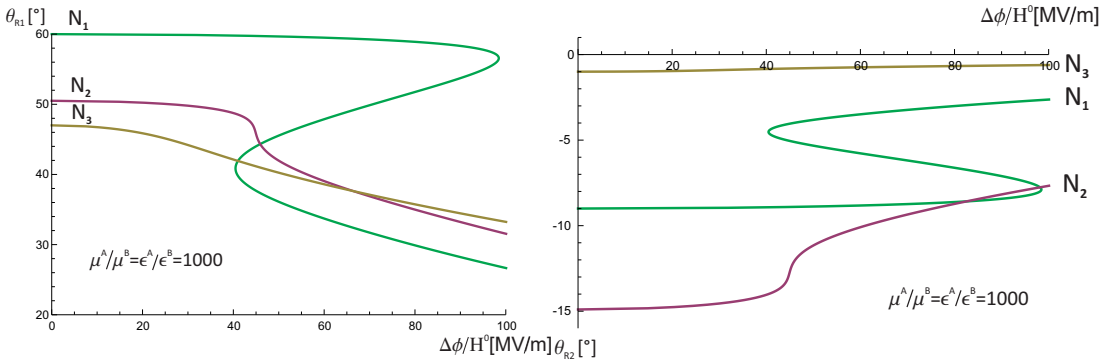

(a) (b)

Figure 4.21: Current configuration with increasing applied nominal electric field at a contrast of 1000 of (a) anisotropic phase and (b) homogeneous phase of a rank-2 laminate with no shear strain considered.

The current lamination angles are shown in figure 4.21 and it is evident that the reference configuration has some differences to the now current configuration at certain applied nominal electric field values. What is apparent when considering the three curves together in figure 4.21(a) is that the greater the starting value in θ_{R1}, the larger the range of applied nominal electric field in which θ_{R1} is near constant. A noticeable change in θ_{R1} then begins to be observed on curves N_1, N_2 and N_3 at applied voltages of 98 MV/m, 30 MV/m and 10 MV/m, respectively. This means that when the laminate is set to its optimum value for θ_{R1}, it presents an ability to maintain this optimum configuration and only changes

when the applied nominal electric field is sufficiently high. The magnitude of the increase in θ_{R2} from 0-100 MV/m for figure 4.21(b) is smaller than the magnitude in decrease of θ_{R1} with increasing applied nominal electric field. This has already been presented for our reference boundary-value problem with a contrast of 100 in figure 4.20 and thus confirms this phenomenon. With regards to N_2, it is evident for both lamination angles that there is a specific electric field at which the material continues to re-orientate without an increase in applied nominal electric field implying that the material is attempting to re-perturb itself due to electromechanical instability.

It is also useful to present the evolution of λ with each of the lamination angles presented so as to confirm if there is truly a non-linear effect as well as understanding how this may vary with extreme presence, or minimisation of the instability. This is now presented in figure 4.22 and the curves relating to N_1 and N_2 show the non-linearity present due to their slight curvature with increasing λ. While for N_3, this effect is less enhanced due to the absence of the inflexion earlier discussed. It is therefore evident that the closer one approaches optimum laminate configuration at contrasts of 1000 and higher, greater care needs to taken to consider instability due to the increased sensitivity of the material.

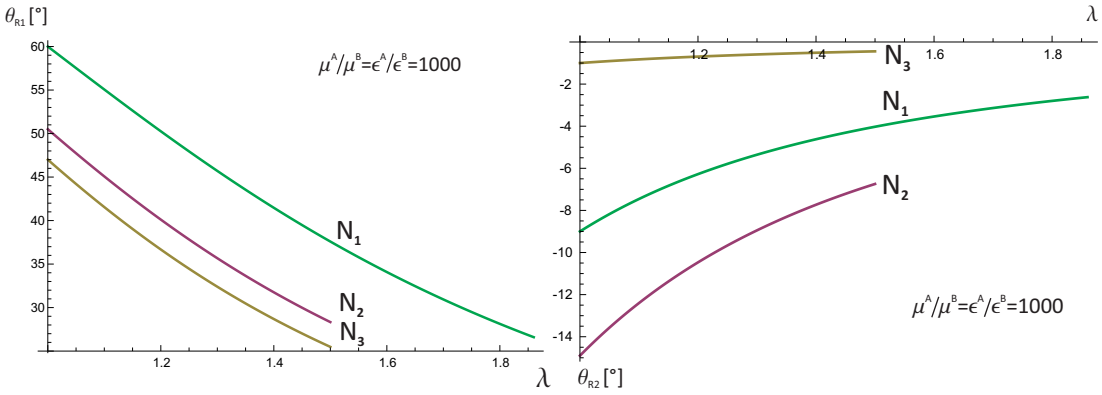

Figure 4.22: Current configuration with increasing longitudinal stretch at a contrast of 1000 of (a) anisotropic phase of and (b) homogeneous phase of a rank-2 laminate with no shear strain considered.

4.3.6 Electric field macroscopic and microscopic contributions in rank-2 laminates

We have already discussed how an applied nominal electric field in a rank-2 laminate gives rise to deformation such that the lamination angles can be re-configured to provide a microstructure for optimum performance. We shall take a closer look

at the resulting influence of this electric field once the optimum configurations have been determined. We have already defined the absolute values of electric fields $E^{0\text{av}}$ and E^{av} in Chapter 3 and determined the weighted contribution in each phase of the Lagrangian electric field $\mathbf{E}^{0\text{av}}$ to provide equations $[3.12_{1,2}]$. Now it is possible to obtain the values for α and $\tilde{\beta}$ for a given configuration and applied nominal electric field in the rank-2 laminate. It should be remembered that the rank-1 laminate embedded in the rank-2 laminate has its own set of α and $\tilde{\beta}$ values distinct from those of the holistic rank-2 laminate. This means that the weighted contribution of electric field and electric displacement for phases "A_{R1}", "B_{R1}" and "B_{R2}" can be determined in order to discover the influence of homogenized macroscopic electric field on the microscopic response of the rank-2 laminate, in a manner analogous to table 4.2. Also, one cannot begin to discuss the realistic electric field in a rank-2 laminate without considering the onset of instabilities and their possible influence on the macroscopic and microscopic electric field magnification.

Despite the numerous step changes in complexity of the present boundary-value problem, DeBotton (2005) notes that in the boundary-value problem of a transversely isotropic sequentially coated laminate made out of stiff inclusions and a softer matrix phase (i.e. $\mu^a > \mu^b$), the core layers at each lamination stage are always stiffer than than the (dilute) layers of the matrix. This implies the possibility that all the intermediate laminates within the composite are stable, and consequently the possibility that the sequentially-coated laminate with the stiffer inclusions is a stable material. When the inclusion phase is the softer one, as is in this boundary-value problem, at each lamination stage the core layers are softer than the (dilute) layers of the matrix phase. For an applied nominal electric field of 100 MV/m, the absolute values of microscopic electric fields are presented in figures 4.23 and 4.24 which also include boundary-value problems to be investigated in the next chapter.

As shown in figure 4.23, an applied nominal electric field of 100 MV/m produces a maximum absolute value of microscopic electric field in the soft phase of the core at a magnification of approximately 15. This alludes the fact that the working applied nominal electric electric field is several times higher than that was being considered throughout the text[5]. Also displayed in figure 4.23 are the microscopic electric fields in each of the phases throughout the rank-2 laminate, with figure 4.24 displaying the corresponding electric fields in the anisotropic phase. The non-linear effects reveal the fact that even an applied nominal electric field of 100 MV/m leads in actuality to an absolute value of macroscopic electric field of 110 MV/m in plane strain with no shear strain considered. In

[5]Rudykh et al. (2011) obtained similar behaviour and obtained a ten-fold enhancement in electromechanical coupling

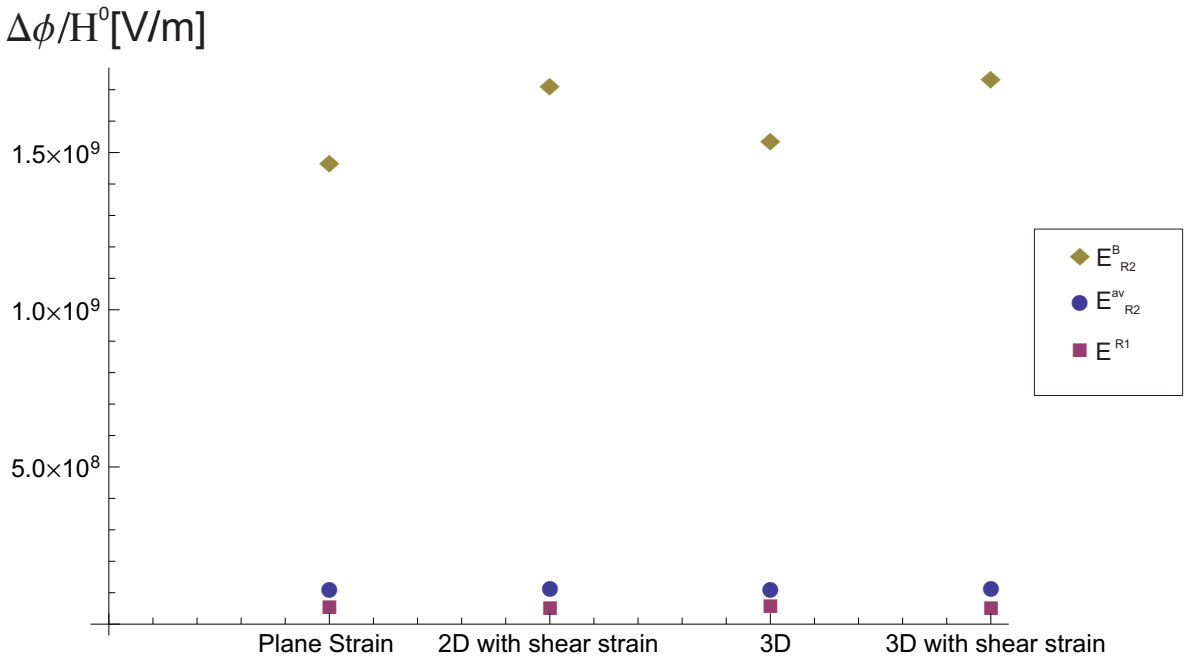

Figure 4.23: Absolute values of applied electric field and corresponding microscopic phase electric fields in rank-2 laminates for various boundary conditions at a contrast of 100.

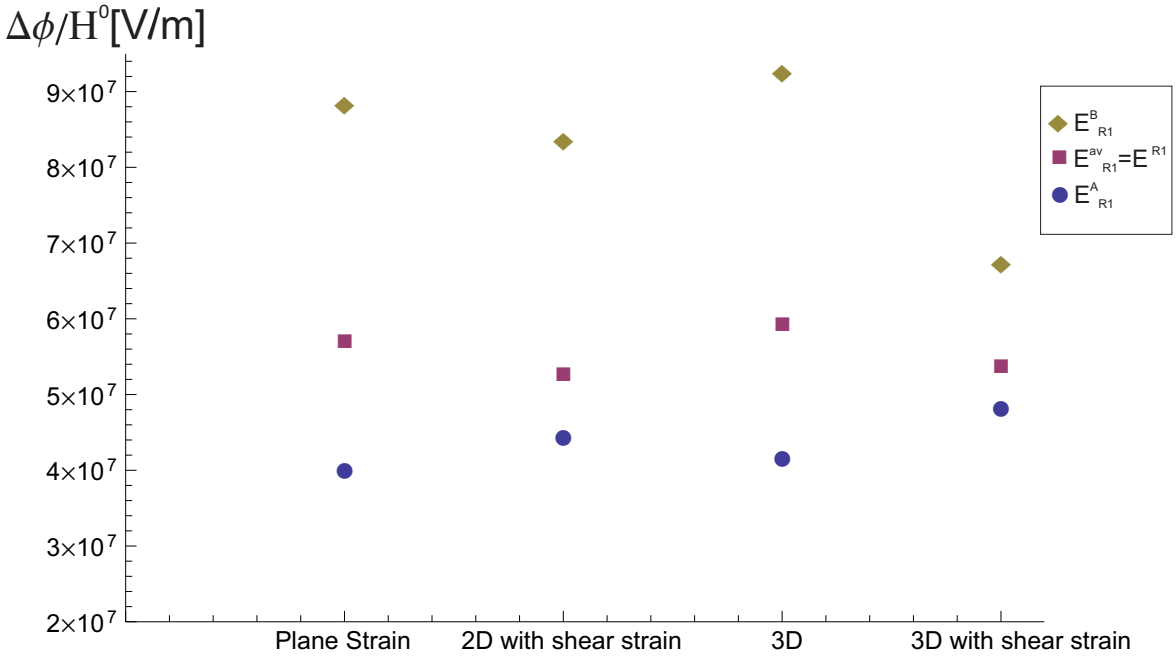

Figure 4.24: Absolute values of applied electric field and corresponding microscopic phase electric fields in rank-1 anisotropic phases embedded in rank-2 laminates for various boundary conditions at a contrast of 100.

order to explain this behaviour is useful to re-visit the set of equations [3.12] in Chapter 2, this time in terms of the rank-2 material. The electric field in each phase is amplified by the corresponding value of $\tilde{\beta}$ at the specific point of λ_{max} i.e. the magnitude of the electric field in the isotropic layers is proportional to the applied field divided by their volume fraction. It has already been established that the electric field is continuous along the interface which implies a severe magnification of the soft phase within the material. This is also witnessed in the embedded rank-1 material whose microscopic electric fields are presented in figure 4.24 such that the soft phase will always present the largest value of microscopic electric field in either the rank-1 or rank-2 material. Also, the rank-1 layers are composed of alternating stiff and soft sub-layers such that their compliant mode corresponds to a shear of the soft sub-layers with rotation of the stiffer ones, as already presented when the rank-1 lamination angle evolved by a greater amount than that of the laminated soft homogeneous phase in the rank-2 laminate in section 4.3.5. In order to obtain a maximum microscopic electric field of 100 MV/m in plane strain with no shear strain considered, it was found that the required applied nominal electric field is 6.95 MV/m.

4.4 Conclusions

In this chapter, it has been presented that:

- The homogeneous actuation in large strain was 6% greater than in small strain while a 12% improvement in λ_{max} from the homogeneous actuation was obtained in large strain, similar to results by Tian et al. (2012) in small strain.
- For rank-1 laminates, when shear strains are considered in a plane strain environment, the value for λ_{max} at optimum laminate configuration is lower than when shear strains are not considered.
- Considering the volume fraction of rank-1 laminates, the distribution of C^A_{R1} and C^B_{R1} is equal (0.5) for all boundary conditions investigated, leading to symmetrical behaviour at approximately $\pi/2$ for λ.
- For rank-2 laminates, comparison of Tian et al. (2012) small strain results with those obtained in large strain show a 20% improvement in λ_{max} for optimum configurations in small strain compared to those in large strain.
- The optimum configuration obtained by Tian et al. (2012) in small strain, when solved in large strain, presented a 12% improvement in λ_{max}.
- When the two plane strain boundary value problems were compared, namely plane strain with shear strain considered and plane strain without shear

strain considered, it was found that the same configuration obtained when no shear strains were considered presented a higher λ_{max} when shear strains were considered by 16% for a contrast of 1000.

- The current electric field of the soft homogeneous phase in the rank-2 laminate at a contrast of 100 reflected the greatest enhancement among all the phases of the factor of 15 in terms of the absolute values.

Chapter 5

Boundary value problems in a three-dimensional environment

5.1 Introduction

In continuation to this study, this chapter will investigate the micro-structural behaviour in a three-dimensional environment with vanishing in-plane tractions and also with shear strains present. This will enable a comparison to be carried out between plane strain results with those that will be obtained in a fully three-dimensional environment for both rank-1 and rank-2 laminates. The presence of electromechanical instability will be highlighted and an attempt to present a type of configuration to reduce this instability, will be executed demonstrably with regards to microstructure optimisation so as to lay the foundation for characterising this instability in future work.

5.2 Tri-axial stretch without shear strain consideration

5.2.1 Initial optimisation: rank-1 laminates

Let us maintain the free conditions in the plane strain problems already encountered given such that $S_{11}^{\text{av}} = 0$ and $S_{22}^{\text{av}} = 0$ but in a scenario in which the stretches in all three directions are considered. The deformation gradient for this three-dimensional boundary-value problem is given as follows

$$\boldsymbol{F}^{\text{av}} = \begin{bmatrix} \lambda_1 & 0 & 0 \\ 0 & \lambda_2 & 0 \\ 0 & 0 & \frac{1}{\lambda_1 \lambda_2} \end{bmatrix}, \qquad [5.1]$$

with $\lambda_1\lambda_2\lambda_3 = 1$ and $S_{33}^{\text{av}} = 0$ implying that the principal strain directions are all now free to deform macroscopically in a manner similar to the homogeneous example presented in section 2.6.1. As already described, λ_1 refers to the longitudinal stretch and now λ_2 refers to the perpendicular stretch with λ_3 relating to the transverse or out-of-plane stretch. Let us begin with a rank-1 laminate and consider the influence of the lamination angle as executed in figure 4.10(b) in section 4.3 for a volume fraction whereby $C_{R1}^B = 0.5$. Figure 5.1 shows the variation of longitudinal, perpendicular and transverse stretch with lamination angle for a rank-1 laminate for the range $40° \leq \theta_{R1} \leq 250°$. The maximum value of λ_1 is found to correspond with the minimum value of λ_2 while the symmetry discussed in section 4.3 in figure 4.10(b) is reflected once again in figure 5.1. The first peak of the λ_1 curve occurs at $\theta_{R1} = 52°$, the middle peak at $\theta_{R1} = 128°$ while the third peak occurs at $\theta_{R1} = 232°$. At $\theta_{R1} = 142.5°$, the λ_1 curve reaches a minimum as well as at $\theta_{R1} = 217.5°$ and these points correspond with maximum values of λ for the λ_2 curve. In this range, the maximum value of λ_3 occurs at $\theta_{R1} = 90°$ while the minimum occurs at $\theta_{R1} = 180°$. The periodic behaviour of the curves in figure 5.1 is modified by the liberation of the transverse traction which accounts for the shift in the lamination angles at which maximum longitudinal stretch occurs, such that symmetry does occur exactly at $\pi/2$ instances as observed in plane strain.

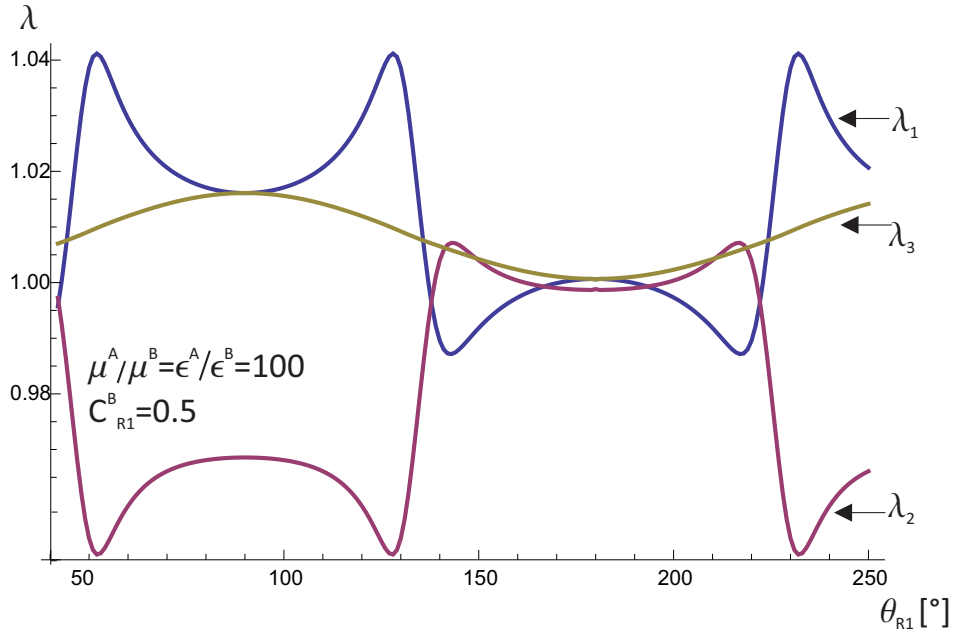

Figure 5.1: Influence of evolving lamination angle on longitudinal stretch (blue curve), perpendicular stretch (purple curve) and transverse stretch (yellow curve) at a contrast of 100. $C_{R1}^A = C_{R1}^B = 0.5$.

At the point at which λ_3 is minimum, it is the direction in which the largest value of stretch in any direction is experienced. This means that this point corresponds with the worst overall behaviour of the rank-1 laminate when optimisation for longitudinal stretch is not considered. This is due to the fact that the direction of the applied nominal electric field is now acting at an angle of 90° to the phases in the laminate. The optimum configuration for this contrast of 100 is therefore when $\theta_{R1} = 52°$ and it was also found that volume fraction is optimum when $C^B_{R1} = 0.5$. Despite the fact that the maximum value of λ_1 coincides with the minimum value of λ_2, it should be noted that the rates of deformation are not identical. The rate at which λ_1 is increasing with increasing lamination angle is far greater than the rate at which θ_{R2} is decreasing, due to the presence of λ_3. This can be confirmed if one considers the difference between λ_1 for the points at $\theta_{R1} = 52°$ and $\theta_{R1} = 90°$ which is 0.025, and the corresponding difference for λ_2 for the same two points which is 0.017.

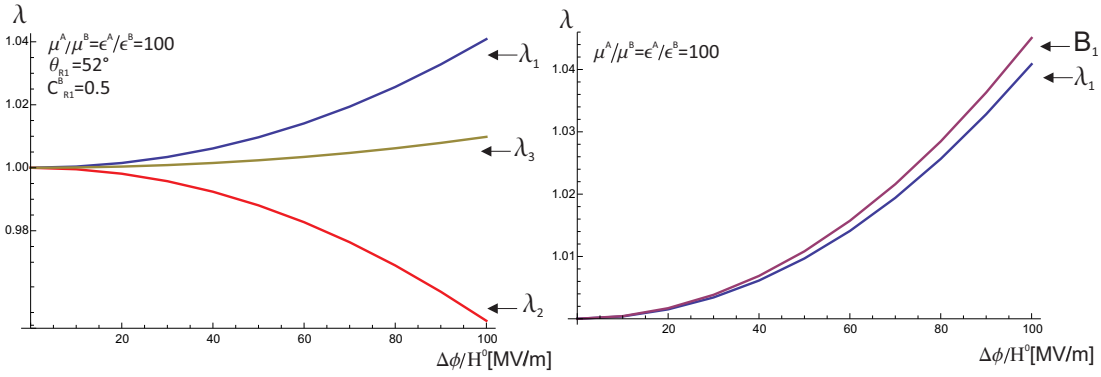

Figure 5.2: (a) Influence of increasing applied nominal electric field on longitudinal stretch (blue curve), perpendicular stretch (purple curve) and transverse stretch (yellow curve) at a contrast of 100 for a rank-1 laminate. (b) Rank-1 laminate longitudinal stretch (blue curve) compared with curve B_1 in section 4.3 at a contrast of 100.

The influence of applied nominal electric field on the three stretches is presented in figure 5.2(a). Comparing this with figure 4.10(a), particularly, the curve for a contrast of 100, it can be argued that for a rank-1 laminate the longitudinal stretch in the presented three dimensional boundary-value problem i.e. λ_1 can possibly be used to approximate λ in the plane-strain boundary-value problem and vice versa due to the minimal deformation in the λ_3 direction. This is displayed in figure 5.2(b) where the difference between λ_{max} for the plane strain boundary-value problem named B_1 in section 4.3 and λ_1 for the three-dimensional boundary-value problem is less than 1%. It is clear that when transitioning from boundary-value problems in plane strain to a three dimensional boundary-value problem where no shear strains are considered, there is no change in the optimum

θ_{R1} and C^B_{R1}. There is however, a decrease in longitudinal strain from the plane strain environment due to λ_3.

5.2.2 Influence of increasing contrast on rank-1 laminates

The effect of varying applied nominal electric field on the stretches in the three directions for a three-dimensional boundary-value problem for all contrasts investigated in this study are presented in figures 5.3, 5.4(a) and 5.4(b). As already indicated for a contrast of 100, there are maximum and minimum responses associated with λ_1 and λ_2, with $\lambda_2 \leq \lambda_1$ at all instances as presented by table 5.1. Non-linear effects are observed in figure 5.4(b) whereby the contrast of 10 000 presents a greater transverse stretch than the contrast of 1000. Also for these two contrasts, the curves for λ_1 in figure 5.3 provide near identical values for λ up until $\Delta\phi/H^0 = 70$ MV/m. This behaviour is also observed for the corresponding λ_2 curves such that λ_3 curves enable better observation of the behaviour between these two contrasts. As discovered in plane strain, it is also found that the volume fraction presents no variation with increasing contrast, with C^B_{R1} =0.5 providing the maximum value for λ_1.

As already discussed for plane strain in figure 4.10(b), the influence of lamination angle on a constant applied nominal electric field of 100 MV/m for varying contrasts is presented in figures 5.5 and 5.6. For λ_1, we observe a small difference in the curves corresponding to contrasts of 1000 and 10 000 as in plane strain. When optimising for λ_1 as we have carried out, an increase in contrasts leads to an increase in possible maximum achievable longitudinal stretch while volume fraction remains constant. Periodic behaviour in a rank-1 laminate is also present once again in figures 5.5 and 5.6(a) confirming observations in plane strain in figure 4.10(b) for rank-1 laminates.

Curve	$\mu^A/\mu^B = \epsilon^A/\epsilon^B$	λ_1	λ_2	λ_3	C^B_{R1}	$\theta_{R1}[^\circ]$
Yellow	10	1.02205	0.96646	1.01238	0.5	55.7
Red	100	1.04086	0.95143	1.00979	0.5	52.0
Green	1000	1.07534	0.92138	1.00929	0.5	51.0
Blue	10 000	1.10356	0.89769	1.00944	0.5	51.4

Table 5.1: Rank-1 laminate configurations for a three dimensional boundary-value problem with no shear strain considered at contrasts of $\{10^x,\ x = 1, 2..., 4\}$ and corresponding longitudinal, perpendicular and transverse stretch determined at an applied nominal electric field of 100 MV/m. Configurations are presented in figures 5.3, 5.4(a) and 5.4(b).

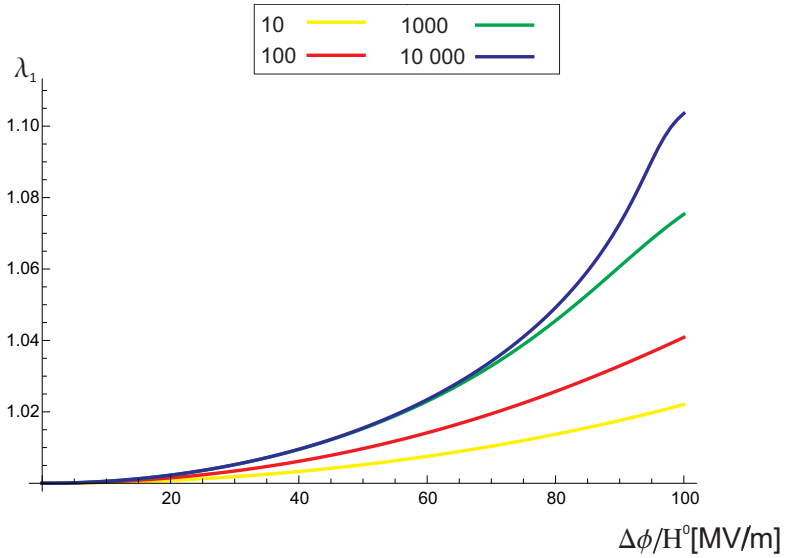

Figure 5.3: Influence of applied nominal electric field on maximum longitudinal stretch at contrasts of $\{10^x,\ x = 1, 2..., 4\}$ for rank-1 laminates relating to a three dimensional boundary-value problem with no shear strains. Configurations are presented on table 5.1.

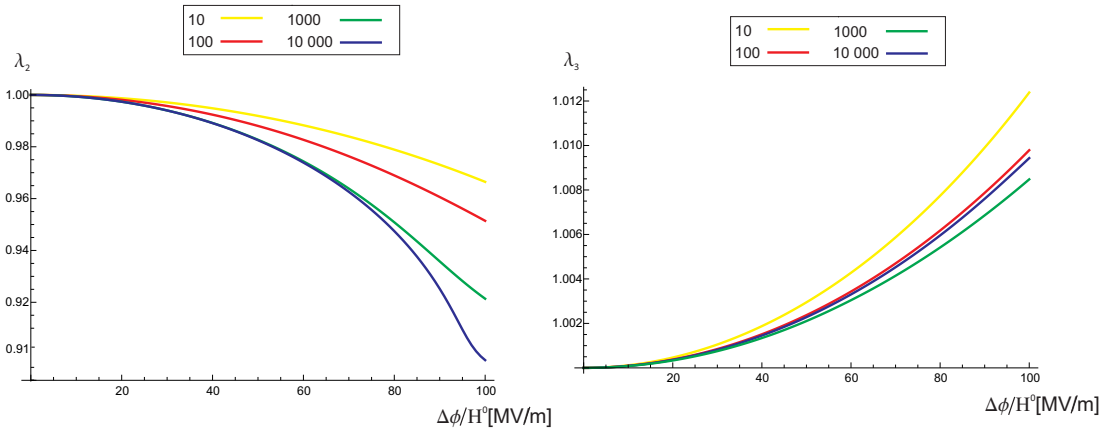

Figure 5.4: Influence of applied nominal electric field on (a) Perpendicular stretch and (b) transverse stretch at contrasts of $\{10^x,\ x = 1, 2..., 4\}$ for rank-1 laminates relating to a three dimensional boundary-value problem with no shear strains. Configurations are presented on table 5.1.

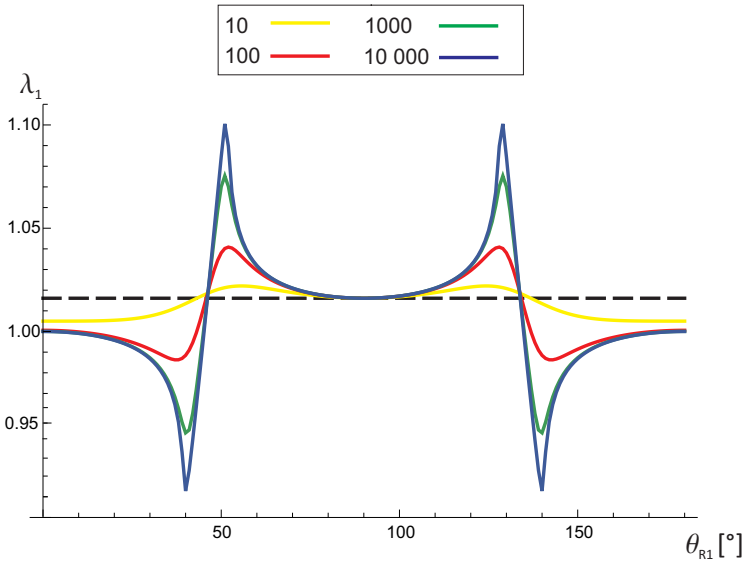

Figure 5.5: Influence of lamination angle on maximum longitudinal stretch at contrasts of $\{10^x, x = 1, 2..., 4\}$ for rank-1 laminates relating to a three dimensional boundary-value problem with no shear strains. Dotted line refers to a soft material such that the actuation is homogeneous. Configurations are presented on table 5.1.

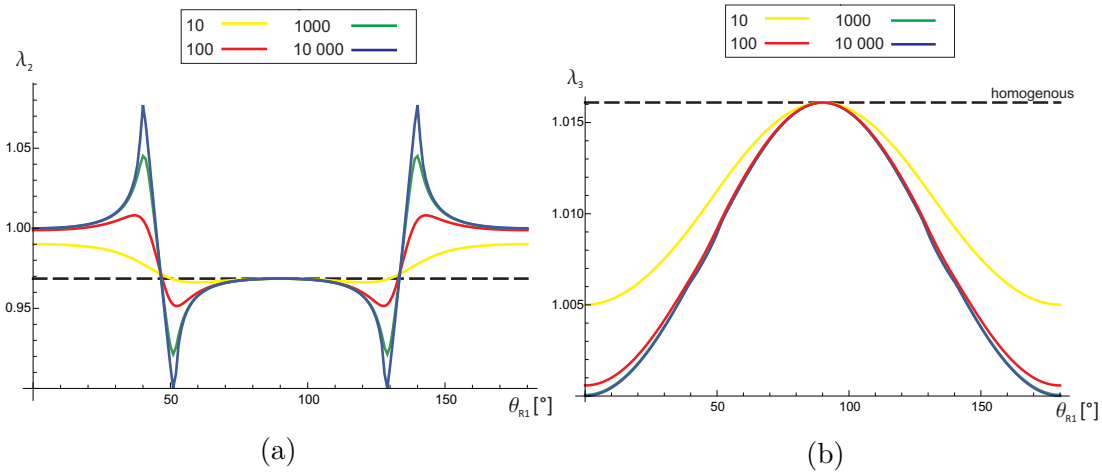

Figure 5.6: Influence of lamination angle on (a) Perpendicular stretch and (b) transverse stretch at contrasts of $\{10^x, x = 1, 2..., 4\}$ for rank-1 laminates relating to a three dimensional boundary-value problem with no shear strains. Dotted line refers to a soft material such that the actuation is homogeneous. Configurations are presented on table 5.1.

5.2.3 Initial optimisation: rank-2 laminates

For a rank-2 laminate, we will execute a similar initial approach as completed for the rank-1 equivalent in section 5.2.1. Figure 5.7(a) displays the influence of increasing electric field on maximum longitudinal stretch at a contrast of 100 which has an optimum configuration with $\theta_{R1} = 51.2°$, $\theta_{R2} = -1°$, $C^B_{R1} = 0.501$ and $C^{R1} = 0.965$. Figure 5.7(b) shows a comparison between the red curve in figure 4.12 for a contrast of 100 in plane strain, which is also curve C_3 from section 4.3.4, and the λ_1 curve in figure 5.7(a). As evident, there is only a 0.14% difference in the values corresponding with λ_{max} for these two boundary-value problems. Therefore as in the rank-1 boundary-value problem, using the method of lamination presented in this study, the overall stretch in a plane strain boundary-value problem can be used to approximate the longitudinal stretch in a three-dimensional boundary-value problem for rank-2 laminates when shear is not considered. This can be attributed to the minimal change in transverse stretch which implies that the perturbation of the laminate longitudinally is in a manner analogous to the plain strain boundary-value problem.

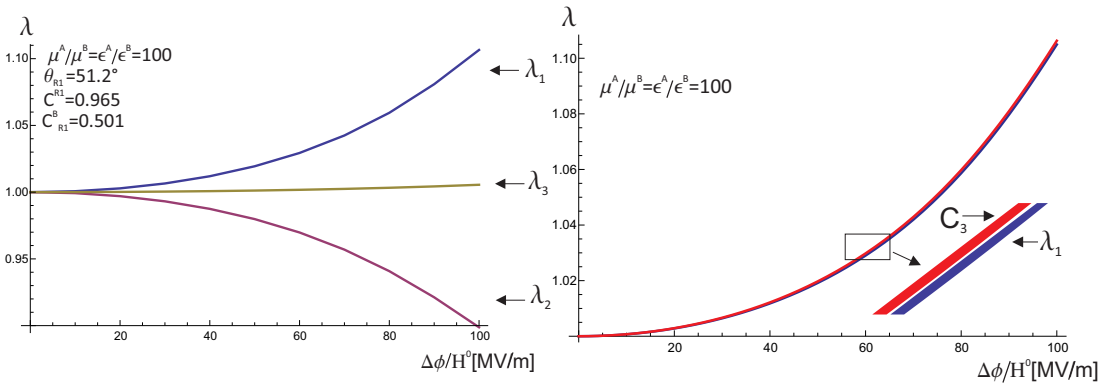

Figure 5.7: (a) Influence of increasing applied nominal electric field on longitudinal stretch (blue curve), perpendicular stretch (purple curve) and transverse stretch (yellow curve) at a contrast of 100 for a rank-2 laminate. (b) Rank-2 laminate in a three-dimensional boundary-value problem (blue curve) compared with curve C_3 from section 4.3.4 for increasing applied nominal electric field and corresponding longitudinal strain at a contrast of 100.

The variation of θ_{R1} and θ_{R2} with λ_1, λ_2 and λ_3 is also presented in figure 5.8 for the optimum configuration at a contrast of 100. Once again the occurrence of maximum λ_1 at the minimum value of λ_2 is found to be present with λ_3 maintaining near-constant behaviour throughout the range presented. For $\theta_{R2} = -1°$ in figure 5.8(a), it is presented that there is symmetry due to the fact that the lamination angle of the rank-2 laminate is almost zero, implying a near horizontal position of the soft homogeneous phase. For $\theta_{R1} = 51.2°$ in figure 5.8(b), varying

θ_{R2} for optimum configuration at a contrast of 100 reveals the non-linear nature of this investigation in a new manner. At $\theta_{R2} = -51.2°$ and $\theta_{R2} = 51.2°$, the rank-2 lamination angles are exactly parallel to each other such that the configuration is that of a rank-1 laminate. This is illustrated by the appearance of near constant λ in figure 5.8(b) at points near these aforementioned values.

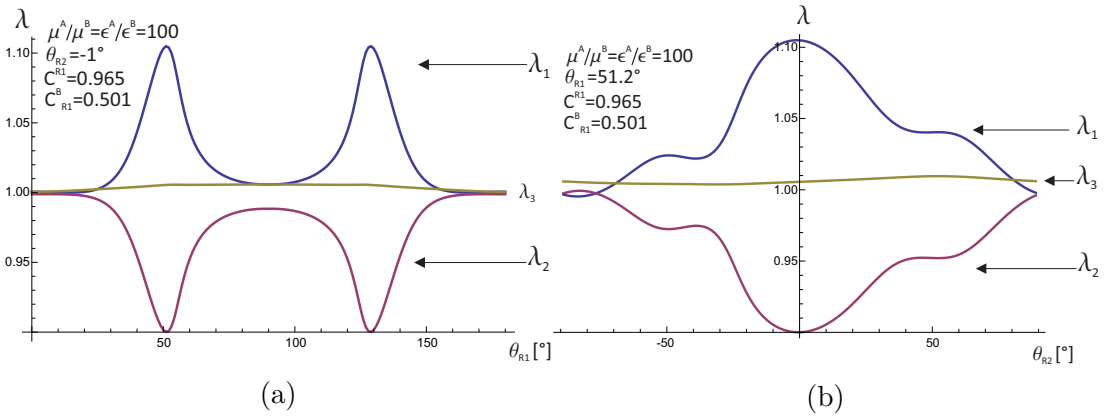

Figure 5.8: Influence of evolving (a) lamination angle of embedded rank-1 in rank-2 laminate for the range $0° \leq \theta_{R1} \leq 180°$ and (b) rank-2 lamination angle for the range $-90° \leq \theta_{R2} \leq 90°$ on longitudinal stretch (blue curve), perpendicular stretch (purple curve) and transverse stretch (yellow curve) at a contrast of 100.

Figures 5.8(a) and 5.8(b) collectively show that for a rank-2 laminate, the lamination angle of the rank-1 anisotropic phase embedded in the rank-2 laminate has a greater influence on the optimisation of λ_1, as compared to the lamination angle of the rank-2 laminate. A reason for this is that the anisotropic phase, as observed for rank-2 laminates so far, occupies a greater proportion of the rank-2 laminate in terms of volume fraction (i.e. $C^{R1} = 0.965$) and combining this with the fluctuation of the electric field due to the anisotropy means that when this lamination angle is perturbed a greater fluctuation in λ_{max} would be observed. The lamination angle of the rank-2 laminate can rather be described as having an effect on the electromechanical stability as can be observed by its influence on the unpredictable fluctuation of λ in figure 5.8(b). However the contribution of θ_{R2} due to the enhancement of the rank-2 longitudinal stretch should not be entirely neglected as holistically, it is the combination of the four factors relating to the rank-2 laminate discussed in section 3.3.2 that are key to the performance enhancement of rank-2 laminates.

5.2.4 Influence of increasing contrast on rank-2 laminates

Non-monotonic behaviour of rank-2 laminates in 3D

We have already established the trade-off required between minimising observable electromechanical instability and maximising λ_{max} in section 4.3.4 and this trade-off shall now be presented for a three-dimensional boundary-value problem. The effect of increasing applied nominal electric field on λ is presented in figures 5.9 and 5.10 for each direction of stretch. For λ_1, the presented behaviour can be compared to that observed for longitudinal stretch in figure 4.12. Two new directions in which this electromechanical instability can be observed are now present i.e. λ_2 and λ_3. At contrasts of 1000 and 10 000, electromechanical instability is observed in the three directions, with the transverse direction also presenting the specific point at which this is triggered in figure 5.9. This implies that for higher contrasts, there is a set electric field which triggers observable electromechanical instability in rank-2 laminates such that the transverse stretch becomes a transverse shrinking when electromechanical instability is triggered. For contrasts of 10 and 100, it is clear that no electromechanical instabilities are observable once again, with a steady increase in λ with increasing applied nominal electric field also evident. One observation on table 5.2 with regards to C^{R1} is that it is increasing with increasing contrast while θ_{R2} is becoming more negative with increasing contrast.

Now considering figure 5.9(a) and 4.12, it is evident that for contrasts of 1000 and 10 000, one value of applied nominal electric field can provide more than one corresponding value of λ, this then implies that the Newton-Raphson method may present some difficulty when applied nominal electric field is used as the independent variable. In section 4.3.2 it was emphasised how the electromechanical loading path for these contrasts produced curves only just within the range between 0 and 100 MV/m. Thus for rank-2 laminate optimisation it is advisable to utilise a two-step method of first determining the optimum configuration at the applied nominal electric field required, and only then, having established the corresponding λ_{max}, using this as a guideline for visualising the electromechanical loading path using λ as the independent variable to ensure this path also lies within a specific range.

Curve	$\mu^A/\mu^B = \epsilon^A/\epsilon^B$	λ_1	λ_2	λ_3	C^B_{R1}	$\theta_{R1}[^\circ]$	C^{R1}	$\theta_{R2}[^\circ]$
Yellow	10	1.02245	0.96828	1.01009	0.554	53.5	0.875	5.1
Red	100	1.10494	0.90007	1.00551	0.501	51.2	0.965	-1.0
Green	1000	1.85543	0.53601	1.00550	0.493	60.0	0.987	-9.0
Blue	10 000	2.00846	0.49706	1.00167	0.509	57.0	0.993	-9.0

Table 5.2: Rank-2 laminate configurations for a three dimensional boundary-value problem with no shear strain considered at contrasts of $\{10^x,\ x = 1, 2..., 4\}$ and corresponding longitudinal, perpendicular and transverse stretch determined at an applied nominal electric field of 100 MV/m. Configurations are presented in figures 5.9 and 5.10.

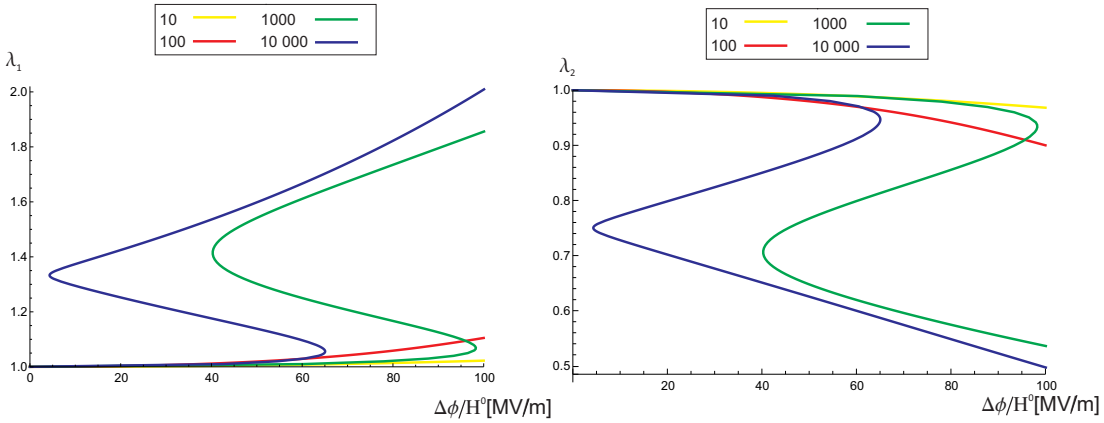

Figure 5.9: Influence of lamination angle on (a) maximum longitudinal stretch and (b) perpendicular stretch at contrasts of $\{10^x,\ x = 1, 2..., 4\}$ for rank-2 laminates relating to a three dimensional boundary-value problem with no shear strains. Configurations are presented on table 5.2.

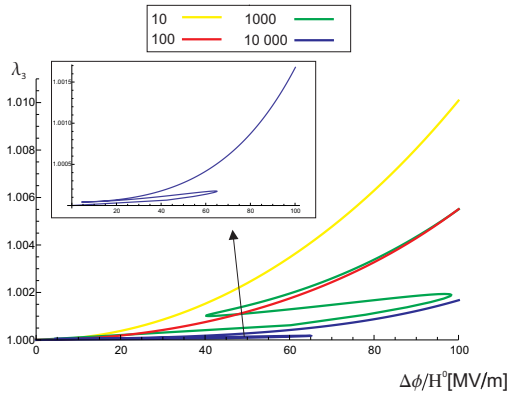

Figure 5.10: Influence of lamination angle on corresponding transverse stretch at contrasts of $\{10^x,\ x = 1, 2..., 4\}$ for rank-2 laminates relating to a three dimensional boundary-value problem with no shear strains considered. Blue curve is enhanced with corresponding configurations presented on table 5.2.

An optimisation for strict monotonic behaviour

In a manner analogous to that executed in section 4.3.3, an attempt shall be made at optimising the rank-2 laminates presented in figures 5.9 and 5.10 in order to determine example configurations which present the limit of monotonic behaviour. We have already established in section 5.2.3 that θ_{R1} contributes to greater fluctuation of λ_{max} when perturbed as compared to θ_{R2}. Using this observed stronger influence of θ_{R1}, it was discovered that θ_{R1} presented the most influential change on the presence of monotonic behaviour for the range of applied nominal electric field up to 100 MV/m, as also presented earlier in section 4.3.3. Thus in order to produce a configuration that presents strict monotonic behaviour, this discovery was applied by maintaining all other parameters to those on table 5.2 and strictly perturbing θ_{R1} initially then visualising the electromechanical loading path before optimising the remaining parameters. The configurations corresponding to types of geometries at the limit of monotonic behaviour are presented on table 5.3. During this process, we have already presented the absolute maximum longitudinal stretch and the corresponding configurations such that it is not vital to emphasise or discuss other parameters as this would reflect a "sub-optimum" configuration which we are not concerned with. This section merely focuses on which of the four variables mentioned in section 3.3.2 provides the greatest weighting with regards to the trade-off required between λ_{max} and stability so as to present sample configurations in a three-dimensional environment, as already performed in plane strain. It is obvious that an infinite number of configurations are possible if one only requires to observe monotonic behaviour.

Curve	$\mu^A/\mu^B = \epsilon^A/\epsilon^B$	λ_1	λ_2	λ_3	C^B_{R1}	$\theta_{R1}[^\circ]$	C^{R1}	$\theta_{R2}[^\circ]$
Yellow	10	1.02245	0.96828	1.01009	0.554	53.5	0.875	5.1
Red	100	1.10494	0.90007	1.00551	0.501	51.2	0.965	-1.0
Green	1000	1.45765	0.69390	1.00312	0.507	52.0	0.985	-8.0
Blue	10 000	1.51682	0.65872	1.00085	0.506	49.3	0.993	-12.0

Table 5.3: Rank-2 laminate configurations for figures 5.11(a), 5.11(b) and 5.12 at contrasts of $\{10^x,\ x = 1, 2..., 4\}$ for rank-2 laminates relating to a three dimensional boundary-value problem with no shear strains considered for sample geometries at the limit of monotonic behaviour.

The curves relating to the limit of monotonic behaviour are presented in figures 5.11 and 5.12 in the same manner as that performed for the rank-2 optimum configurations. What is initially evident is that the longitudinal stretch has decreased due to the reduction in angle of the anisotropic phase, in agreement with figure 5.8(a) and 4.15. Mention has already been made of an inflexion point at higher contrasts for the optimum configurations but in figure 5.12 the transverse stretch reveals the exact point at which the concavity of curves changes for configurations which present the limit of monotonic behaviour. This point can be described as relating to a point in the evolution of the laminate at which

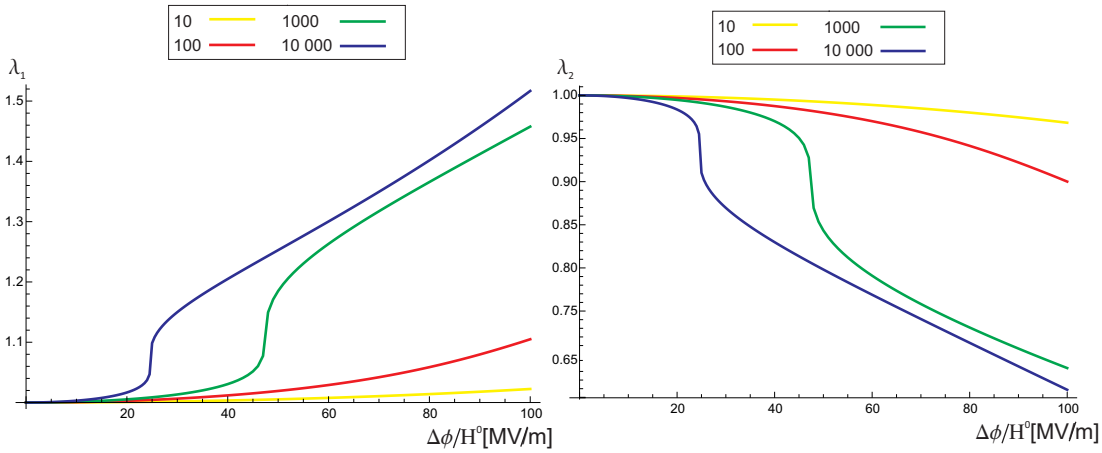

(a) (b)

Figure 5.11: Influence of applied nominal electric field for rank-2 laminates on (a) maximum longitudinal stretch and (b) perpendicular stretch at contrasts of $\{10^x,\ x = 1, 2..., 4\}$ for rank-2 laminates relating to a three dimensional boundary-value problem with no shear strains considered for strict monotonic behaviour.

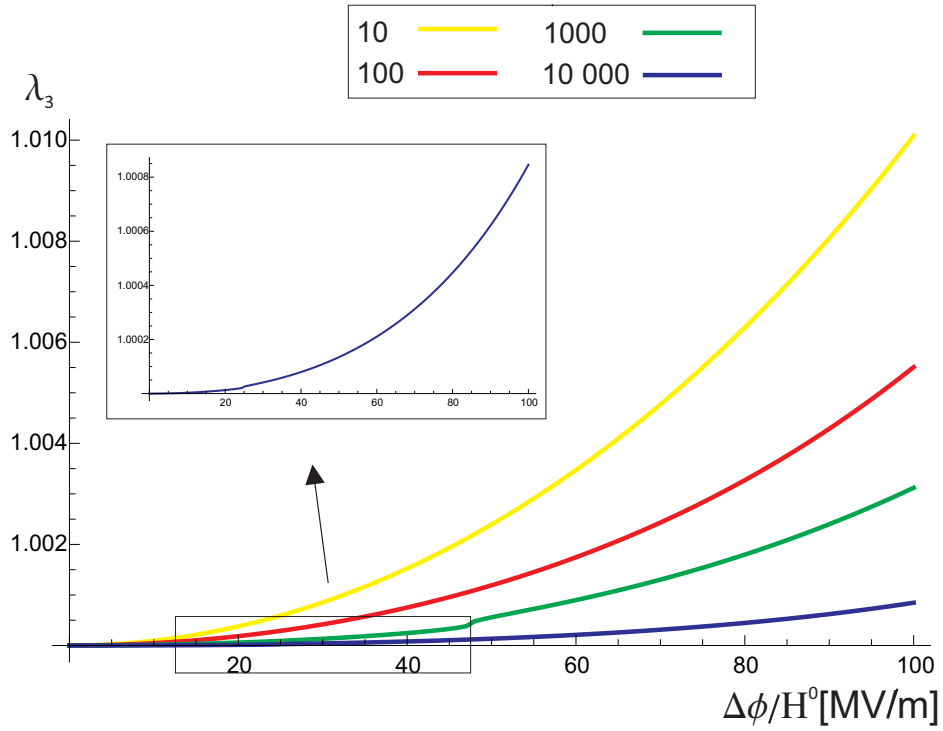

Figure 5.12: Influence of applied nominal electric field on transverse stretch at contrasts of $\{10^x,\ x = 1, 2..., 4\}$ for rank-2 laminates relating to a three dimensional boundary-value problem with no shear strains considered showing showing the position at which electromechanical instability is triggered at contrasts of 1000 and higher.

λ increases greatly as applied nominal electric field is increased. For contrasts of 1000 and 10 000, the corresponding points lie when $\Delta\phi/H^0$ =46 MV/m and $\Delta\phi/H^0$ =24 MV/m respectively. This demonstrates that when considering tri-axial stretch, λ_3 provides crucial information towards the overall behaviour of rank-2 laminates that cannot be obtained under plane strain.

5.3 Tri-axial stretch with in-plane vanishing tractions

5.3.1 Influence of increasing contrast on rank-1 laminates

Having already considered laminates in a three-dimensional configuration as well as laminates with vanishing in-plane tractions, let us now consider laminates whose behaviour is characterised by both of these phenomena, combined. The expected deformation gradient is therefore given as

$$\boldsymbol{F}^{\text{av}} = \begin{bmatrix} \lambda_1 & \xi\lambda_2 & 0 \\ 0 & \lambda_2 & 0 \\ 0 & 0 & \frac{1}{\lambda_1\lambda_2} \end{bmatrix}, \qquad [5.2]$$

where all of the following conditions are enforced

$$S_{11}^{\text{av}} = 0, \qquad S_{12}^{\text{av}} = 0, \qquad S_{22}^{\text{av}} = 0, \qquad S_{33}^{\text{av}} = 0. \qquad [5.3]$$

The assignment of λ_1, λ_2 and λ_3 applies in the same manner as that earlier utilised in this chapter. The optimum configurations for rank-1 laminates are presented on table 5.4, which can be compared with table 4.2. Stretch λ_{max} has decreased from the plane strain boundary-value problem while ξ has increased. The liberation of the perpendicular and transverse stretch has allowed for deformation to be experienced in these directions such that the amount of shear has increased. For the soft material such that the actuation is homogeneous, $\lambda_1 = \lambda_3$, confirming the assumptions made in the example boundary-value problem in section 2.6.1. With increasing contrast, the effects of λ_1 are enhanced as also shown in figure 5.13. One condition however, remains immutable, acting as further confirmation of already presented results. The optimum volume fraction is 0.5 at all investigated contrasts. The lamination angle has changed only slightly with increasing contrast implying that, once one determines the optimum lamination angle at any contrast where the ratio of the shear and dielectric moduli are equal, this can be assumed to be optimum at all contrasts for rank-1 laminates under the same conditions. Also comparing figures 5.14 and 5.4, when shear strains are considered there is evidently little to no variation in λ_2 with increasing contrast.

Curve	$\mu^A/\mu^B = \epsilon^A/\epsilon^B$	λ_1	λ_2	λ_3	ξ	C^B_{R1}	$\theta_{R1}[^\circ]$
Black	Homogeneous	1.01610	0.96857	1.01610	0		
Yellow	10	1.01951	0.96876	1.0125	-0.00968	0.5	56.1
Red	100	1.02097	0.96885	1.01095	-0.01388	0.5	56.0
Green	1000	1.02115	0.96885	1.01077	-0.01437	0.5	56.0
Blue	10 000	1.02117	0.96886	1.01075	-0.01443	0.5	56.0

Table 5.4: Rank-1 laminate configurations for a three dimensional boundary-value problem with shear strain considered at contrasts of $\{10^x,\ x = 1, 2..., 4\}$ and corresponding amount of shear and longitudinal, perpendicular and transverse stretch determined at an applied nominal electric field of 100 MV/m. Dotted line refers to a soft material such that the actuation is homogeneous. Corresponding curves are in figures 5.13, 5.14(a) and 5.14(b).

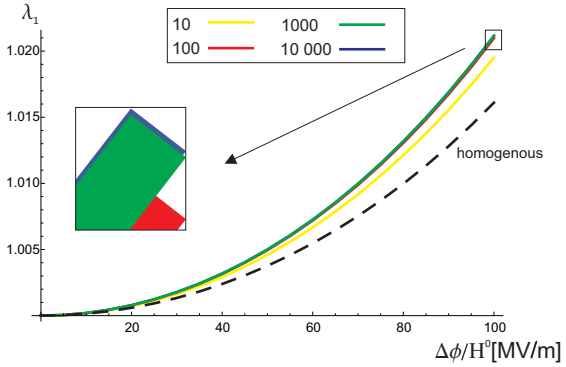

Figure 5.13: Influence of applied nominal electric field on maximum longitudinal stretch at contrasts of $\{10^x,\ x = 1, 2..., 4\}$ for rank-1 laminates relating to a three dimensional boundary-value problem with shear strains considered. Dotted line refers to a soft material such that the actuation is homogeneous. Configurations are presented on table 5.4.

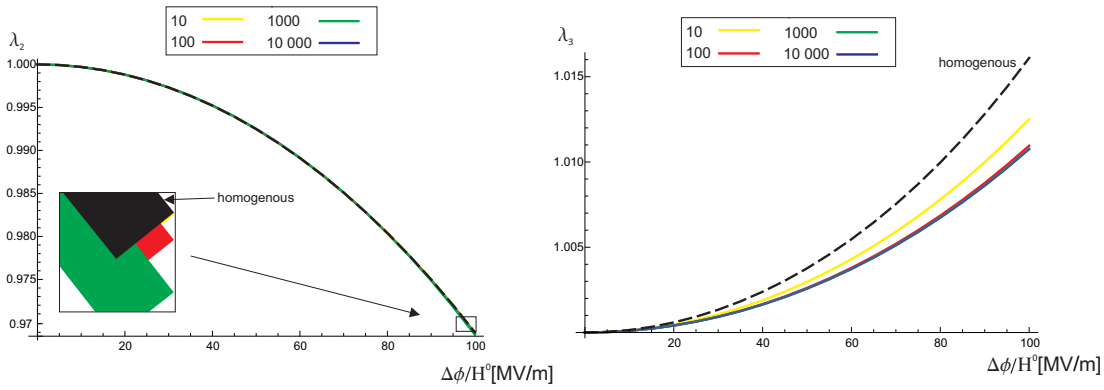

Figure 5.14: Influence of applied nominal electric field on (a) perpendicular stretch and (b) transverse stretch at contrasts of $\{10^x,\ x = 1, 2..., 4\}$ for rank-1 laminates relating to a three dimensional boundary-value problem with shear strains considered. Configurations are presented on table 5.4.

The influence of lamination angle on λ_{max} is also presented in figures 5.15 and 5.16 and the evolution presented is similar to that already presented in figures 5.5 and 5.6. What is interesting however is that the homogeneous value of λ_3 is greater than at all other contrasts. The value given for ξ for a soft material such that the actuation is homogeneous hints as to why this is so as it is evident that there is no shear experienced such that considerable stretch in proportion to the other directions is shifted to the transverse direction. There is also a dampening of fluctuation of λ_1 and λ_2 observed in comparison to figures 5.5 and 5.6. This dampening can also be observed if one compares the figures 4.2(b) and 4.10(b). Thus for rank-1 laminates, vanishing in-plane tractions lead to a reduction in maximum attainable longitudinal stretch, as well as dampening in the fluctuation of λ for a range of θ_{R1} angles.

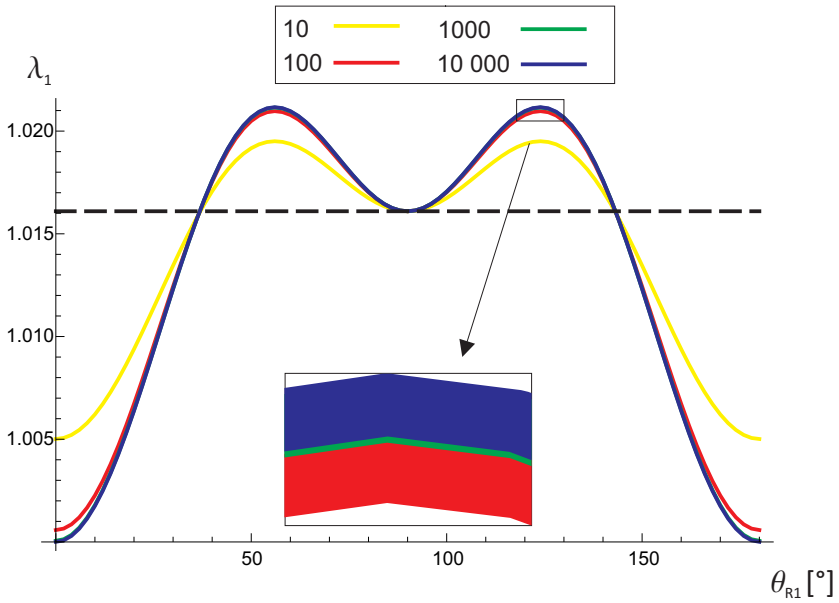

Figure 5.15: Influence of lamination angle on maximum longitudinal stretch at contrasts of $10^x, x = 1, 2..., 5$ for rank-1 laminates relating to a three dimensional boundary-value problem with shear strains considered. Dotted line refers to a soft material such that the actuation is homogeneous. Configurations are presented on table 5.4.

The presence of ξ likewise drives an optimisation process for ξ_{max} which will be compared to the plane strain boundary-value problem. Let us therefore determine rank-1 laminate configurations for maximum amount of shear in a three dimensional boundary-value problem with shear strain considered. Table 5.5 and figure 5.17 display the results of this optimisation process, showing behaviour comparable to that on table 4.3 and figure 4.4. The optimum lamination angle has increased by 0.1° for each corresponding configuration from the plane strain boundary value problem with shear strains considered. It is also observed

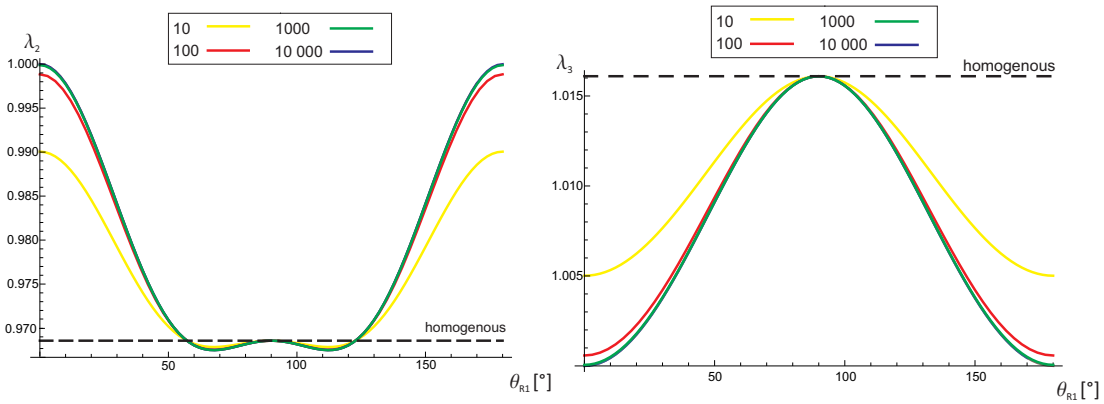

Figure 5.16: Influence of lamination angle on (a) perpendicular stretch and (b) transverse stretch at contrasts of $\{10^x,\ x = 1, 2..., 4\}$ for rank-1 laminates relating to a three dimensional boundary-value problem with shear strains considered. Configurations are presented on table 5.4.

that once again the shear at contrasts above 100 shows only infinitesimal change, while C^B_{R1} is optimum at 0.5 at all contrasts in figure 5.17(b) similar to all rank-1 boundary-value problems investigated so far.

Curve	$\mu^A/\mu^B = \epsilon^A/\epsilon^B$	ξ_{max}	λ_1	λ_2	λ_3	C^B_{R1}	$\theta_{R1}[^\circ]$
	Homogeneous	0	1.01610	0.96857	1.0161		
Yellow	10	-0.02047	1.01391	0.97862	1.00784	0.5	30.9
Red	100	-0.02988	1.01307	0.98271	1.00446	0.5	31.0
Green	1000	-0.02976	1.01297	0.98320	1.00407	0.5	31.0
Blue	10 000	-0.02998	1.01296	0.98325	1.00403	0.5	31.0

Table 5.5: Rank-1 laminate configurations optimised for maximum amount of shear for a three dimensional boundary-value problem with shear strain considered at contrasts of $\{10^x,\ x = 1, 2..., 4\}$ and corresponding longitudinal, perpendicular and transverse stretch determined at an applied nominal electric field of 100 MV/m. Corresponding curves are in figures 5.17(a) and 5.17(b).

5.3.2 Influence of increasing contrast on rank-2 laminates

Moving on to the more intricate problem regarding rank-2 laminates, the optimum configurations are presented on table 5.6 and the corresponding figures 5.18 and 5.19. What is immediately evident are the very high values of λ_{max} for contrasts of 1000 and 10 000. Compare this with the enhancement experienced for rank-2 laminates for the plane strain boundary-value problem with shear strains considered on table 4.6. It is evident that boundary conditions which take into account shear strain for rank-2 laminates provide a significant enhancement of

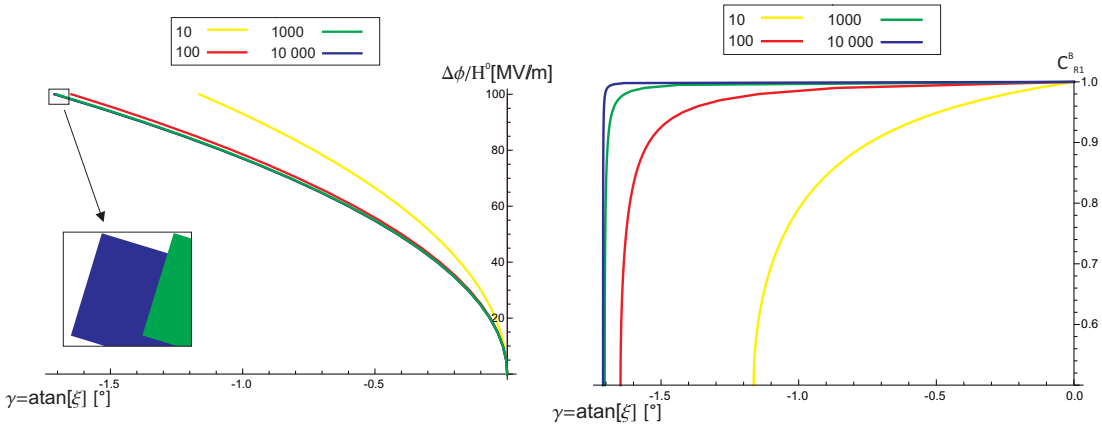

Figure 5.17: (a) Influence of increasing applied nominal electric field on Shear angle and (b) influence of volume fraction on shear angle for a three dimensional boundary-value problem with shear strain considered at contrasts of $\{10^x,\ x = 1, 2..., 4\}$ for rank-1 laminates. Corresponding configurations are presented on table 5.5.

λ_{max} from their rank-1 equivalents.

On figure 5.19(a), the curve relating to λ_2 presents a similar evolution the its corresponding λ_1 curve, as would be expected by now. However with regards to λ_3, some new non-linear performance is observed. Unexpectedly, λ_3 corresponding to a contrast of 10 000 shows the largest value, while the new behaviour is such that the curve relating to a contrast of 10 presents the second largest value for λ_3 at $\Delta\phi/H^0$ =100 MV/m. What this reveals is a higher out of plane stretch occurring at a contrast of 10 000 than a contrast of 10 due to the much higher amount of shear.

Curve	$\mu^A/\mu^B = \epsilon^A/\epsilon^B$	λ_{max}	λ_2	λ_3	ξ	C^B_{R1}	$\theta_{R1}[°]$	C^{R1}	$\theta_{R2}[°]$
Yellow	10	1.02231	0.96866	1.00982	0.00039	0.562	55.4	0.824	5.5
Red	100	1.12312	0.88476	1.00726	0.11421	0.508	64.4	0.964	11.0
Green	1000	2.32532	0.42543	1.01086	1.53061	0.501	85.0	0.986	25.0
Blue	10 000	7.30968	0.13508	1.01307	6.23386	0.496	90.0	0.99	47.0

Table 5.6: Rank-2 laminate configurations for a three dimensional boundary-value problem with shear strain considered at contrasts of $\{10^x,\ x = 1, 2..., 4\}$ and corresponding amount of shear and longitudinal, perpendicular and transverse stretch determined at an applied nominal electric field of 100 MV/m. Corresponding curves are in figures 5.18, 5.19(a) and 5.19(b).

Table 5.7 and figure 5.20 display the resulting curves for ξ_{max} optimisation with notice taken of the fact that the shear angle has been limited to not go beyond -40° in figure 5.20, in a manner analogous to figure 4.7. This is due to an attempt to reduce the effect of shear strain as earlier described in section 4.2.4 as

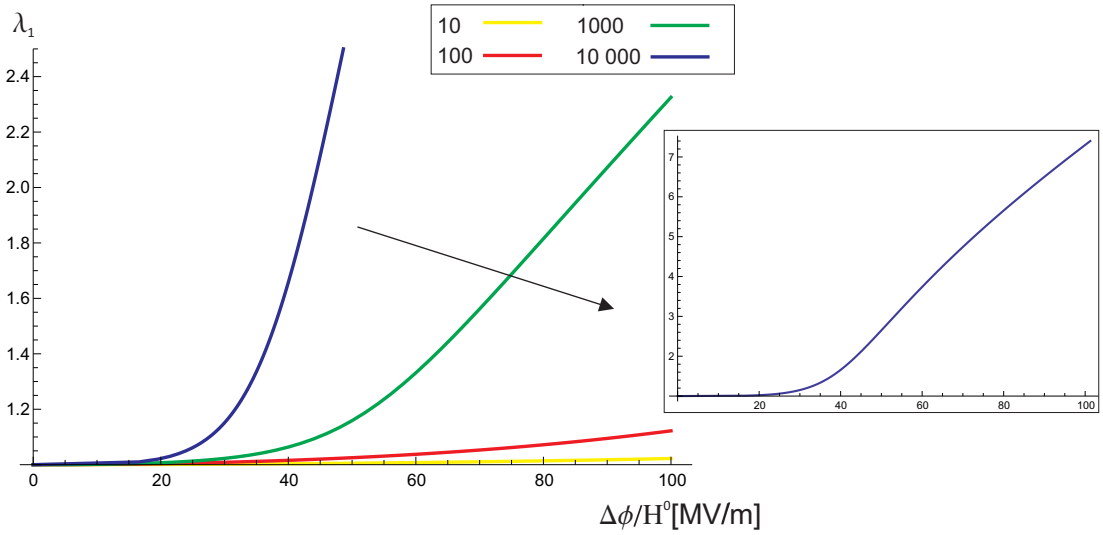

Figure 5.18: Influence of lamination angle on maximum longitudinal stretch at contrasts of $\{10^x,\, x = 1, 2..., 4\}$ for rank-2 laminates relating to a three dimensional boundary-value problem with shear strains considered. Sub-image displays the full curve at a contrast of 10 000. Configurations are presented on table 5.6.

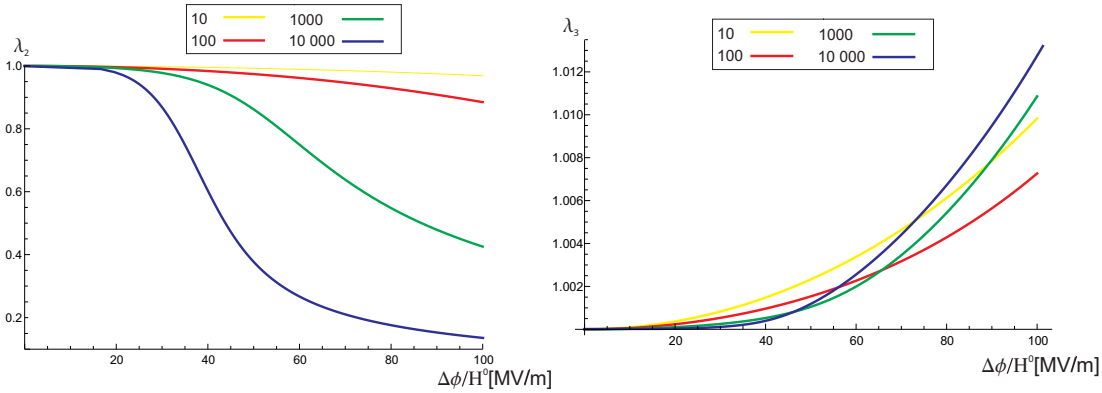

(a) (b)

Figure 5.19: Influence of lamination angle on (a) perpendicular stretch and (b) transverse stretch at contrasts of $\{10^x,\, x = 1, 2..., 4\}$ for rank-2 laminates relating to a three dimensional boundary-value problem with shear strains considered. Configurations are presented on table 5.6.

high shear strains imply high shear forces present at interfaces possibly leading to failure of the composite. Thus, despite the fact that in both plane strain and three-dimensional problems with in-plane vanishing tractions the improvement of λ_{max} is highly favourable, it is crucial that a trade-off between λ_{max} and ξ is accomplished in microstructure optimisation. It is therefore possible that optimisation in terms of ξ can be used to minimise shear strains as well as determine contrasts which provide acceptable shear strains. Comparing figure 5.20 with

figure 4.7, the curves show some similarities in terms of varying orientation with contrast, however at contrasts of 10 and 1000 the overall inclinations of the rank-2 laminate have become negative. This can be attributed to the additional out of plane behaviour now possible in a three-dimensional environment as compared to the plane strain problem in figure 4.7. This also explains the difference in curvature in plane strain in figure 4.7 and three-dimensions in figure 5.20 at a contrast of 1000. This further enforces the fact that a three-dimensional environment contributes to improved electromechanical stability of rank-2 laminates by liberating the transverse direction in which the laminate may reorient itself with increased electrical excitation.

Curve	$\mu^A/\mu^B = \epsilon^A/\epsilon^B$	ξ_{max}	λ_1	λ_2	λ_3	C^B_{R1}	$\theta_{R1}[^\circ]$	C^{R1}	$\theta_{R2}[^\circ]$
Yellow	10	-0.02047	1.01382	0.97873	1.00781	0.499	30.9	0.998	30.9
Red	100	0.27005	1.06063	0.93437	1.00906	0.505	90.0	0.965	34.1
Green	1000	1.98480	2.3142	0.42733	1.01118	0.505	90.0	0.987	23.0
Blue	10 000	-21.35195	7.07379	0.13997	1.00999	0.499	59.0	0.993	-90.0

Table 5.7: Rank-2 laminate configurations optimised for maximum amount of shear for a three dimensional boundary-value problem with shear strain considered at contrasts of $\{10^x, x = 1, 2..., 4\}$ and corresponding longitudinal, perpendicular and transverse stretch determined at an applied nominal electric field of 100 MV/m. Corresponding curves within the range -$40^\circ \leq \gamma \leq 40^\circ$ are presented in figure 5.20.

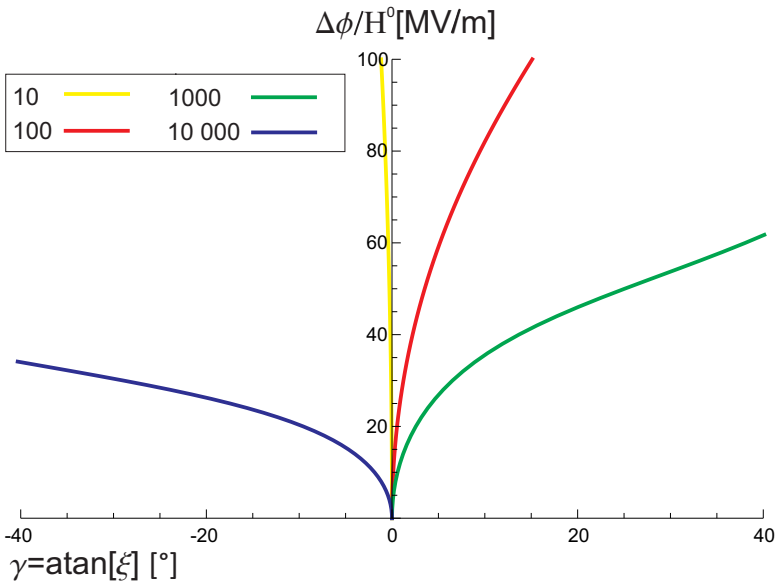

Figure 5.20: Influence of increasing applied nominal electric field on Shear angle and for a three dimensional boundary-value problem with shear strain considered at contrasts of $\{10^x, x = 1, 2..., 4\}$ for rank-2 laminates limited to the range -$40^\circ \leq \gamma \leq 40^\circ$. Corresponding configurations are presented on table 5.5.

5.4 Comparison between three-dimensional boundary value problems for rank-2 laminates

In a manner analogous to that executed in section 4.3.4, A comparison of the influence of shear strains on three-dimensional behaviour shall be executed. The configurations can be described as follows, curves titled Q_1 relate to a configuration that provides λ_{max} where $\lambda_1 = \lambda_{max}$ at a contrast of 1000 when shear strains are considered, identical to the green curves in figures 5.18 and 5.19. Curves titled Q_2 relate to a configuration optimised for ξ_{max} at a contrast of 1000, identical to the green curve in figure 5.20. Curves Q_3 and Q_4, in a manner analogous to that executed for contrasts of 100 and 1000 in section 4.3.4, represent corresponding stretches for identical configurations when shear strains are considered, and when they are not considered, respectively. Curves presented for Q_4 are identical to the green curves presented in section 5.2.4 in figures 5.9 and 5.10. Due to the three-dimensional environment, it is now possible to compare the influence of shear for perpendicular and transverse stretch as well.

Curve	λ_1	λ_2	λ_3	ξ	C^B_{R1}	$\theta_{R1}[^\circ]$	C^{R1}	$\theta_{R2}[^\circ]$
Q_1	2.32532	0.42543	1.01086	1.53061	0.501	85.0	0.986	25.0
Q_2	2.3142	0.42733	1.01118	1.98480	0.505	90.0	0.987	23.0
Q_3	2.16782	0.45798	1.00723	-0.40509	0.493	60.0	0.987	-9.0
Q_4	1.85543	0.53601	1.00550		0.493	60.0	0.987	-9.0

Table 5.8: Various Rank-2 laminate configurations and corresponding longitudinal stretch and amount of shear at a contrast of 1000 and applied nominal electric field of 100 MV/m. Q_1 - optimum configuration when shear strains are considered, Q_2 - optimum configuration to obtain maximum amount of shear and corresponding longitudinal stretch, Q_3 - optimum configuration when shear strains are not considered and resulting longitudinal stretch and amount of shear when computed in an environment taking into account shear strain and Q_4 - optimum configuration when shear strains are not considered. Corresponding curves presented in figures 5.21 and 5.22.

From Q_4 to Q_3 an enhancement of longitudinal strain was obtained of 17%, which can be compared to the improvement obtained in section 4.3.4 in a plane-strain environment. Likewise, the elimination of non-monotonic behaviour was also observed from Q_4 to Q_3 confirming the fact that in terms of longitudinal stretch, the observable electromechanical instability can be reduced by considering shear strains. It should also be noted that a greater transverse stretch was obtained for Q_2 than for Q_1 for a greater amount of shear in figure 5.22(a), implying that the transverse direction may more than likely be able to provide information relating to the behaviour of a rank-2 laminate in terms of shear strain. On figure 5.22, It is evident that this particular contrast presents a bias towards positive shear inclination. However this performance presents a maximum amount of shear for both Q_1 and Q_2 outside of the range of $-40^\circ \leq \gamma \leq 40^\circ$

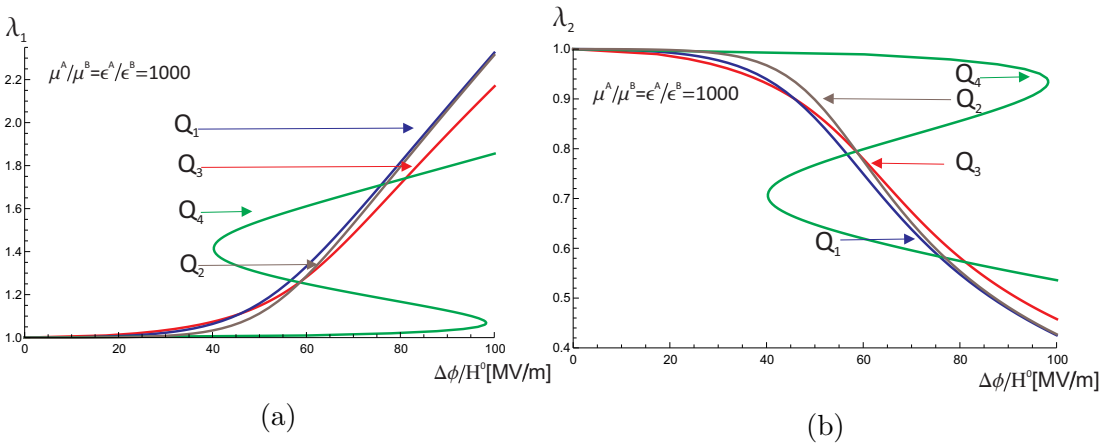

Figure 5.21: (a) Influence of increasing applied nominal electric field on (a) longitudinal stretch and (b) perpendicular stretch for laminate configurations Q_1, Q_2, Q_3 and Q_4 described on table 5.8.

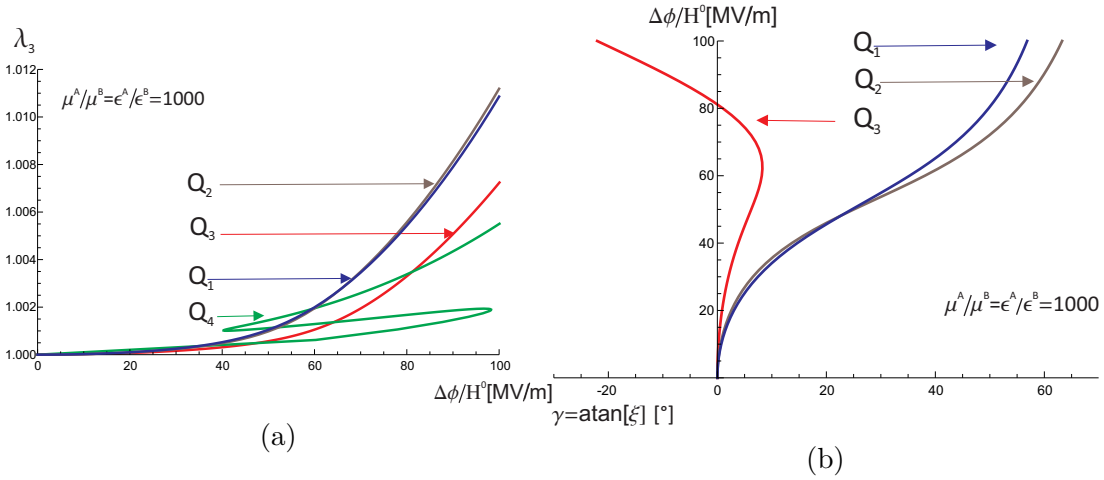

Figure 5.22: (a) Influence of increasing applied nominal electric field on transverse stretch for laminate configurations Q_1, Q_2, Q_3 and Q_4 presented on table 5.8. (b) Influence of applied nominal electric field on shear angle for laminate configurations Q_1, Q_2 and Q_3 presented on table 5.8.

previously mentioned in section 5.3.2. The difference between Q_3 and Q_2 in figure 5.22 completely illustrates the possibility of accomplishing a trade-off between λ and ξ when perturbing the microstructure of rank-2 laminates.

Another way these curves can be interpreted is to compare figures 5.22 and 4.19 in order to illustrate the ability of a three-dimensional environment to contribute to the electromechanical stability of rank-2 laminates. Configuration C_5 in figure 4.18(b) and Q_1 in figure 5.22(b) illustrate that non-monotonic behaviour can also be eliminated in terms of the shear angle evolution. These configura-

tions, as it should be emphasised, relate to λ_{max} therefore there has been no attempt to optimise ξ in any manner for C_5 and Q_1. Also, C_7 in figure 4.18(b) and Q_3 in figure 5.22(b) reflect similar curvature. This indicates that when transitioning from a constrained environment with no shear strains considered, to a liberated environment where shear strains are considered, electromechanical instability may manifest itself in the shear angle evolution of rank-2 laminates due to the change in concavity of Q_3 and C_7. This therefore means that even at low shear angles, there may be shear forces at the interfaces between phases due to the presence of electromechanical instability.

5.5 Conclusions

In this chapter it has been presented that

- Longitudinal stretch λ_1 in tri-axial strain can be used to approximate λ_{max} in plane strain for both rank-1 and rank-2 laminates.
- The rate of change of stretch with increasing applied nominal electric field of λ_1 is greater than the rate of change of stretch of perpendicular stretch, λ_2.
- When transitioning from boundary-value problems without shear strain considered to those with shear strain considered for rank-1 laminates, dampening of λ with varying θ_{R1} is present.
- The angle θ_{R1} is more dominant in determination of the optimum configuration that provides λ_{max} compared to θ_{R2}.
- At higher contrasts, shear angles are unsuitably high at λ_{max} such that a trade-off needs to be established between λ and ξ when optimising the microstructure of rank-2 laminates.
- When three-dimensional boundary value problems where compared with each other, a 17% enhancement of λ_{max} was obtained for the same configuration from tri-axial stretch with no shear strain considered to tri-axial stretch with shear strain considered at a contrast of 1000.

Chapter 6

Holistic design parameter optimisation

6.1 Introduction

So far, we have analysed the effective behaviour of rank-1 and rank-2 laminates with equal ratios of shear and dielectric moduli in the two phases. It has been presented that for the boundary-value problems in this study, an increase in contrast results in an increase in maximum attainable longitudinal stretch and shear strain from that of the previous contrast. This leaves one to wonder whether or not a material with unequal shear and dielectric ratios would provide enhancement in the same manner and if so, what the response would be for such a laminate under the presented boundary conditions. Therefore this chapter shall be dedicated to exactly this enquiry, followed by presenting the current configuration of the rank-2 laminates and phase electric fields of rank-2 laminates with these unequal ratios. This will then enable the development of a prescription for laminate design with the aim of establishing a framework for future studies.

6.2 Material with unequal shear and dielectric ratios

6.2.1 Initial optimisation: rank-1 and rank-2 laminates

Consider now, rank-1 and rank-2 laminates composed of materials "A" and "B" resembling soft actuators presented in figures 3.1 and 3.2, with proportions of shear and dielectric moduli presented in table 6.1.

In this arrangement, the shear modulus of the softer phase has been decreased to establish a softer material whose ratio of shear to dielectric moduli are not

μ^A	μ^B	ϵ^A	ϵ^B
10^3 MPa	0.1 MPa	$10^3\epsilon_0$	10 ϵ_0

Table 6.1: Shear and dielectric parameters of the stiff and less dielectric phase "A" and the softer, more dielectric phase "B" for a rank-1 and rank-2 laminate.

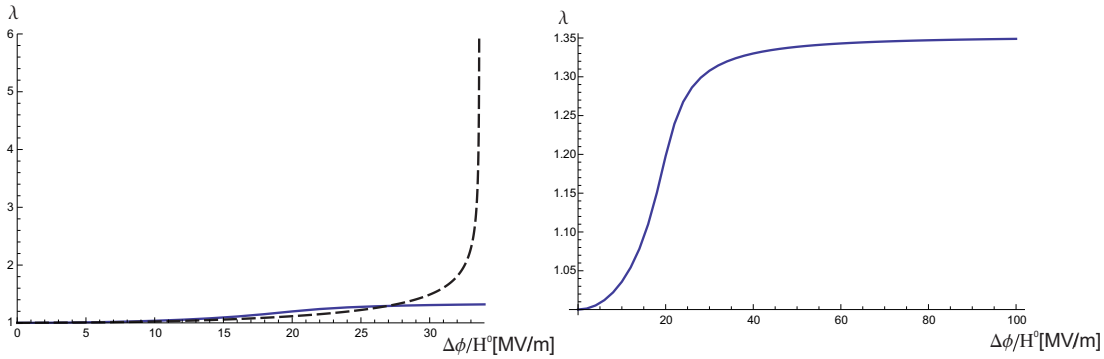

(a) (b)

Figure 6.1: Influence of increasing applied nominal electric field on maximum longitudinal stretch in plane strain with no shear strain considered at an applied nominal electric field of 20 MV/m for (a) homogeneous phase (black dashed line) and rank-1 laminate (blue curve) and (b) close up of rank-1 laminate. Corresponding λ values at $\Delta\phi/H^0$ =20 MV/m are presented on table 6.2.

equal. In the context of the contrasts presented in section 4.1, the dielectric ratio is 100 and the shear ratio is 10 000. The proportions of the shear and dielectric moduli can be likened to real world materials with material "A" referring to a contrast similar to that presented as poly(vinylidene fluoride) (PVDF) with $BaTiO_3$ nanowires, synthesized by Choi et al. (2016), while material "B" can be representative of a silicone-based material as presented by Skov et al. (2016). These ratios will initially be applied to rank-1 and rank-2 laminates with a deformation gradient and boundary conditions presented in section 4.3 such that the laminates are experiencing plane strain with no shear strains considered.

Figure 6.1(a) displays the homogeneous actuation of the soft phase of a rank-1 laminate with increasing applied nominal electric field with λ as the dependent variable. What is immediately apparent is that after $\Delta\phi/H^0 = 34$ MV/m, stiffening of the rank-1 laminate occurs while the homogeneous curve presents opposite behaviour in the form of infinite compliance. In order to provide favourable and optimum laminate configurations for the rank-2 laminate it would therefore be unwise to optimise the laminate at applied nominal electric fields higher than 34 MV/m. It should also be noted that behaviour of a similar nature was obtained by Gei et al. (2013) for higher applied nominal electric fields, thus confirming

these results. The fact that a rank-1 curve of this nature can be obtained when the stiffer phase is laminated with the homogeneous soft phase reveals the electromechanical coupling effect of a 2-phase laminate. Thus the applied nominal electric field, for purposes of investigating this set of shear and dielectric moduli, will be limited to 20 MV/m in order to ensure the behaviour experienced is in a region where electrical excitation presents a satisfactory electromechanical response.

The configurations providing λ_{max} for a rank-1 and rank-2 laminate are presented in table 6.2 and figure 6.2. With regards to the three curves in figure 6.2, λ_{max} has improved from the homogeneous value to the rank-1 and then further improved for the rank-2 laminate which is consistent with the general idea regarding this study. The rank-2 laminate in particular presents a remarkable variation in the evolution of the curve for λ with increasing applied nominal electric field. A drastic change in the gradient of the rank-2 curve is observed in the region $9\,\text{MV/m} \leq \Delta\phi/H^0 \leq 14$ MV/m. This behaviour is observed at a relatively low applied nominal electric field of 20 MV/m which can be attributed to the reduction in shear modulus of the softer phase "B" for the same dielectric modulus, increasing the electrical influence of this particular material.

What is also peculiar is the corresponding value of applied nominal electric field at which this behaviour begins to occur. If the stiffening in figure 6.1(b) occurred near 34 MV/m then one would expect that limiting this applied nominal electric field to 20MV/m would mean that only steady increase of λ would be observed. The reason why this variation in concavity occurs at this particular value of applied nominal electric field is most likely due to the fact that this region ($9\,\text{MV/m} \leq \Delta\phi/H^0 \leq 14$ MV/m) in figure 6.2 corresponds to the first observable difference in values for λ between the rank-2, rank-1 and a soft material such that the actuation is homogeneous as applied nominal electric field is increased. In the range $0\,\text{MV/m} \leq \Delta\phi/H^0 \leq 9$ MV/m, the corresponding values of λ in figure 6.2, indicated by the curvature, for the three curves are almost indistinguishable and only after this region is when the corresponding configuration of each composite begins to present an influence in the amplification of λ. A sharp increase in the curve corresponding to the rank-2 laminate is then observed at $\Delta\phi/H^0 = 13$ MV/m. This also means that, despite limiting applied nominal electric field to 20MV/m, the electrical excitation needs to be sufficiently high for a rank-2 laminate configuration to perform better than its rank-1 equivalent.

It is useful now to retrace the procedure executed in order to highlight the electromechanical enhancement that occurs when the shear and dielectric moduli are not equal. A soft material such that the actuation is homogeneous (figure 6.1) presented infinite compliance at approximately $\Delta\phi/H^0 = 34$ MV/m. Secondly,

Curve	λ_{max}	C^B_{R1}	$\theta_{R1}[^\circ]$	C^{R1}	$\theta_{R2}[^\circ]$
R1	1.19792	0.5	59.1		
R2	1.64039	0.51	57.0	0.939	-13.0
homogeneous	1.11543				

Table 6.2: Laminate configurations and corresponding maximum longitudinal stretch using contrasts presented on table 6.1 for a boundary-value problem of plain strain with no shear strains considered at an applied nominal electric field of 20 MV/m. Corresponding curves are presented in figure 6.2.

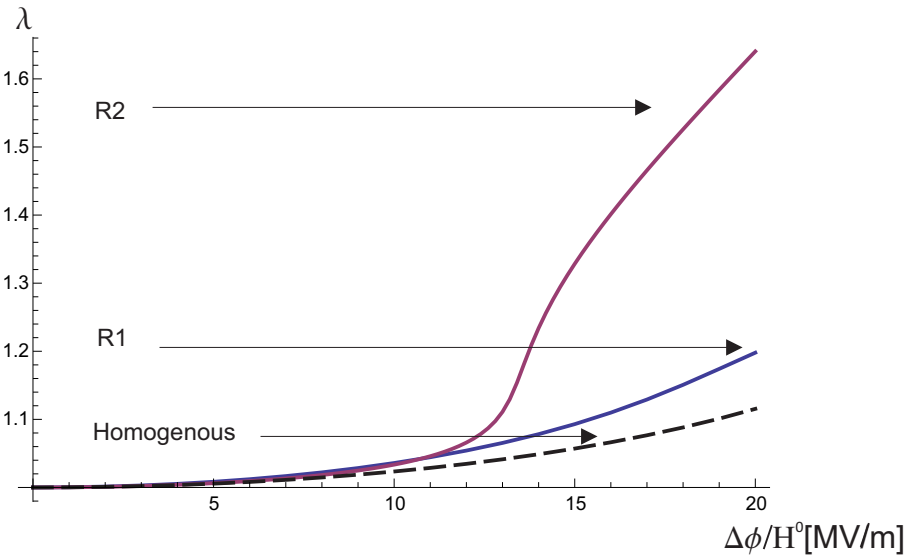

Figure 6.2: Influence of increasing applied nominal electric field on longitudinal stretch for rank-1, rank-2 and homogeneous softer material using contrasts presented on table 6.1 for a boundary-value problem of plain strain with no shear strains considered. Corresponding configurations are presented on table 6.2.

a rank-1 laminate, which is essentially the homogeneous soft phase, with a stiff phase now included at a weighted fraction of approximately half of the material, presented stiffening at approximately the same amount of applied nominal electric field. Then finally, we further only slightly reduce this stiff phase ($C^A_{R1} = 0.49$) when optimizing the rank-2 laminate on table 6.2 and observe indistinguishable behaviour at electrical excitations below 9 MV/m. The conclusion of this evolution when considering the three volume fractions of the rank-2 laminate on table 6.2, is that a stiff phase is not only required in order to provide a favourable contrast for electrical excitation, but it also contributes to the overall stability of both rank-1 and rank-2 laminates when shear and dielectric ratios are equal as well as unequal. This enhanced electromechanical stability then enables deformation to occur at sufficiently high electrical excitations to provide an enhancement in the longitudinal stretch of rank-1 and rank-2 laminates. It should also be considered that in terms of volume fractions, phase "$\mathrm{B_{R2}}$" is very small ($C^B_{R2} = 1 - C^{R1}$)

but its addition to the rank-1 laminate greatly improves the influence of applied nominal electric field in figure 6.2. Thus the influence of θ_{R1}, θ_{R2}, C^B_{R1} and C^{R1} is ever more present for rank-1 and rank-2 laminates whose shear and dielectric ratios are unequal.

6.2.2 A comparison between all boundary-value problems: rank-1 laminates

For rank-1 laminates, all four boundary-value problems previously studied will now be applied and compared. The shear and dielectric ratios presented on table 6.1 will be maintained. The applied nominal electric field will also be limited to 20 MV/m. The configurations obtained and the boundary-value problem for each are presented on table 6.3 and figures 6.3 and 6.4. With regards to plane strain, it is evident that λ_{max} is greater when shear strains are not considered in a manner consistent with that already presented earlier in section 4.3.4. The same phenomenon is observed for the three-dimensional equivalent boundary-value problems which is more than enough confirmation that if shear strains are not taken into account for rank-1 laminates then λ_{max} will be greater.

What is also important to note for these contrasts is that λ_{max} for a boundary-value problem of plane strain with no shear considered presents the largest value of λ_{max} throughout the whole study. This answers the initially posed argument in this chapter that a rank-1 laminate whose materials have unequal ratios of shear and dielectric moduli provides better enhancement of longitudinal stretch than contrasts where the ratios of contrasts and dielectric ratios are equal. Another observation is that the optimum volume fraction of the soft phase for all rank-1 laminates presented is 0.5 where there are equal amounts between hard and soft material in rank-1 laminates. This is similar to all other rank-1 laminates presented in this study.

Curve	Case	λ_{max}	λ_2	λ_3	ξ	C^B_{R1}	$\theta_{R1}[^\circ]$
Blue	Plane Strain	1.19792				0.5	59.1
Yellow	Plane strain with Shear strain	1.12836			-0.04661	0.5	63.0
Red	3D	1.19258	0.79132	1.05965		0.5	60.3
Green	3D with Shear strain	1.11592	0.83964	1.06727	-0.05776	0.5	63.0
Black	Homogeneous	1.11543					

Table 6.3: Rank-1 laminate configurations and corresponding maximum longitudinal stretch using contrasts presented on table 6.1 for various boundary-value problems at an applied nominal electric field of 20 MV/m. Corresponding curves are presented in figures 6.3 and 6.4.

A distinct working range is observed of the lamination angle of the rank-1 laminate on table 6.3 of $59^\circ \leq \theta_{R1} \leq 63^\circ$ for all boundary-value problems with

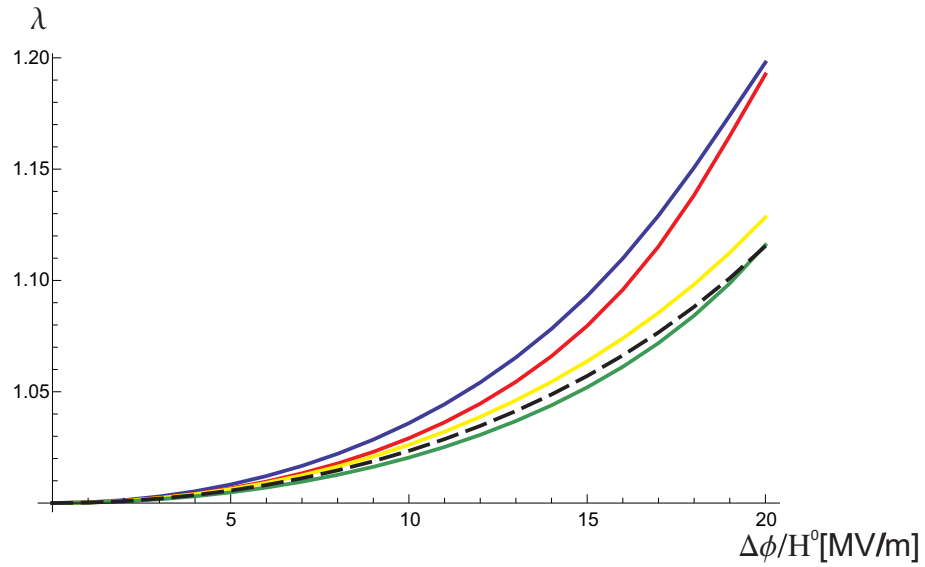

Figure 6.3: Influence of applied nominal electric field on longitudinal stretch for rank-1 laminates under various boundary-value problems at an applied nominal electric field of 20 MV/m. Corresponding configurations are presented on table 6.3.

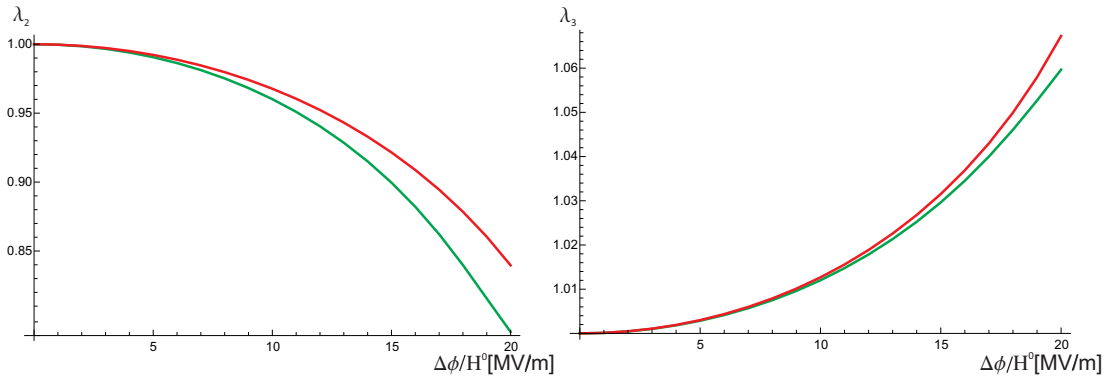

(a) (b)

Figure 6.4: Influence of increasing applied nominal electric field on corresponding (a) perpendicular stretch and (b) transverse stretch at an applied nominal electric field of 20 MV/m for rank-1 laminates sharing a three-dimensional environment. Green curves refer to a boundary-value problem when shear strains are considered and red to a boundary-value problem when shear strains are not considered. Corresponding configurations are presented on table 6.3.

the exact same optimum lamination angle observed for boundary-value problems where shear strains are considered in plane strain and three-dimensional environments. It is useful to discuss which boundary-value problem that would provide the most optimum as well as realistic behaviour for possible application. The boundary-value problems relating to plane strain provide an unrealistic behaviour as in reality, there would always be three dimensions to consider, despite

the fact that the boundary-value problem of plane strain with no shear strain considered provides the highest value of λ_{max}. This leaves the two boundary-value problems solved in a three dimensional environment, where it is evident that the boundary-value problem that does not take into account vanishing tractions in this environment provides the optimum performance. Indeed, a concern may now be that a more realistic representation of the composite would be to take into account shear in order to limit any high shear strains as established for figure 5.20 in section 5.3.2. However, as evident from the values for shear given on table 6.3, the shear angle in three-dimensions with shear strain considered only reaches -3° implying that the shear forces at the interfaces between the phases for a rank-1 laminate are relatively small. Amount of shear or ξ_{max} optimisation was also performed so as to fully justify this point. Maximum shear angles obtained were -7.4° for a boundary-value problem of plane strain with in-plane vanishing tractions and -7.8° for a boundary-value problem of tri-axial stretch with vanishing in-plane tractions. The implication of this is that for a rank-1 laminate it is possible that the amount of shear experienced in a plane strain environment is very close to that experienced in a three-dimensional environment. This is confirmed by comparing tables 4.3 and 5.5 which present shear optimisation results for the previous rank-1 laminates optimised when the shear and dielectric ratios were equal. This means that for rank-1 laminates not only can the longitudinal stretch plane strain be used to approximate that experienced in tri-axial stretch, but also the amount of shear can be approximated in a likewise manner.

One point to be mindful of is the fact that the value of θ_{R1}, when the configurations laminates relating to the yellow curve and green curve on table 6.3 and figure 6.4(a) are optimised for ξ_{max}, is not the same as previously presented on tables 4.3 and 5.5. Angle θ_{R1} at ξ_{max} for plane strain with shear strain considered was found to be 34.1° while that for tri-axial stretch with shear strain considered was found to be 35.7°. These values are important due to the fact that for all contrasts previously investigated whose ratios of shear to dielectric moduli were equal, θ_{R1} values at ξ_{max} were observed to be almost identical at all contrasts as displayed on tables 4.3 and 5.5. It is therefore apparent that a laminate with unequal shear and dielectric ratios reveals a new non-linear effect when performing optimisation for ξ_{max}. Thus the parameters influencing optimisation of rank-1 laminates when materials have unequal shear and dielectric ratios lead to enhanced non-linear effects. One subtlety that may be easily overlooked is the fact when the curves relating to tri-axial stretch with shear considered (Green curve) and homogeneous curve are compared in figure 6.3, it is noticed that at values below $E^{0\text{av}} = 20$ MV/m the homogeneous curve presents better response than the rank-1 laminate. The homogeneous curve only starts to present the lowest value for λ only at 20 MV/m when $\lambda = \lambda_{max}$ and possibly if the applied nominal electric field were to be increased past this point.

6.2.3 A comparison between all boundary-value problems: rank-2 laminates

Rank-2 laminates shall now be optimised in a manner analogous to that performed for rank-1 laminates. The results are presented on table 6.4 with corresponding curves presented in figures 6.5 and 6.6. The curves relating to shear strain not being taken into account present an inflexion point similar to that experienced for contrasts of 1000 and 10 000 in figures 4.12 and 5.9(a). This suggests that this behaviour is common to all contrasts which have either a shear modulus or a dielectric modulus above a certain threshold. The curve relating to tri-axial stretch with shear considered (green) presents the highest value for λ_{max}. For the curve relating to plain strain with shear strains considered (yellow) it should be noted that the amount of shear experienced corresponds to a shear angle of -53°. In the context of laminate interface interaction, this value is unsuitably high as large shear angles would be unfavourable while for tri-axial stretch with shear strains considered, a more acceptable amount of shear of -2° is experienced.

Curve	Case	λ_{max}	λ_2	λ_3	ξ	C^B_{R1}	$\theta_{R1}[^\circ]$	C^{R1}	$\theta_{R2}[^\circ]$
Blue	2D only	1.79682				0.497	60.0	0.948	-21.0
Yellow	2D + Shear	1.75878			-1.329	0.520	92.0	0.944	14.0
Red	3D only	1.66166	0.57433	1.04816		0.499	58.0	0.979	-29.0
Green	3D + Shear	1.84828	0.51655	1.04742	-0.029146	0.517	59.0	0.957	-32.0

Table 6.4: Rank 2-laminate configurations and corresponding maximum longitudinal stretch using contrasts presented on table 6.1 for various boundary-value problems at an applied nominal electric field of 20 MV/m. Corresponding curves are presented in figures 6.5 and 6.6.

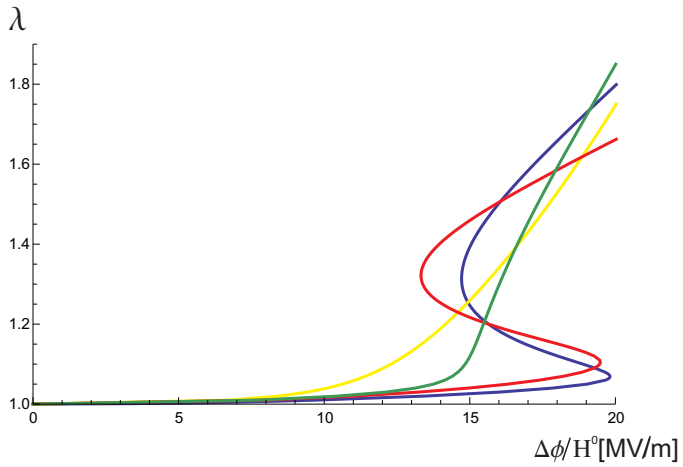

Figure 6.5: Influence of increasing applied nominal electric field on maximum longitudinal stretch at an applied nominal electric field of 20 MV/m for rank-2 laminates sharing a three-dimensional environment. Corresponding configurations are presented on table 6.4.

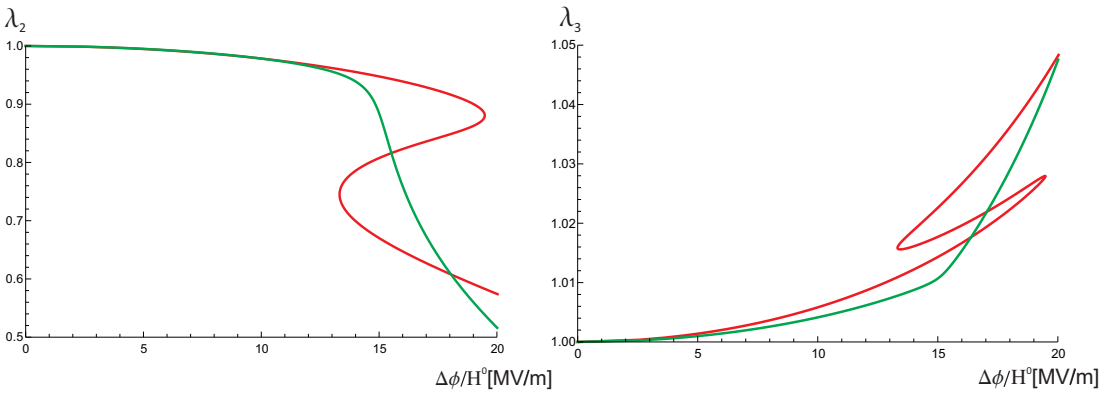

(a) (b)

Figure 6.6: Influence of increasing applied nominal electric field on corresponding (a) perpendicular stretch and (b) transverse stretch at an applied nominal electric field of 20 MV/m for rank-2 laminates sharing a three-dimensional environment. Green curves refer to a boundary-value problem when shear strains are considered and red to a boundary-value problem when shear strains are not considered. Corresponding configurations are presented on table 6.4.

When comparing rank-1 and rank-2 laminate behaviour for each boundary-value problem, the boundary-value problem relating to tri-axial stretch with shear strains considered (yellow) transitions from presenting the lowest value for λ_{max} on table 6.3 for rank-1 laminates to the highest value for λ_{max} among the presented rank-2 laminates. The injection of a matrix phase of soft material appears to present a profound contribution to the enhancement of longitudinal strain as well as shear strains. This is confirmed by the fact that both C^B_{R1} and C^{R1} are quite high for this configuration in comparison to other rank-2 laminates on this table implying a strong influence of the increased soft phase.

With regards to the two-dimensional boundary-value problems, for the first time a boundary value problem with shear strains considered results in a reduction in λ_{max}. Compare this with observations made in section 4.3.4 as well as by comparing tables 4.6 and 5.2. What this implies is a strong influence of the reduction of the shear modulus of material "B" such that the high shear angle observed in plane strain affects laminate performance. This is precisely what was being implied in figure 4.7 when only angles up to $\pm 40°$ were presented. However this is only experienced in plane strain as the configurations in a three-dimensional environment on table 6.4 reflect an enhancement in λ_{max} due to the consideration of shear strains, with surprisingly convenient low shear angle. Using only λ_{max} for comparison, it is possible to speculate where the range of values presented for these unequal ratios would lie on the spectrum of results presented in chapters 4 and 5. The range would most likely lie between $100 \leq \mu^A/\mu^B = \epsilon^A/\epsilon^B \leq 10\ 000$ however it is clear that establishing unequal ratios of shear to dielectric moduli presents improved performance for both rank-1 and rank-2 laminates and would

be the best design framework to establish for rank-1 and rank-2 laminate optimisation.

6.2.4 Current configuration of lamination angles of rank-2 laminates

In a manner similar to that executed in section 4.3.5, it is useful to determine the current configuration of lamination angles for the new combination of materials being investigated in this chapter. In order to accomplish this, the curves earlier presented in figure 6.5 will be presented in their current configuration with focus solely on longitudinal strain. The focus will be limited to longitudinal strain so as to provide comparison with all the various boundary-value problems. The current configurations of lamination angles for rank-2 laminates whose shear and dielectric ratios are not equal are now presented in figures 6.7 and 6.8, starting at the configurations presented on table 6.4 when $\Delta\phi/H^0$ =0 MV/m. What is immediately apparent for the evolution of lamination angle with applied nominal electric field in figures 6.7(a) and 6.8(a) is that as applied nominal electric field is increased, there is little deformation up until electromechanical instability is experienced for boundary-value problems with no shear strains considered. With regards to θ_{R1}, the value decreases at all boundary-value problems implying a clockwise rotation of the anisotropic phase. On figure 6.8(a), θ_{R2} shows an increase for all boundary-value problems except for the plane-strain boundary-value problem where shear strains are not considered, which presents a decrease in θ_{R2}.

Collectively, θ_{R2} angles for all boundary-value problems may appear to be converging to a common angle however this is not the case when one considers the evolution of the longitudinal stretch with both angles in figures 6.7(b) and 6.8(b). The evolutions show that each rank-2 laminate follows its own unique pathway for θ_{R1} and θ_{R2}. The current configuration can be considered to develop as a result of numerous variables and not strictly the input lamination angles as the figures may imply. Therefore the presence of electromechanical instability due to the lamination angles is confirmed due to the fact that there are no inflexion points if λ is presented as the independent variable in figures 6.7(b) and 6.8(b).

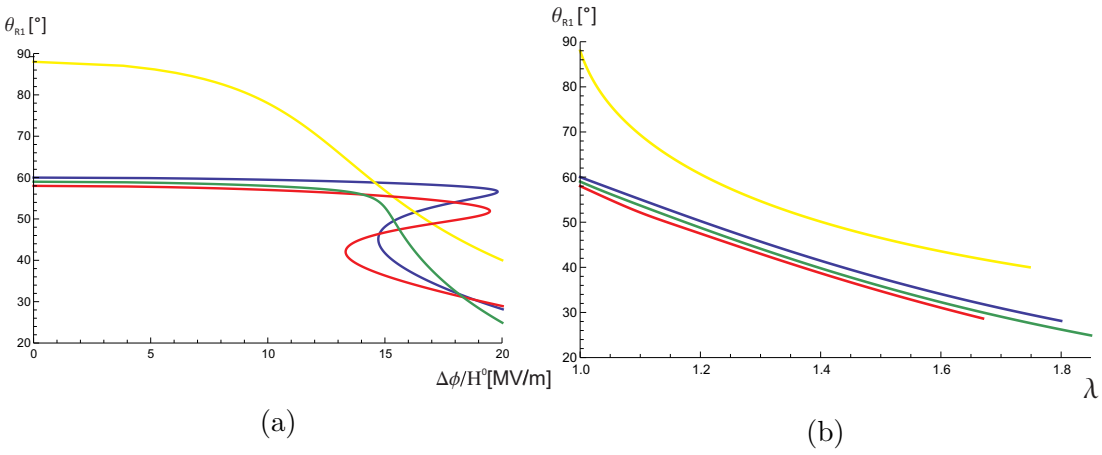

Figure 6.7: Current configuration of presenting (a) influence of increasing electric field on θ_{R1} and (b) influence of increasing longitudinal stretch on θ_{R1} for all rank-2 laminate of unequal shear and dielectric ratios with input configurations presented on table 6.4. Colours also refer to table 6.4.

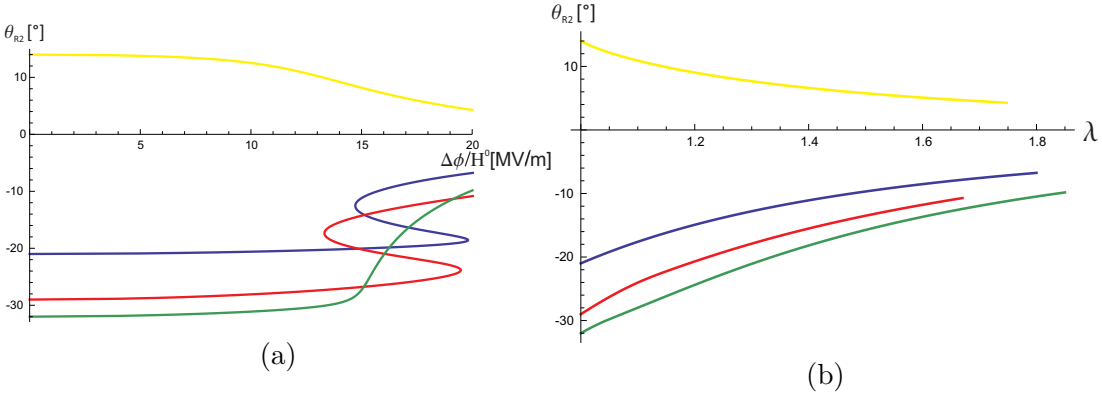

Figure 6.8: Current configuration of presenting (a) influence of increasing electric field on θ_{R1} and (b) influence of increasing longitudinal stretch on θ_{R1} for all rank-2 laminates investigated of unequal shear and dielectric ratios with input configurations presented on table 6.4. Colours also refer to table 6.4.

6.2.5 Electric field microscopic and macroscopic distributions for unequal dielectric and shear moduli

Now that the lamination angles in the current configuration have been presented, it is also useful, in a likewise manner to section 4.3.6, to compare and contrast the actual electric fields experienced in terms of their absolute values in all three phases in rank-2 laminates whose shear and dielectric moduli are unequal. A comparison will be made with the boundary-value problem of equal dielectric and shear moduli at a contrast of 100 presented earlier in figures 4.23 and 4.24. Previously an enhancement of a factor of 15 had been experienced and as now

presented in figures 6.9 and 6.10, enhancement of the soft phase in the matrix is of a factor 20 is experienced and maximum for the case of tri-axial stretch with no shear strain considered. This increase in enhancement can be attributed to the change in contrast of shear modulus of the soft phase presented on table 6.1. The boundary-value problem wiht maximum enhancement of the soft phase is surprisingly the one that reflects the lowest value of λ_{max} of the four presented on table 6.4. The value of C^{R1} is high such that the resulting value of E^B_{R2} is also high if one considers equation $[3.22_2]$. Thus it is logical that the laminate with the the highest amount of C^{R1} will have the greatest amount of strain enhancement. This enhancement highlights the electromechanical coupling present throughout this study. The more dielectric soft phase allows electrical excitation such that the jump in phases leads to a direct correlation between the applied nominal electric field and enhancement of this soft phase through the constant $\tilde{\beta}$ as explained in section 4.3.6.

Comparing the soft phases in the entirety of the rank-2 laminate i.e. E^B_{R1} and E^B_{R2} absolute values in figures 6.9 and 6.10, the plain strain boundary-value problem with shear strain considered presents the lowest enhancement of the four boundary-value problems in figure 6.10. Despite the corresponding configuration presenting a large amount of C^B_{R1}, the orientation of the anisotropic phase whereby $\theta_{R1} = 92^\circ$ means that this near vertical arrangement may not be ideal for electromechanical interactions. It is therefore evident that there is a pronounced influence of boundary-value problems on the absolute values of electric field enhancement for the soft phase due to the optimal laminate configuration.

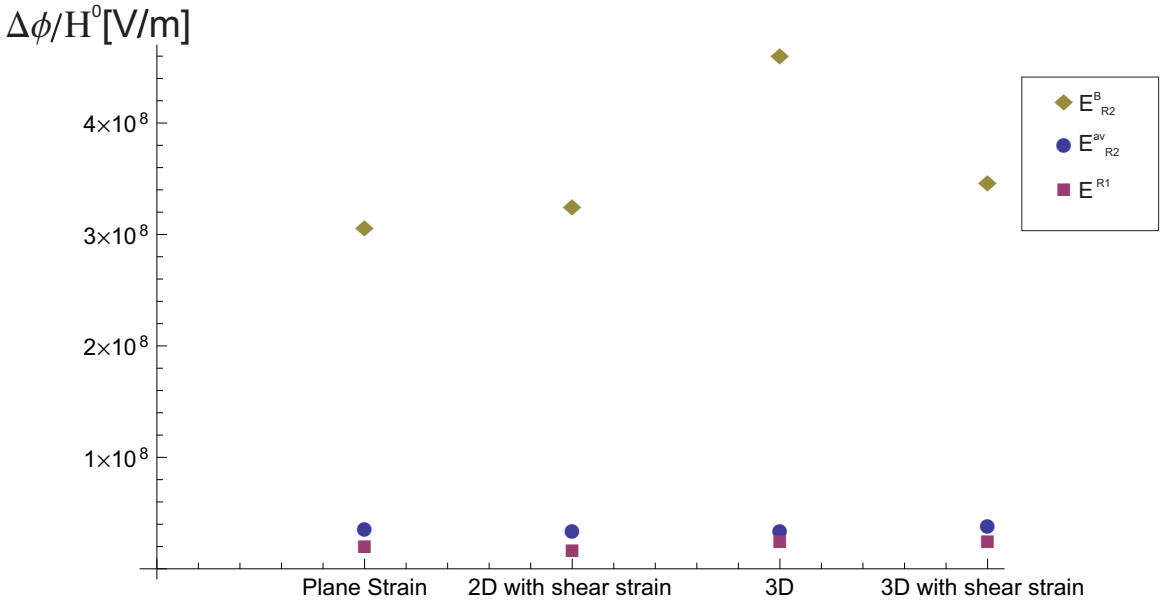

Figure 6.9: Absolute values of applied electric field and corresponding microscopic phase electric fields presented as absolute values in rank-2 laminates for all rank-2 laminates investigated of unequal shear and dielectric ratios with input configurations presented on table 6.4.

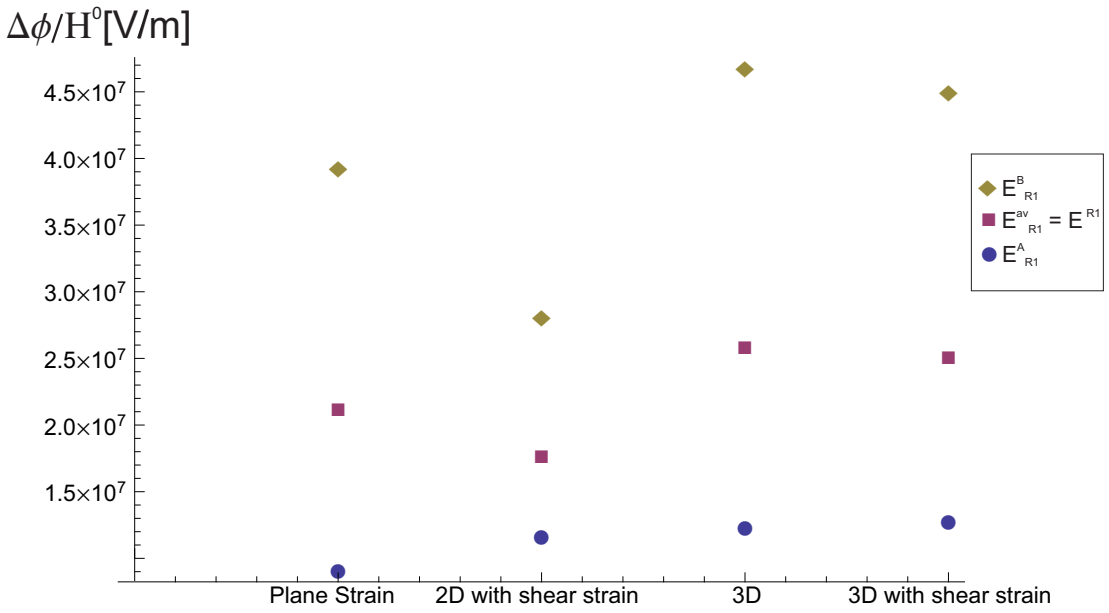

Figure 6.10: Absolute values of applied electric field and corresponding microscopic phase electric fields presented as absolute values in rank-1 anisotropic phases embedded in rank-2 laminates for all rank-2 laminates investigated of unequal shear and dielectric ratios with input configurations presented on table 6.4.

6.3 Design optimisation using material contrast: a prescription for laminate design

By this section, it should now be apparent that there is crucial requirement for laminate optimisation while taking into account both the presence of instability and shear strains when utilising rank-1 and rank-2 laminates whose dielectric and shear moduli are equal as well as unequal for actuation. At this juncture, we are now in a position to put forth a recommendation for strategies to employ in rank-1 and rank-2 sequentially laminated composite design by enlisting all the observations presented throughout this text. This section, in particular, is involved in establishing a designer's perspective as opposed to a rigorous, scientific, optimisation methodology in order to provide a recommendation for the possible combination of contrasts that would be optimum when designing rank-1 and rank-2 laminates. This idea has already been presented in part when laminates of unequal shear and dielectric moduli were presented earlier in this chapter. Optimising the contrast will therefore involve selecting a set of specific parameters to maintain as constant when perturbing the shear and dielectric moduli.

6.3.1 Rank-1 laminate contrast optimisation

As expected, we begin with rank-1 laminates in hope of advancing to possible rank-2 laminate contrast optimisation. It should be noted however, that the term "contrast optimisation" is used loosely due to the already presented numerous non-linear effects such that a non-linear influence when contrasts are perturbed is now most certainly expected. Thus the contrast optimisation results only represent an example optimisation process. In order to determine a logical starting point, we shall recap some of the observations already made in earlier sections. It may be useful to re-visit the configurations on tables 4.2, 4.8, 5.1, 5.4 and 6.3 before proceeding further.

For rank-1 laminates, it has been indisputably determined that the optimum volume fraction, for laminates whose shear and dielectric ratios are equal, that the amount of stiff phase and soft phase required at the optimum configuration are equal. There is also little to no change in the lamination angle with increasing contrast for materials whose shear and dielectric moduli are equal. When shear is considered in both plane strain and three-dimensional environments, the same predictions are valid only considering the fact that lamination angles for λ_{max} and ξ_{max} differ. Taking into account the stiffening for the rank-1 laminate with unequal shear and dielectric moduli encountered in figure 6.1, the applied nominal electric field in this section shall be limited to 20 MV/m. Amounts of stiff and soft phase in this new rank-1 laminate shall be maintained as equal (i.e.

0.5) and the selected lamination angle in plane strain shall be 50° in an effort to consider an angle within an acceptable range of all different boundary conditions presented. The contrast shall be optimised in a plane strain environment where shear strains are not considered, similar to section 4.3, which also contributes to selecting the lamination angle to be 50°. The aim of selecting this boundary-value problem is to consider the boundary-value problem which presented the most severe effect of electromechanical instabilities such that if contrast optimisation is possible under these conditions, then it would likely be possible for boundary-value problems with less restriction on the laminates ability to deform, such as in three dimensions or when shear strains are considered. The parameters are summarised on table 6.5.

$E^{0\text{av}}$ [MV/m]	C^B_{R1}	$\theta_{R1}[^\circ]$
20	0.500	50.0

Table 6.5: Rank-1 laminate parameters for contrast optimisation attempt.

The initial contrast optimisation attempt was carried out for the ranges of $10 \leq \epsilon^A/\epsilon^B \leq 1000$ for the dielectric ratio and $10 \leq \mu^A/\mu^B \leq 1000$ for the shear ratio. The results of this optimisation are presented in figure 6.11 and it is evident that, for the parameters on table 6.5, the initial ranges in which high λ values can be expected are when $\epsilon^A \geq 1000$ and $10 \leq \mu^A \leq 100$. This should come as no surprise as we have already established that there is an amplification of the electric field component in the soft phase, enabled by the dielectric ratio in section 6.2.5. The dielectric constant (or permittivity) ϵ is independent of the deformation such that the shear modulus is the parameter that limits the deformation of the material. This stretch is more present in the soft phase according to table 4.2 therefore the dielectric modulus will be higher than the shear modulus for maximum deformation. Using this new established range for the shear and dielectric moduli, a secondary optimisation for the ranges of $1000 \leq \epsilon^A/\epsilon^B \leq 10\,000$ for the dielectric ratio and $0 \leq \mu^A/\mu^B \leq 100$ for the shear ratio is presented in figure 6.12. The limit of this study of a contrast of 10 000 for either shear or dielectric moduli will also be applied in this case. It is therefore observed that λ continues to increase with increasing dielectric ratio for the parameters on table 6.5 until the limit of this study is reached that of a contrast of 10 000. Therefore for the parameters on table 6.5, a new contrast has been established of a dielectric ratio of 10 000 and a shear modulus of 10.

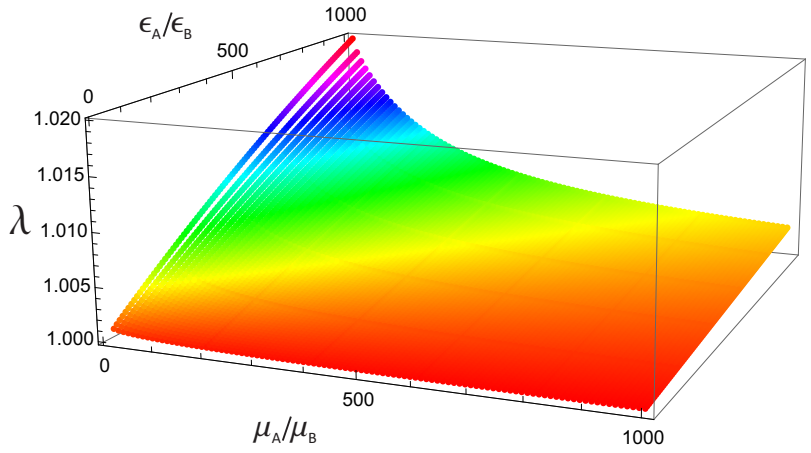

Figure 6.11: Example contrast optimisation search for the ranges $10 \leq \epsilon^A/\epsilon^B \leq 1000$ and $10 \leq \mu^A/\mu^B \leq 1000$ for a rank-1 laminate in a plane strain environment with no shear strains considered at an applied nominal electric field of 20 MV/m. C^B_{R1} =0.5, $\theta_{R1} = 50°$. Each point represents a unique combination of contrasts.

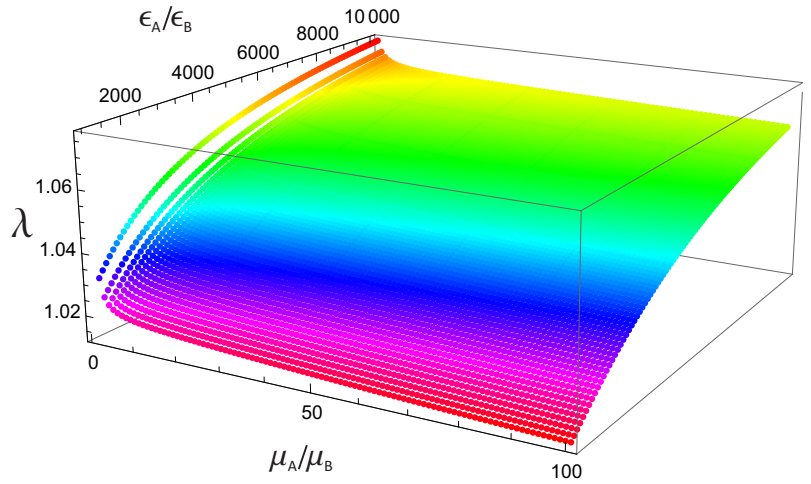

Figure 6.12: Example contrast optimisation for the ranges $1000 \leq \epsilon^A/\epsilon^B \leq 10000$ and $10 \leq \mu^A/\mu^B \leq 100$ for a rank-1 laminate in a plane strain environment with no shear strains considered up to the limit of this study at an applied nominal electric field of 20 MV/m. C^B_{R1} =0.5, $\theta_{R1} = 50°$. Each point represents a unique combination of contrasts.

6.3.2 Rank-2 laminate contrast optimisation

The same process shall be applied to rank-2 laminates, beginning with making an effort to select values for volume fractions and lamination angles representing a large proportion of those obtained for different boundary conditions. In a manner analogous to the previous section, re-visiting tables 4.6, 4.7, 4.9, 5.2, 5.6 and 6.4 is beneficial before proceeding. The volume fraction of the anisotropic phase shall be set at 0.99 while that of the softer phase in the core at 0.5, where both have been determined by an approximation from results on the aforementioned

tables. As has been obtained for rank-2 laminates, θ_{R1} is in the range 50-60° for this boundary-value problem therefore it shall be set to 55°. According to the enhancement of electric field presented in section 6.2.5, θ_{R2} will be set to near horizontal at 10°. This is due to the fact that throughout all the tables 4.6, 4.7, 4.9, 5.2, 5.6 and 6.4, there is an average difference between θ_{R1} and θ_{R2} of approximately 45° for each configuration. Therefore now starting at the configuration on table 6.5 and as we have increased θ_{R1}, it is recommended to set θ_{R2} to 10° i.e. a counter-clockwise rotation from horizontal by the same amount as θ_{R1}. These parameters are summarised on table 6.6.

$E^{0\text{av}}$ [MV/m]	C^{B}_{R1}	$\theta_{R1}[^\circ]$	C^{R1}	$\theta_{R2}[^\circ]$
20	0.500	55.0	0.990	10.0

Table 6.6: Rank 2-laminate parameters for contrast optimisation attempt.

This optimisation was performed in a manner similar to the rank-1 starting at the ranges of $10 \leq \epsilon^A/\epsilon^B \leq 1000$ for the dielectric ratio and $10 \leq \mu^A/\mu^B \leq 1000$ for the shear ratio. Similar to the rank-1 contrast optimisation, for the parameters on table 6.6 the initial range in which high λ values can be expected is when $\epsilon^A \geq 1000$ and $10 \leq \mu^A \leq 100$ in figure 6.13. The optimisation was then carried out up to a dielectric ratio of 10 000. It should be noted that, owing to the non-linear nature of this optimisation process, great care was taken when determining values for λ such that optimisation was performed in stages up until figure 6.14 which presents the final optimisation carried out for the ranges of $8\,000 \leq \epsilon^A/\epsilon^B \leq 10\,000$ for the dielectric ratio and $0 \leq \mu^A/\mu^B \leq 200$ for the shear ratio. Thus a high dielectric modulus and low shear modulus are required for high λ values for the configuration presented on table 6.6. These values for λ for a rank-2 laminate, however are not necessarily higher than for the previously introduced rank-1 laminate which reflects the non-linear nature of this investigation. Minimising the ranges of contrast optimisation would be advisable for future work due to the fact that in this case there has been one configuration defined for an extremely large range of contrasts.

It may now appear tempting to optimise the rank-1 and rank-2 configurations on tables 6.5 and 6.6 and optimum contrasts so as to determine λ_{max}, but this may prove to be naive. These new contrasts determined are under the influence of non-linear effects such that they only represent a myriad of contrast combinations possible when one maintains a set of parameters as performed on tables 6.5 and 6.6. What is evident here is that if the lamination angle, volume fraction and applied nominal electric field are kept constant, it is possible to determine the contrast combinations that would provide a better value for λ. An example

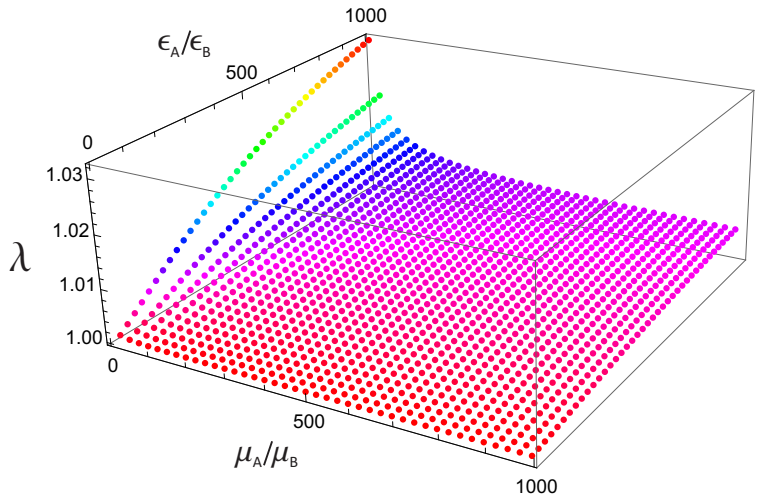

Figure 6.13: Contrast optimisation search for a rank-2 laminate in a plane strain environment with no shear strains considered. C^B_{R1} =0.5, C^{R1} =0.99, $\theta_{R1} = 55°$, $\theta_{R2} = 10°$. Each point represents a unique combination of contrasts.

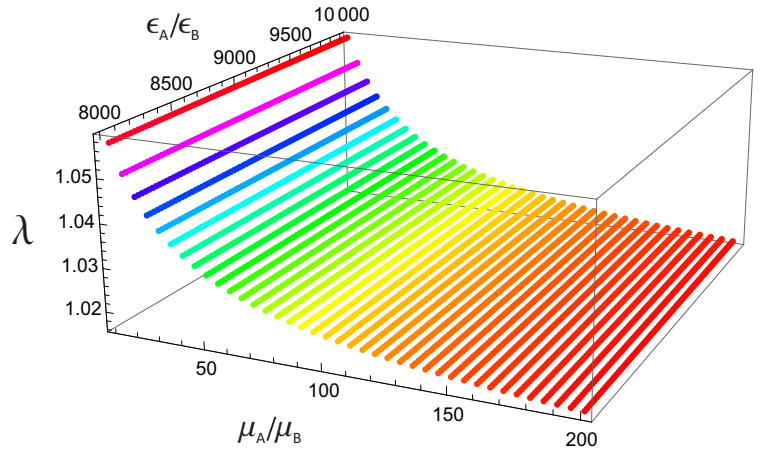

Figure 6.14: Contrast optimisation search for a rank-2 laminate in a plane strain environment with no shear strains considered. C^B_{R1} =0.5, C^{R1} =0.99, $\theta_{R1} = 55°$, $\theta_{R2} = 10°$. Each point represents a unique combination of contrasts.

of how this phenomenon may be used to one's advantage is as follows. Consider the configurations for contrasts of 1000 and 10 000 when shear and dielectric moduli are equal on table 4.6. For these rank-2 laminates, it is evident that λ_{max} improves greatly from a contrast of 1000 to 10 000 however, ξ also presents itself as unsuitably high. Using a designer's mindset, as stated at the beginning of this chapter, it is possible that there is a contrast between 1000 and 10 000 that may present a large enough enhancement of λ_{max}, while simultaneously minimising the shear angle or ξ. Thus, using target values for λ and ξ in the same manner as that executed on table 6.6, it is possible to determine contrasts for shear and

dielectric moduli that would maximise λ while minimising ξ between contrasts of 1000 and 10 000. Even if a sub-par value for λ is obtained, optimisation of the lamination angles and volume fractions could then be performed as a way of "tuning" the laminate to any required configuration. It is therefore pertinent to refer to the contrasts presented on tables 6.5 and 6.6 as "sample" configurations as the possibilities that rank-2 laminates present when one considers contrast optimisation are in-fact, infinite.

Of course one would now wonder why this contrast optimisation would not have been more ideal if executed at the beginning of this entire study in chapter 4 so as to provide an even more exhaustive coverage of rank-1 and rank-2 laminates. However, it should be noted that in order to even execute this so called "contrast optimisation", a general framework of suitable working ranges for all aspects of rank-2 laminates had to first be established such that the assigned initial lamination angles, volume fractions and applied nominal electric field on tables 6.5 and 6.6 would be in a region which provides the greatest probability of generating accurate values. Therefore, a prescription for rank-1 and rank-2 laminate design has thus been presented as an alternative method for approaching rank-1 and rank-2 laminate optimisation.

6.4 Conclusions

In this chapter, it has been presented that:

- Despite limiting applied nominal electric field to 20MV/m, the electrical excitation needs to be sufficiently high for a rank-2 laminate configuration to perform better than its rank-1 equivalent.
- A stiff phase is not only required in order to provide a favourable contrast for electrical excitation, but it also contributes to the overall stability of both rank-1 and rank-2 laminates when shear and dielectric ratios are equal as well as unequal.
- Rank-1 and rank-2 laminates whose shear and dielectric moduli are unequal provide enhanced performance in terms of λ_{max} in comparison to laminates with equal shear and dielectric moduli.
- Electric field enhancement of the soft phase in the matrix of a factor 20 is experienced and maximum for the case of tri-axial stretch with no shear strain considered

- For rank-1 and rank-2 laminates, the initial ranges in which high λ values can be expected are when $1000 \leq \epsilon^A/\epsilon^B \leq 10000$ for the dielectric ratio and $10 \leq \mu^A/\mu^B \leq 100$ for the shear ratio.
- If the lamination angle, volume fraction and applied nominal electric field are kept constant, it is possible to determine the contrast combinations that would provide a better value for λ.

Chapter 7

Conclusion

This study has been conducted in the realm of hyper-electroelasticity whereby rank-1 and rank-2 composites are characterized by a Lagrangian description of kinematics. We have begun with a description of finite elasticity and then presented fundamentals of electroelasticity for Neo-Hookean energy. The lamination procedure explained is that of a stiff, high dielectric phase laminated with a softer, low dielectric phase with electromechanical coupling due to Maxwell stress. Assumptions have been made for the sake of this study and rank-1 and rank-2 homogenized solutions based on the electric fields were then developed. In the context of this work, we initially followed the works of Tian et al. (2012) which related to small strain. These works were then applied to large strain using the methods of lamination introduced by Gei et al. (2013). Four parameters have been classified as ultimately leading to the microstructure optimisation of rank-2 laminates, namely the volume fraction of the soft phase in the core (C^B_{R1}), the volume fraction of the core in the composite (C^{R1}), the lamination angle of the rank-1 laminate (θ_{R1}) and the lamination angle of the rank-2 laminate (θ_{R2}).

For rank-1 laminates, the study commenced by comparing results obtained by Tian et al. (2012) in small strain with those obtained using the homogenized solutions in large strain when the ratios of shear and dielectric moduli of the phases was equal to provide a contrast of 100. The contrast of 100 was selected as the reference contrast for any initial optimisation presented in the study. The two sets of results provided the foundation of significant enhancement of longitudinal strain as well as non-linear effects present in large strain. The homogeneous actuation in large strain was 6% greater than in small strain while a 12% improvement in λ_{max} from the homogeneous actuation was obtained in large strain, similar to results by Tian et al. (2012) in small strain. It was also evident for all rank-1 laminates that there is a symmetry of approximately $\pi/2$, depending on the boundary conditions applied. When shear strains were considered in a plane strain environment, the value for λ_{max} at optimum laminate configuration was

lower than when shear strains were not considered for rank-1 laminates. This was evident when comparisons between the two boundary-value problems were made for rank-1 laminates. Considering the volume fraction of rank-1 laminates, the distribution of C_{R1}^{A} and C_{R1}^{B} was equal (0.5) at all boundary conditions investigated when the shear and dielectric moduli were equal.

It was also evident that an increase in contrast led to an amplification in the response of rank-1 laminates through various angles as well as for maximum longitudinal stretch. This was attributed to the increase in contrast providing a more efficient interaction of the electric field with the electromechanical coupling effect. It was useful to note that in plane strain, while the no shear strain considered boundary-value problem showed a curvilinear decrease in λ_{max} with increasing C_{R1}^{B}, the boundary-value problem where shear strains were accounted for presented a more rapid decrease in λ_{max}. Also, the lamination angle corresponding with λ_{max} was not the same as the lamination angle corresponding to ξ_{max} at an applied nominal electric field of 100 MV/m for rank-1 laminates. It was also presented that for rank-1 laminates in plane strain with no shear strain considered, the absolute value of the phase electric field in the softer phase is much higher than that for the stiffer phase such that the deformation of a rank-1 laminate is dominated by the soft phase. The equal amounts of stiff and soft phase, along with the lack of change of optimum lamination angle with increasing contrast, also enforced this fact that the soft phase is dominant in the deformation of rank-1 laminates.

It was clear that when transitioning from boundary-value problems relating to plane strain to those in a three dimensional boundary-value problem, there was little change in the optimum θ_{R1} and no change in optimum C_{R1}^{B}. To confirm if the equal weighting of stiff to soft phases applies to all rank-1 laminates regardless of contrast, it would be advisable to optimise rank-1 laminates with ratios of shear to dielectric moduli opposite to those presented at the beginning of chapter 6 in a manner analogous to section 6.2.2. It was also argued that for a rank-1 laminate, the longitudinal stretch in a three dimensional boundary-value problem i.e. λ_1 can be used to approximate λ in a plane strain boundary-value problem and vice versa. The rate of change in stretch with increasing applied nominal electric field of λ_1 was also found to be greater than the rate of change in stretch of perpendicular stretch, λ_2. For a three-dimensional boundary-value problem that does not consider shear strain, an increase in contrast past 100 did not seem to induce any further notable transverse stretch, i.e. λ_3 in rank-1 laminates. As also observed in the plane strain solution, there was a slight decrease in the optimum lamination angle with increasing contrast.

When the applied nominal electric field was varied with shear strain con-

sidered in a three dimensional environment, there was little difference in λ_{max} at increasing contrasts for rank-1 laminates. The influence of lamination angle on λ_{max} remained unassailable revealing the ferocity of performance-enhancing influence of lamination angle on maximum longitudinal stretch in a rank-1 laminate. Consideration of shear strains meant that the electromechanical coupling phenomenon was greatly reduced when shear strains were considered. In terms of the magnitude of shear stresses, it was also determined that they are very small in a three-dimensional boundary-value problem where shear strains are considered. When transitioning from boundary-value problems without shear strain considered to those with shear strain considered for rank-1 laminates, dampening of λ with varying θ_{R1} was also observed. Rank-1 laminates, in the context of microstructure optimisation, are crucial in providing a baseline enhancement which will enable a better understanding of the severe non-linear nature of rank-2 laminates.

For rank-2 laminates, the initial optimisation at a contrast of 100 was carried out for plane strain with shear strain considered. Comparison of Tian et al. (2012) small strain results with those obtained in large strain led to a 20% improvement in λ_{max} being obtained for optimum configurations in small strain compared to those in large strain. The optimum configuration obtained by Tian et al. (2012) in small strain, when solved in large strain, presented a 12% improvement in λ. When all contrasts were compared for optimum configurations presented in large strain with those obtained in small strain by Tian et al. (2012) for plane strain with shear strain considered, significant enhancement of λ_{max} was achieved, enforcing the non-linear nature of this study. It was also presented that the rank-2 laminate configuration can be optimised for maximum amount of shear as a method of understanding if high shear strains may affect phase interface interactions, possibly leading to composite failure. The volume fraction of the anisotropic phase was also found to present the greatest influence on shear angle and λ.

When shear strains were not considered in plane strain for rank-2 laminates, a lower λ was obtained compared to when shear strains were considered. However, there was observed electromechanical instability at contrasts of 1000 and 10 000. Microstructure perturbation in order to reduce the observable electromechanical instability was presented for example configurations. It was also found that a reduction in applied nominal electric field could be performed to achieve this effect in addition. This then helped to enforce the fact that there exists a different optimum configuration at each different value of operational applied nominal electric field for rank-2 laminates. It was found that when θ_{R1} was parallel to θ_{R2} when shear strains were not considered, λ_{max} values were the same due to the the fact that the rank-2 laminate configuration was in a manner similar to

the rank-1 configuration. There was also no change in the volume fraction of the soft phase in the core i.e. C_{R1}^{B} from that of the rank-1 laminate which further confirmed the behaviour. Also for a laminate that was at very low contrasts at which the dielectric and shear moduli were equal, there was little increase in λ_{max} for a rank-2 laminate as opposed to a rank-1 laminate for actuation purposes.

When the two plane strain boundary value problems were compared, namely plane strain with shear strain considered and plane strain without shear strain considered, it was found that the same configuration obtained when no shear strains were considered presented a higher λ when shear strains were considered by 16% for a contrast of 1000. Also, for a configuration that presents non-monotonic behaviour when shear strains are not considered, monotonic behaviour can be obtained when shear strains are considered implying a vanishing in observable electromechanical instability. Having determined optimum configurations, the current configuration of a rank-2 laminate when applied electric field was increased revealed that θ_{R1} reflects greater change in current angle and again electromechanical instability was reflected in the current state of the laminate. The electric field of the soft homogeneous phase in the rank-2 laminate at a contrast of 100 reflected the greatest enhancement among all the phases of the factor of 15 in terms of the absolute values. This enhancement was found to be of a factor of 20 for a laminate whose shear and dielectric moduli were not equal for a three-dimensional case with no shear strains considered. This was due to the fact that the magnitude of the electric fields in the isotropic layers is proportional to the applied electric field divided by their volume fraction. It was found that in order to obtain a maximum electric field in any phase of 100 MV/m when the ratios of shear and dielectric moduli were equal at a contrast of 100, the required applied nominal electric field was found to be 6.95 MV/m.

In a three-dimensional environment, it was also found that λ_1 can be used to approximate λ in plane strain. It was again discovered, through lamination angle perturbation, that θ_{R1} is more dominant in λ_{max} determination compared to θ_{R2}. Electromechanical instabilities were also observed when shear strains were not considered in a three-dimensional environment. All contrasts from 10 to 10 000 were also presented for example configurations which illustrated the limit of strict monotonic behaviour. When shear strains were considered in a three-dimensional environment, there was a reduction in λ_{max} up to contrast of 1000 in comparison to the plane strain equivalent problem which was attributed to the presence of the transverse stretch. An increase in contrast also resulted in an increase in ξ_{max} in agreement with plane strain results. It was conclusively determined in this section that at higher contrasts, shear angles are unsuitably high at λ_{max} such that a trade-off needs to be established between λ and ξ when optimising the microstructure of rank-2 laminates. Lastly when three-dimensional

boundary value problems were compared with each other, a 17% enhancement of λ was obtained for the same configuration from tri-axial stretch with no shear strain considered to tri-axial stretch with shear strain considered at a contrast of 1000. This confirmed enhancement of λ occurs in both plane strain and three-dimensional boundary-value problems.

The influence of non-linear effects and microstructure sensitivity exposed in chapters 4 and 5 should be re-iterated as the contrast optimisation executed in chapter 6 represents only a very small region in the vastness of strategies available for laminate optimisation. The number of combinations possible if one considers lamination angles, volume fractions, amount of applied nominal electric field, direction of applied nominal electric field, method of lamination as well as contrast of laminating materials are possibly infinite. This should then be followed up by consideration of the trade-off required between λ, ξ and electromechanical instability. This study has thus provided exhaustive coverage of only a particular combination of all these aforementioned variables and therefore there is no claim here that this optimisation strategy is inviolable. If anything, this study demonstrates the multitude of design approaches possible in finite strain with only a slight undertone of electromechanical instabilities occurring in rank-2 laminated composites when shear strains are not considered in plane strain and tri-axial stretch. The investigation of the electromechanical instabilities and their classification would represent a separate study altogether and is recommended as future work. As a starting point, chapter 6 would be recommended as a foundation for advancement in complexity of laminate microstructure optimisation for a targeted performance for rank-2 or higher rank laminates.

As presented in sections 4.3.6 and 6.2.5, the amount of applied nominal electric field considered in this study has proven to be considerably high in terms of absolute values of the phase electric fields actually experienced. A different approach would be to reduce this applied nominal electric field in order to achieve a specific target electric field in a specific phase of the laminate. However, this approach is not as straightforward as the statement suggests as simply reducing the electric field may seem trivial in execution but in reality the boundary conditions as well as the contrast also contribute to the non-linear effect. This means that a new type of behaviour would possibly occur if too many parameters are perturbed in comparison to this study. Also, reducing the applied nominal electric field also has its limits as the nominal applied electric field should be sufficiently high enough to justify optimising rank-1 and rank-2 laminates. This is because at low applied nominal electric fields, there may be only very little difference in λ_{max} between rank-1 and rank-2 laminates as discussed in section 6.2.1 such that there would be no justification for optimising the microstructure in such a case.

The jump conditions presented in chapter 3 also contribute to electric field enhancement through the method of lamination such that if this method is to be altered it may present a significant influence on electric field enhancement in the three phases through the jump conditions and the new homogenized solution in terms of the electric field. The method of lamination can be thus considered in future work in terms of considering three materials in the rank-2 laminate as opposed to two, with an expectation that results obtained in such a study would be vastly different to those experienced in this study. In the context of the homogenised solution, the electric displacement has been of little to no mention in this study and this may be another aspect of future study. One can also imagine that in reality, material shear and dielectric moduli would not be exactly of values presented in this study therefore one could begin by selection of a set of different contrasts representative of real world materials and then proceed to optimise the laminates with the aid of chapter 6.

The Newton-Raphson method has presented some difficulty when applied nominal electric field is used as the independent variable. It is well known that this method depends on the initial estimation such that when electromechanical instability is present in the form of non-monotonic behaviour, it is possible to not obtain all true points on the desired electromechanical loading path. If one considers the number of equations and parameters to be solved simultaneously discussed in section 3.3.2, it means that each parameter requires an accurate initial estimation, with the number of parameters increasing for the more complex boundary-value problems. Therefore, it would be recommended to consider an exploration of various numerical methods possible for providing *accurate* and *precise* solutions on the corresponding electromechanical loading path. In section 4.3.2, it was also emphasised how the electromechanical loading path for contrasts of 1000 and 10 000 produced curves only just within the range $0 \leq \Delta\phi/H^0 \leq 100$ MV/m. Thus for rank-2 laminate optimisation another method of applying the Newton-Raphson method would be to utilise a two-step method of first determining the optimum configuration at the applied nominal electric field required, and only then, having established the corresponding λ_{max}, using this as a guideline for visualising the electromechanical loading path using λ as the independent variable to ensure this path also lies within the selected range.

In the context of prioritising the parameters defined in this study, the lamination angles of rank-1 and rank-2 laminates have been determined to provide the greatest weighting of all the optimisation parameters as they present a profound influence on the longitudinal stretch and electromechanical stability. Of course, the combination of lamination angles and volume fractions for rank-2 laminates is ultimately what influences maximum longitudinal stretch but the

main observation presented in this text is that the lamination angles provide a more dominant influence on the maximum longitudinal stretch, amount of shear and electromechanical stability of rank-2 laminates. Mention has also been made of shear strains as they have been observed through a comparison of boundary-value problems where shear strains are considered and when shear strains are not considered.

Another possible future region of study would be to illuminate in more detail the influence of ξ_{max} optimisation on programming rank-2 laminates. Indeed the shear angle has been found to increase with increasing contrast up to an unfavourable extent which may not be suitable for laminate performance. However, if the contrast and amount of applied nominal electric field are modified one may find a suitable region which would provide lower shear strains for a suitably high maximum longitudinal stretch. Mention can be made to section 6.3.2 as an example of such a case where shear modulus of the soft phase was low and dielectric modulus of the soft phase high such that one may expect phase pressures and shear stresses to be low. The high shear strains may even be found to be influential on the electromechanical stability of laminates as well. For laminates of equal shear and dielectric moduli, there has also proven to be a specific contrast at which electromechanical instability is present such that if one desires to determine the contrast at which this instability is triggered a further study may be executed in this manner. However this could prove severely challenging due to the non-linear nature of rank-2 laminates, as illustrated when laminates composed of materials of unequal shear and dielectric moduli were investigated.

This study was limited to ratios of shear and dielectric moduli up to 10 000 and mention should be made that this limit was merely selected as initial results were being compared to previous authors but the region of contrast investigation is unrestricted. Although, there may be no use going past such a ratio of moduli as this may not represent currently available real-world materials, which is ultimately what one hopes this study would eventually achieve. It may not be clear, also, if some of the rank-2 configurations obtained in this study relate to a realistic type of microstructure. For example, a lamination angle in the rank-2 laminate of -1° may prove to be difficult to manufacture. However this study, ultimately, has shown that for whichever parameter that cannot be greatly modified, one can optimise all other parameters for improved laminate performance. One hopes that an advancement in areas such as 3D printing or more modern methods could aid in solving this problem and over time may lead to a widespread application of dielectric composite actuators.

References

Ashley, S. (2003), 'Artificial muscles', *Scientific American* pp. 53–59.

Bertoldi, K. & Gei, M. (2011), 'Instabilities in multilayered soft dielectrics', *Journal of the Mechanics and Physics of Solids* **59**(1), 18–42.

Boyce, M. C. & Arruda, E. M. (2000), 'Constitutive Models of Rubber Elasticity: A Review', *Rubber Chemistry and Technology* **73**(3), 504–523.

Brochu, P. & Pei, Q. (2010), 'Advances in dielectric elastomers for actuators and artificial muscles', *Macromolecular Rapid Communications* **31**(1), 10–36.

Carpi, F., Rossi, D. D., Kornbluh, R., Pelrine, R. & Sommer-Larsen, P. (2008), *Dielectric elastomers as electromechanical transducers : fundamentals, materials, devices, models and applications of an emerging electroactive polymer technology*, Elsevier Science, Oxford, UK.

Choi, W., Choi, K., Yang, G., Kim, J. C. & Yu, C. (2016), 'Improving piezoelectric performance of lead-free polymer composites with high aspect ratio BaTiO3 nanowires', *Polymer Testing* **53**, 143–148.

DeBotton, G. (2005), 'Transversely isotropic sequentially laminated composites in finite elasticity', *Journal of the Mechanics and Physics of Solids* **53**(6), 1334–1361.

Dorfmann, A. & Ogden, R. W. (2005), 'Nonlinear electroelasticity', *Acta Mechanica* **174**(3-4), 167–183.

Dorfmann, L. & Ogden, R. W. (2017), 'Nonlinear electroelasticity : material properties , continuum theory and applications', *The Royal Society* **473**(2204).

Fu, Y. B. & Ogden, R. W. (2001), *Nonlinear Elasticity: Theory and Applications*, Lecture note series / London mathematical society, Cambridge University Press, Cambridge, UK.

Garcia-Mayoral, R. & Jimenez, J. (2011), 'Drag reduction by riblets', *Philosophical Transactions of the Royal Society A: Mathematical, Physical and Engineering Sciences* **369**(1940), 1412–1427.

Gei, M., Springhetti, R. & Bortot, E. (2013), 'Performance of soft dielectric laminated composites', *Smart Materials and Structures* **22**(10), 8.

Lopez-Pamies, O. (2006), On the Effective Behavior, Microstructure Evolution and Macroscopic Stability of Elastomeric Composites, PhD thesis, University of Pennsylvania.

Lopez-Pamies, O. (2014), 'Elastic dielectric composites: Theory and application to particle-filled ideal dielectrics', *Journal of the Mechanics and Physics of Solids* **64**(1), 61–82.

McMeeking, R. M. & Landis, C. M. (2005), 'Electrostatic Forces and Stored Energy for Deformable Dielectric Materials', *Journal of Applied Mechanics* **72**(4), 581.

Ogden, R. W. (1974), 'On the overall moduli of non-linear elastic composite materials', *Journal of the Mechanics and Physics of Solids* **22**(6), 541–553.

Ogden, R. W. (1997), *Non-linear Elastic Deformations*, Dover Civil and Mechanical Engineering, Dover Publications, New York.

Pelrine, R. E., Kornbluh, R. D. & Joseph, J. P. (1998), 'Electrostriction of polymer dielectrics with compliant electrodes as a means of actuation', *Sensors and Actuators A: Physical* **64**(1), 77–85.

Rudykh, S. (2012), Electroactive Polymer Composites : Microscopic and Macroscopic Stability, PhD thesis, Ben-Gurion University of the Negev.

Rudykh, S., Lewinstein, A., Uner, G. & DeBotton, G. (2011), 'Giant Enhancement of the Electromechanical Coupling in Soft Heterogeneous Dielectrics', pp. 0–2.

Skov, A. L., Pei, Q., Opris, D., Spontak, R. J., Gallone, G., Shea, H. & Benslimane, M. Y. (2016), Dielectric Elastomers (DEs) as EAPs: Materials, *in* F. Carpi, ed., 'Electromechanically Active Polymers: A Concise Reference', Springer International Publishing, Cham, chapter 31, pp. 687–714.

Spinelli, S. A. & Lopez-Pamies, O. (2015), 'Some simple explicit results for the elastic dielectric properties and stability of layered composites', *International Journal of Engineering Science* **88**, 15–28.

Suo, Z., Zhao, X. & Greene, W. H. (2008), 'A nonlinear field theory of deformable dielectrics', *Journal of the Mechanics and Physics of Solids* **56**(2), 467–486.

Tevet-Deree, L. (2008), Electroactive Polymer Composites - Analysis and Simulation, PhD thesis, Ben-Gurion University of the Negev.

Tian, L., Tevet-Deree, L., Debotton, G. & Bhattacharya, K. (2012), 'Dielectric elastomer composites', *Journal of the Mechanics and Physics of Solids* **60**(1), 181–198.